Response to the Editor: acp-2016-850

On behalf of all co-authors, I would like to thank the three anonymous reviewers for detailed and thoughtful comments on the manuscript: Carbon Dioxide and Methane Measurements from the Los Angeles Megacity Carbon Project: 1. Calibration, Urban Enhancements, and Uncertainty Estimates" *by* K. R. Verhulst et al. The reviewer comments were both thoughtful and insightful and helped improve the clarity and content of the manuscript, especially with regards to the topic of background estimation. We also thank another reviewer for a short comment that helped clarify text in the manuscript related to the annual averages. We have posted separate responses to comments made by Referees 1-3 online and incorporated the suggested changes into a revised version of the manuscript. Attached below is a copy of the revised manuscript, with all changes highlighted using "track changes." Where applicable, we included typographical and stylistic changes, as well as additional references suggested by the reviewers. We also conducted our own internal reviews, which resulted some in stylistic and typographical edits throughout the text that are also tracked here. Additionally, we were able to update our latest carbon dioxide and methane datasets up to June 2016, and these data are now included in Figures 2-4. Finally, in Table 1 we included the location of an additional site that was installed in November 2016 (Canoga Park) in Table 1. Although we are not able to present results from this site at this time, the location will become part of the regular Los Angeles in situ network going forward and we thought it would be appropriate to include the coordinates with the list of other sites in Table 1.

Carbon Dioxide and Methane Measurements from the Los Angeles Megacity Carbon Project: 1. Calibration, Urban Enhancements, and Uncertainty Estimates

Kristal R. Verhulst[1,2], Anna Karion[3], Jooil Kim[4], Peter K. Salameh[4], Ralph F. Keeling[4], Sally Newman[5,a], John Miller[6,7], Christopher Sloop[8], Thomas Pongetti[1], Preeti Rao[1,b], Clare Wong[1,5,c], Francesca M. Hopkins[1,d], Vineet Yadav[1], Ray F. Weiss[4], Riley M. Duren[1], and Charles E. Miller[1]

[1]NASA Jet Propulsion Laboratory, California Institute of Technology, Pasadena, CA, USA
[2]University of California, Los Angeles, Joint Institute for Regional Earth System Science and Engineering, Los Angeles, CA, USA
[3]National Institute of Standards and Technology (NIST), Gaithersburg, MD, USA
[4]Scripps Institution of Oceanography, University of California, San Diego, La Jolla, CA, USA
[5] California Institute of Technology, Division of Geological and Planetary Sciences, ,Pasadena, California, USA
[6]NOAA/ESRL/GMD, Boulder, CO, USA
[7]CIRES, University of Colorado, Boulder, CO, USA
[8]Earth Networks, Inc., Germantown, MD, USA
[a]Now at: Bay Area Air Quality Management District, Planning and Research Division, Climate Protection Section, San Francisco, CA, USA
[b]Now at: University of Michigan, School of Natural Resources and Environment, Ann Arbor, MI, USA.
[c]Now at: California State University, Northridge, Institutional Research Office, Northridge, California, USA
[d] Now at: University of California, Riverside, Dept. of Environmental Sciences, Riverside, CA, USA

Correspondence to: K. R. Verhulst (Kristal.R.Verhulst@jpl.nasa.gov)

Abstract. We report continuous surface observations of carbon dioxide (CO_2) and methane (CH_4) from the Los Angeles (LA) Megacity Carbon Project during 2015. We devised a calibration strategy, methods for selection of background air masses, calculation of urban enhancements, and a detailed algorithm for estimating uncertainties in urban scale CO_2 and CH_4 measurements. These methods are essential for understanding carbon fluxes from the LA megacity and other complex urban environments globally. We estimate background mole fractions entering LA using observations from four "extra-urban" sites including: two "coastal/marine" sites located south of LA in La Jolla and offshore on San Clemente Island, one "continental" site located in Victorville, in the high desert northeast of LA, and one "continental/mid-troposphere" site located on Mount Wilson in the San Gabriel Mountains. We find that a local marine background can be established to within ~1 ppm CO_2 and ~10 ppb CH_4 using these local measurement sites. Overall, atmospheric carbon dioxide and methane levels are highly variable across Los Angeles. "Urban" and "suburban" sites show moderate to large CO_2 and CH_4 enhancements relative to a marine background estimate. The USC site near Downtown LA exhibits median hourly enhancements of ~20 ppm CO_2 and ~150 ppb CH_4 during 2015 and ~15 ppm CO_2 and ~80 ppb CH_4 during mid-afternoon hours (12-16:00 LT, local time), which is the typical period of focus for flux inversions. The estimated measurement uncertainty is typically better than 0.1

Deleted: roughly

Deleted: We also show that continental sites may not be relevant for selecting background observations during summer months due to the prevalence of onshore flow, which could transport CO_2 and CH_4 from the LA Basin to relatively remote sites.

Deleted: to

Deleted: An urban site

Deleted: has a

Deleted: roughly

Deleted: during all hours

Deleted: roughly

Deleted: midday

Deleted: roughly

ppm CO_2 and 1 ppb CH_4 based on the repeated standard gas measurements from the LA sites during the last two years, similar to Andrews et al. (2014). The largest component of the measurement uncertainty is due to the single-point calibration method; however, the uncertainty in the background mole fraction is much larger than the measurement uncertainty. The background uncertainty for the marine background estimate is ~10% and ~15% of the mid-afternoon enhancement near Downtown LA for CO_2 and CH_4, respectively. Overall, analytical and background uncertainties are small relative to the local CO_2 and CH_4 enhancements, however, our results suggest that reducing the uncertainty to less than 5% of the enhancement will require detailed assessment of the impact of meteorology on background conditions.

Deleted: 1-2
Deleted: observations being elevated relative to the
Deleted: The approach to identifying background mole fractions
Deleted: described here results in
Deleted: ranging
Deleted: from roughly 5
Deleted: and 15
Deleted: downtown
Deleted: , during afternoon hours

1 Introduction

Improved understanding of carbon dioxide (CO_2) and methane (CH_4) emissions from cities has been identified as a priority for both carbon cycle science and to support climate change mitigation efforts (Hutyra et al., 2014; Pacala et al., 2011). More than half of the global population currently resides within cities, with the fraction living in urban areas projected to increase in the future (United Nations, 2014). Currently, more than 70% of anthropogenic greenhouse gases (GHG) are emitted from cities globally (IEA, 2008). The combination of carefully designed urban-scale atmospheric CO_2 and CH_4 monitoring networks, tracer transport modelling, and functionally resolved emissions data sets has the potential to offer significant advances in understanding and managing urban carbon emissions (Duren and Miller, 2012).

Carbon fluxes can be estimated using both top-down, bottom-up, or a combination of both methods using measurements in an inverse model framework (Asefi-Najafabady et al., 2014; Gurney et al., 2005; Lauvaux et al., 2016). Top-down and bottom-up approaches are complementary to one another and when combined can be beneficial for informing policy. Top-down approaches typically estimate carbon sources and sinks from measured patterns of variability based on atmospheric observations. By contrast, bottom-up methods require an investigation of activity data and local processes, such as fossil fuel production and consumption data, and/or construction of models that combine fossil fuel usage data with estimates of the carbon content of the fuel type (Asefi-Najafabady et al., 2014; Gurney et al., 2009, 2012). An integrated top-down approach can be very useful, especially given the complex mixtures of anthropogenic and biogenic CO_2 and CH_4 sources found in urban ecosystems, which may be difficult to quantify using bottom-up methods (Duren and Miller, 2012; Hutyra et al., 2014). Furthermore, combining top-down and bottom-up approaches in an iterative process can lead to a better understanding of gaps in bottom-up emissions models. Top-down measurements are advantageous in that they can be reported with fully traceable and rigorously defined uncertainties. For these reasons, measurement records with both high precision and long-term stability are crucial to the objective evaluation of reported emissions at local, regional, and continental scales (roughly 10^2 km^2 to 10^6 km^2; e.g., Andrews et al., 2014).

Deleted: “
Deleted: ”
Deleted: or “
Deleted: ”
Deleted: Both
Deleted: attempt to
Deleted: , such as
Deleted: ing
Deleted: from each source sector
Deleted: also
Deleted: In this way
Deleted: -10^6
Deleted: e.g.

In recent years, there has been growing international interest in using top down atmospheric approaches to quantify urban GHG fluxes (e.g., Duren and Miller, 2012; McKain et al., 2012, 2015). Large, organized urban greenhouse gas

Deleted: e.g.

monitoring projects have emerged in many cities, including Paris (CO$_2$-Megaparis: http://co2-megaparis.lsce.ipsl.fr; e.g., Bréon et al., 2015; Xueref-Remy et al., 2016), Boston (McKain et al., 2015), Indianapolis (Influx: http://influx.psu.edu; e.g., Turnbull et al., 2015), Salt Lake City (http://lair.utah.edu/page/project/uta/pilot/; e.g., McKain et al., 2012), the San Francisco Bay Area, (e.g., Shusterman et al., 2016) and, in this study, the Los Angeles Megacity (https://megacities.jpl.nasa.gov/portal/; see also Feng et al., 2016). To date, most of these research efforts to quantify greenhouse gas emissions in cities have been largely disconnected. The data and methods for greenhouse gas monitoring in urban regions should be fully disclosed and documented with a small degree of latency to make the best use of these atmospheric data for emissions verification and/or for informing policies more generally.

The Megacities Carbon Project was established through a multi-agency and multi-institution collaboration to develop and demonstrate policy-relevant carbon monitoring in some of the world's largest and most complex cities, and to help address gaps in our knowledge of greenhouse gas emissions (Duren and Miller, 2012). The Los Angeles (LA) testbed project involves continuous and discrete flask sampling of air to monitor greenhouse and trace gas concentrations, together with isotopic ratios of CO$_2$ at multiple surface sites. This study describes the Los Angeles surface measurement network. The LA project has dramatically expanded the number of greenhouse gas observing sites in the South Coast Air Basin since 2013, allowing unprecedented spatio-temporal measurement coverage in this region. In this study, we describe the Los Angeles Megacity surface network, sampling strategy, and calibration methods. We also discuss some preliminary results on CO$_2$ and CH$_4$ enhancements in the LA Basin and some detailed metrics for evaluating uncertainties in our observations.

California's South Coast Air Basin (SCB) is home to approximately 16.3 million residents and has a geographical area of roughly 17,100 km^2 (Figure 1; CARB, 2014). Observations from the LA network will be useful for future assessment of GHG emissions in the SCB, which encompasses more than 42% of the CA statewide population. Policies and strategies for mitigation of CO$_2$ and CH$_4$ emissions are currently being implemented in California, with measures being passed at the state and local levels. The California Global Warming Solutions Act of 2006 (AB 32) requires California to reduce its GHG emissions to 1990 levels by 2020, a 15% reduction below emissions expected under a business-as-usual scenario.

The SCB presents unique challenges in terms of the complexity of the land surface, meteorology, and spatial-temporal variability of its CO$_2$ and CH$_4$ emissions. The SCB is bordered by the Pacific Ocean to the west and by mountains to the north and east. The mesoscale circulation patterns observed over the LA megacity are challenging to represent in atmospheric transport models (e.g., Angevine et al., 2012; Conil and Hall, 2006; Feng et al., 2016). Complex topography within the Basin can allow formation of micrometeorological zones, which may result in concomitant transport complexity. Prior studies suggest a dense measurement network with a high-degree of spatial and temporal resolution is required to provide robust, spatially-resolved greenhouse gas flux estimates for the Los Angeles megacity (Kort et al., 2013).

Deleted: e.g.

Deleted: e.g.

Deleted: e.g.

Deleted: e.g.

Deleted: se

Deleted: More information flow between existing urban observational networks and the science and applications communities is needed to understand greenhouse gas emissions from cities.

Deleted: , and https://megacities.jpl.nasa.gov/portal/)

Deleted: pilot

Deleted: The Los Angeles Megacity

Deleted: >15

Deleted: spans

Deleted: in California's South Coast Air Basin (SCB,

Deleted:

Deleted:)

Deleted: also

Deleted: South Coast Air Basin

Deleted: 43

Moved down [1]: Urban and suburban areas in the SCB have high population densities and a large variety of anthropogenic CO$_2$ and CH$_4$ emissions sources, as well as non-zero CO$_2$ fluxes expected from the terrestrial biosphere (Feng et al., 2016; Newman et al., 2013, 2016) and potential for CH$_4$ from natural geologic seeps (e.g. Peischl et al., 2013).

Deleted: e.g.

Urban and suburban areas in the SCB have high population densities and contain a complex mixture of natural and anthropogenic CO_2 and CH_4 emissions sources. Urban CO_2 emissions can originate from both anthropogenic and biospheric processes. Urban anthropogenic CO_2 sources mainly reflect fossil fuel usage – including combustion of gasoline in cars and combustion of natural gas for electricity production for household use and seasonal cooling and heating – while biospheric CO_2 fluxes include above- and below-ground respiration and photosynthesis (Djuricin et al., 2010; Hutyra et al., 2014; Newman et al., 2013, 2016). CH_4 can be produced via biogenic and thermogenic processes. Biogenic CH_4 is produced as a result of microbial decomposition of organic matter under anaerobic conditions (e.g., due to waste disposal in landfills and wastewater treatment plants), and is also produced via enteric fermentation in the gut of livestock and from manure. Thermogenic CH_4 is derived from natural geologic processes that produce fossil fuels, and therefore is naturally present in fossil fuel deposits including oil fields, and geologic seeps (Etiope and Ciccioli, 2009). Thermogenic CH_4 can also be emitted through intentional venting and fugitive leaks in the extraction, storage, refining, transport, and use of natural gas, as well as from incomplete combustion of fossil fuels.

In the LA Basin, many anthropogenic sources of CO_2 and CH_4 are co-located with each other and with potential natural sources. LA is a major industrial and shipping hub, with a dense network of roads and freeways for transport, the Port of Los Angeles, the Los Angeles International Airport, and also has extensive oil drilling infrastructure, with more than 10 local oil refineries and storage facilities. The LA Basin is also known for its naturally occurring geologic seeps, such as the La Brea Tar Pits. In addition to extensive natural gas pipeline networks, LA also has a variety of other CH_4 sources, including landfills, wastewater treatment plants, fossil fuel extraction and refining, natural gas storage facilities, compressor stations, and vehicle-fueling stations, and dairy agriculture, all of which can result in fugitive emissions (e.g., Hopkins et al., 2016; Peischl et al., 2013; Viatte et al., 2016; Wennberg et al., 2012). The complex mixture of sources and intense human impacts of urbanization complicate CO_2 and CH_4 source attribution in the LA Basin.

Several previous efforts have been made to characterize CO_2 and CH_4 in LA using in situ and remote sensing observations. Some of the earliest published measurements of CO_2 in Los Angeles date back to the 1970s (Newman et al., 2008). Since then, there have been numerous studies investigating atmospheric CO_2 and CH_4 in the LA Basin using in situ observations, including continuous and flask-based sampling from Mt Wilson (MWO; Hsu et al., 2010; Wennberg et al., 2012), Pasadena (CIT) and Palos Verdes Peninsula (PVP; Newman et al., 2008, 2013, 2016), and remote-sensing studies, including ground-based and space-based measurements (Kort et al., 2012; Viatte et al., 2016; Wong et al., 2016, 2015, Wunch et al., 2009, 2016). Periodic intensive field campaigns using aircraft have allowed brief "snap-shot" assessments (days to weeks in duration) of CO_2 and CH_4 levels and emissions in LA, including the campaigns ARCTAS-CA in 2008 (Jacob et al., 2010) and CalNex-LA in 2010 (Brioude et al., 2013; Cui et al., 2015; Peischl et al., 2013; Ryerson et al., 2013), which were major field studies involving collaboration between the California Air Resources Board (ARB) and several partner agencies to improve the accuracy of emissions inventories for greenhouse gases and atmospheric pollutants, as well as a smaller, more recent campaign (Conley et al., 2016).

Moved (insertion) [1]

Deleted: a large variety of anthropogenic CO_2 and CH_4 emissions sources, as well as non-zero CO_2 fluxes expected from the terrestrial biosphere (Feng et al., 2016; Newman et al., 2013, 2016) and potential for CH_4 from natural geologic seeps (e.g. Peischl et al., 2013). Urban areas such as Los Angeles

Deleted: (

Deleted: including

Deleted:),

Deleted: sources

Deleted: photosynthesis and

Deleted: coal beds,

The local enhancement, or the difference between the observed mole fraction at an urban site relative to an inferred “background” mole fraction (referred to in this study as CO$_2$xs and CH$_4$xs), is of particular interest for urban studies. Prior studies have consistently reported large enhancements of CO$_2$ (e.g., 20 ppm to 100 ppm CO$_2$xs at the surface and 2 ppm to 8 ppm XCO$_2$ enhancement in the column averaged dry-air mole fraction) and CH$_4$ (e.g., 10’s to 1000’s of ppb CH$_4$xs at the surface and 0.2 ppb to 50 ppb XCH$_4$xs), with significant temporal variability of the signals (Kort et al., 2012; Newman et al., 2013, 2016; Viatte et al., 2016; Wecht et al., 2014; Wennberg et al., 2012; Wong et al., 2015; Wunch et al., 2009). For CO$_2$, radiocarbon (^{14}C) isotopic tracer measurements have also been made at a limited number of sites in Southern California (Djuricin et al., 2010, 2012, Newman et al., 2013, 2016; Riley et al., 2008). Djuricin et al. (2010) demonstrated that fossil fuel combustion contributed up to 50% to 70% to CO$_2$ sources during winter, while aboveground biological respiration was found to contribute more CO$_2$ than other sources during spring, when fossil fuel contributions were smaller. Recently, Newman et al. (2016) determined that fossil fuel combustion is the dominant source of CO$_2$ for inland Pasadena using three-isotope approach, using ^{14}C along with ^{13}C and ^{18}O stable isotopes, similar to Djuricin et al., (2010). In California, gasoline is approximately 10% ethanol by volume. Ethanol that is derived from biofuel (i.e. from C4 grasses, such as corn) will increase the ratio of atmospheric ^{13}C/^{12}C when gasoline is combusted, adding complexity to the attribution of fossil CO$_2$ emissions (Djuricin et al., 2010; Newman et al., 2016). For CH$_4$, emissions estimates based on top down methods indicate that bottom-up methods systematically underestimate CH$_4$ emissions in the LA megacity by roughly 30% to >100% (Cui et al., 2015; Jeong et al., 2013; Peischl et al., 2013; Wecht et al., 2014; Wennberg et al., 2012; Wong et al., 2016, 2015; Wunch et al., 2009). Recent evidence from stable isotopes of CH$_4$ and light alkanes (e.g., ethane, propane, and butane) suggest that fossil emissions are the predominant source of CH$_4$ (Hopkins et al., 2016; Peischl et al., 2013; Wennberg et al., 2012; Townsend-Small et al., 2012), particularly leakage from natural gas infrastructure and from local fossil CH$_4$ sources.

In contrast to some of these earlier studies, the monitoring network described here provides near-continuous and systematic monitoring of in situ CO$_2$ and CH$_4$ levels (as well as CO, which is not discussed in this work) at multiple sites in the LA metropolitan area. The LA network allows continuous spatial and temporal measurement coverage at multiple sites, spanning multiple years, which can be used in future top-down atmospheric inversion studies. The first part of this study focuses on the sampling strategy and calibration method (Section 2). Next, we estimate hourly average CO$_2$ and CH$_4$ mole fractions (Section 3) and discuss observation-based selection criteria for determining the background CO$_2$ and CH$_4$ mole fractions using data from "extra-urban" sites (Section 4). One important result from this analysis is the near equivalence of continental and marine boundary layer background estimates for this region. We then use a marine background estimate to calculate urban CO$_2$ and CH$_4$ enhancements from the LA surface network during afternoon hours, the typical period of focus for atmospheric flux inversions (Section 5). We also present a framework for estimating detailed time-dependent uncertainties in the enhancement based on the combined uncertainty in the air sample data collected from the measurement system and the background estimate (Section 6). We compare data collected from analyzers in the field and independent data collected at the NOAA/ESRL and Scripps Institution of Oceanography laboratories to estimate measurement uncertainties

Deleted: robust

Deleted: 30

Deleted: –

Deleted: CO$_2$

Deleted: roughly

Deleted: –

Deleted: CH$_4$

Deleted: roughly

Deleted: CH$_4$

Deleted: column averaged dry-air mole fraction

Deleted: -

Deleted: also

and provide suggestions for future accommodation of additional high mole fraction tanks in our network. In addition to providing a foundation for subsequent flux studies for LA, the sampling strategy, calibration methods, and uncertainty calculations described here are intended to provide a blueprint for other surface observation networks in complex cities around the world.

Deleted: be extensible to

2 Methods

2.1 Site selection criteria

The Los Angeles network design strategy began with a preliminary analysis based on a network receptor footprint sensitivity analysis for CO_2 using the wind fields generated with the Weather Research and Forecasting (WRF) model to drive the Stochastic Time-Inverted Lagrangian Transport (STILT) model (Kort et al., 2013) and Vulcan fossil fuel CO_2 emissions (Gurney et al., 2009, 2012). Kort et al. (2013) found that a minimum of eight optimally located in-city surface observation sites were required for accurate monitoring of fossil fuel CO_2 emissions in the LA megacity. Such a network was estimated to distinguish fluxes to within approximately 12 g C m^{-2} d^{-1} (roughly 10% of average peak fossil CO_2 flux in the LA domain) on 8-week time scales and 10 km spatial scales. In general, we do not expect the surface sites to be equally sensitive for CO_2 and CH_4, as the network design was only optimized for detection of fossil-fuel CO_2 emissions (Kort et al., 2013). We initially assessed the logistics of deploying instruments at or near each of the locations specified by Kort et al. (2013). Site evaluation and siting criteria involved one or more of the following steps: (1) visual inspection of maps and satellite imagery to investigate whether suitably tall structures were available and to assess potential impacts of terrain and nearby strong greenhouse gas emission sources; (2) on-site surveys; (3) mobile measurement surveys in the region of interest (Hopkins et al., 2016); and/or (4) short-term deployment of a continuous CRDS analyzer on a short tower (approx. 10 meters) for roughly 1-2 weeks prior to more permanent, fixed installation.

Deleted: , which

Moved (insertion) [3]

Deleted: t

Deleted: o

Where possible, measurement locations were sought on open-lattice communications towers. These structures were favored as they tend to reduce the influence of perturbed airflow from the supporting structure itself and remote locations minimize the influence of nearby emissions (Prasad et al., 2013). In the SCB, access to tall towers (>100 meters above ground level) was limited to the surrounding mountain ranges, which would present unique complexities for modelling and interpretation of the data. Therefore, towers within the Basin were limited to shorter cellular tower sites (<60 m), where available. Although there are a large number of shorter cellular towers in the SCB, these structures were often inaccessible due to permitting or other restrictions. When no tower sites were available in a critical sampling area, we sought secure locations on the rooftops of tall, multi-story buildings in the area of interest. The siting criteria and sampling design framework were based on recommendations from Prasad et al. (2013) and McKain et al. (2015). In cases where rooftop sites were evaluated, Large Eddy Simulations were performed to study the impact of recirculation and nearby structures on the flow field around a building rooftop (Prasad et al., 2013).

2.2 Sampling locations

We established a network of eleven new surface observation sites distributed throughout three counties in the SCB (Figure 1). The geographic coordinates, inlet heights, species measured, and installation dates are summarized in Table 1. The tower sites include: Compton (COM), Granada Hills (GRA), Ontario (ONT), Victorville (VIC), and San Clemente Island (SCI). The building/rooftop sites are all located on university campuses in the following cities: Los Angeles (USC, University of Southern California), Pasadena (CIT, California Institute of Technology), Fullerton (FUL, California State University Fullerton), and Irvine (UCI, University of California, Irvine). The La Jolla site (LJO) is located on Scripps pier, near a flask sampling location that has been discussed previously in the literature (e.g., Graven et al., 2012). The Palos Verdes Peninsula (PVP) and Pasadena (CIT) measurements have been described previously in the literature, but are not discussed in this study (Newman et al., 2013, 2016).

The measurement methods discussed below apply to the eleven new observation sites discussed here. All are equipped with similar instrumentation and use an internally consistent sampling protocol and calibration strategy (see Section 2.3-2.4). The LJO, SCI, VIC, and MWO sites are located outside the SCB boundary and are considered here as “extra-urban” sites, which can be used to estimate background or boundary condition for the SCB (Figure 1). We use an observation-based method to select background mole fractions from “extra-urban” sites, in part due to their remote locations (see Sections 3 and 4 for further discussion).

2.3 Instrumentation

The Los Angeles Megacity greenhouse gas-monitoring network utilizes wavelength-scanned cavity ring-down spectroscopy (CRDS) instruments (Picarro Inc., series G2301 and G2401; Rella et al., 2013; Welp et al., 2013) . All the CRDS instruments measure CO_2, CH_4, and water vapor, while sites with Picarro G2401 instruments also measure CO (Table 1). There are 3 standard configurations for the sites discussed in this study: 1) towers with a single inlet height, 2) towers with multiple inlet heights, and 3) rooftop sites, which follow a 4-corner sampling strategy. Table 1 also indicates the site type, number of air inlets, and approximate heights for the air inlets. Air inlet heights vary from 13 meters (m) above ground level (agl) to 100 m agl for tower sites, and from 20 to 55 m agl for the rooftop sites. Many of the measurement sites discussed in this study were installed, maintained, and/or operated by Earth Networks (EN, Germantown, MD, https://www.earthnetworks.com/).

Deleted: to 100

Deleted: eters

Deleted: m

The gas-handling configuration for the EN greenhouse gas monitoring stations is shown in the Supplemental Materials (Figure S1, adapted from Welp et al., 2013). The Earth Networks Sample Module houses a Valco 8-port low-pressure, dead-end flow path selector with standard bore size of 0.75 mm (VICI, Valco Instruments Co. Inc., http://vici.com/vval/sd.php), housed inside a heated box maintained at 38° C. The selector valve determines the sample type entering the CRDS cell (either outside air or standard/calibration gases).

Deleted: Appendix

Deleted: A

All tower and rooftop sites are equipped with EN meteorological stations (Weatherbug, Inc., http://download.aws.com/manuals/RedBugBoxInstall.pdf), which measure wind speed, wind direction, ambient pressure, ambient temperature, humidity, dew point temperature, and incident solar radiation. Rain gauges are installed below the gas inlets. For tower sites, the wind measurements are co-located with the uppermost air inlet for the in situ greenhouse gas analyzers. For rooftops, the air inlets and wind sensors are installed on the four corners of the building, with masts typically positioned roughly 3 m to 5 m above the roofline and roughly 90 degrees from the walls or edge of the building's rooftop. Co-located meteorological measurements will allow better determination of the sensitivity of rooftop sites to local and regional emissions (i.e., when the winds are stronger or more consistent), relative to potential emissions from the building itself (i.e., when the winds are calm).

Deleted: -5

Deleted: m

Deleted: i.e.

Deleted: i.e.

The EN sample modules used in the LA surface network include a Nafion dryer housed in a thermostatic box (see Figure S1 and description by Welp et al., 2013). The drying system consists of a 183 cm (72-inch)-long Nafion membrane dryer (PermaPure, Inc., model MD-050-72S-1). An MKS640 pressure controller maintains a constant pressure to the Nafion dryer during routine sampling of ambient air and calibration gases (set point roughly 800 mb, 600 Torr). Both sample air and reference gases pass through a Nafion dryer before entering the CRDS cavity (Figure S1). The water vapor concentrations in the sample and standard gases are roughly 0.1±0.01% H_2O after passing through the Nafion dryer. The analyzer pump redirects roughly 30% of the dry gas exiting the Nafion to the outer shell side of the dryer. Welp et al. (2013) provide further discussion on the design, testing, and implementation of this drying inlet system. Both the sample air and reference gases are delivered to the Nafion at the same pressure in order to reduce the drying bias due to permeation through the Nafion during routine operation, based on recommendations from Welp et al. (2013). The CRDS water vapor correction and uncertainty due to the treatment of water vapor are described in more detail in Section 6.

Deleted: A

Deleted: see Appendix,

Deleted: A

Before each analyzer was deployed, the Picarro factory default orifice (O'Keefe A-18-NY) was replaced with a smaller one (O'Keefe A-9-NY) to reduce the flow to about 70 sccm (cm^3/minute at STP). A second critical orifice (O'Keefe A-6-NY) was installed downstream of the Nafion to reduce the counterflow rate to about 30 sccm, and filters were added upstream of the critical orifice to prevent particles from disrupting the flow. A separate small pump (ALITA AL-6SA Air pump) module is installed for each air inlet and delivers a constant stream of sample air at 10 standard liters per minute (sL/min) to the EN sample module. The air inlets consist of 9.525 mm (3/8") Synflex tubing and an air intake filter consisting of either a stainless steel (SS) or titanium wire mesh screen (100 Mesh SS or Monel mesh).

The CRDS analyzers communicate data directly with a Linux mini-computer on-site that receives the data stream through a TCP connection. The site computer runs software (GCWerks, http://www.gcwerks.com), which controls the port sampling sequence in the EN sample module. The software acquires all the high-frequency data points from the CRDS (i.e., roughly 2.5 second time interval), EN sample module, and weather stations at each site, and records extensive engineering data. GCWerks also sends out pre-programmed email alarms so that instrument issues can be diagnosed remotely. All high-

Deleted:

resolution data (Level 0 data) are retained. The GCWerks software then applies some basic automated quality control flags and filters to the Level 0 data (the uncorrected, roughly 2.5 second resolution CRDS reading) and also rejects some data points to create higher-level data products (see Supplementary materials and Table S1).

Deleted: Appendix

Deleted: A1 and

Deleted: A1

2.4 Calibration gases and sampling

Each measurement site is equipped with two natural air standard gas tanks. In the field, Parker Veriflo regulators (p/n: 45100653, Model: 95930S4PV3304) are used to deliver gas from the calibration tanks, and are connected to the Earth Networks sample module via 0.16 cm O.D. (1/16") SS tubing. Field standards are prepared by the National Oceanic and Atmospheric Administration Earth System Research Laboratory (NOAA/ESRL) and/or Scripps Institute of Oceanography (SIO) laboratory and are calibrated relative to World Meteorological Organization (WMO)-scales before and after deployment in the field. The NOAA/ESRL ambient-level standards are natural air tanks filled at Niwot Ridge, Colorado and calibrated against standards on the WMO-scale maintained by NOAA/ESRL (X2007 for CO_2, X2004A for CH_4, http://www.esrl.noaa.gov/gmd/ccl/; (Dlugokencky, 2005; Zhao and Tans, 2006). In addition to the ambient-level calibration and target tanks, the VIC and LJO sites had high mole-fraction standard tanks installed at the time of this study. These high mole fraction tanks were prepared by NOAA/ESRL and calibration assignments were provided prior to deployment (roughly 500 ppm CO_2 and 2600 ppb CH_4). The NOAA/ESRL high mole fraction tanks are prepared by adding a 10% CO_2-in-air mixture to natural air during the pressurization of the cylinder at Niwot Ridge, Colorado (and a similar procedure is used for CH_4). The cylinder is then moved to the NOAA calibration laboratory in Boulder, CO where it is calibrated relative to NOAA/WMO secondary standards. For all standard tanks, we retrieve the most recent tank assignments from the NOAA Central Calibration Laboratory (http://www.esrl.noaa.gov/gmd/ccl/refgas.html). The SIO standards are filled using a similar procedure, except tanks are filled with natural coastal air from Scripps Pier in La Jolla, California, and the tanks are also calibrated against standards on the same WMO-scales. All mole fractions are reported in units of µmol gas per mol dry air (ppm) or nmol gas per mol dry air (ppb). All ambient-level tanks have mole fractions close to clean-air ambient conditions (roughly 400 ppm CO_2 and 1850 ppb CH_4). Our calibration strategy ensures compatibility within the LA surface network, and with other global atmospheric observations tied to the WMO scales.

Deleted: that are calibrated on the World Meteorological Organization (WMO) scales for CO_2 and CH_4

Deleted: Both

Moved (insertion) [4]

Deleted: In addition to the ambient-level calibration and target tanks, the VIC and LJO sites had high mole-fraction standard tanks installed at the time of this study. These tanks were prepared by NOAA/ESRL and calibration assignments were provided prior to deployment (roughly 500 ppm CO_2 and 2600 ppb CH_4).

The current calibration strategy for the LA surface network relies on a single-point calibration, tied to the WMO/NOAA scale. One of the near-ambient tanks is assigned as the calibration standard, and the other tank is a target standard, which is treated as an unknown sample. This calibration method assumes a linear response in the analyzer. This calibration framework has been used extensively for calibration of gas chromatography (GC-MS) instruments in remote monitoring networks, such as the Advanced Global Atmospheric Gases Experiment (ALE/GAGE/AGAGE network, see e.g., Prinn et al., 2001). The details of the calibration gas composition will be discussed in a separate publication.

Deleted: (e.g.

The CRDS analyzer samples each standard tank approximately every 22 hours (i.e., approximately daily). The target tank measurement is staggered roughly 8-12 hours after the calibration gas (as well as the high mole fraction tank, where applicable). All tanks are sampled for 20 minutes. The first 10 minutes of each tank run are rejected and only the data from the last 10 minutes of any are used in the calibration of CO_2 and CH_4 mole fractions to account for the stabilization of air in the CRDS after the inlet is switched (Welp et al., 2013). Variations in the measured target values and deviations from the assigned values are used to track the performance of the analyzer over time and determine uncertainties for the air data (Section 6.1).

The instrument sensitivity (S) is calculated for each standard tank (the calibration tank, the target tank, and the high mole fraction tank) and is determined as the ratio between the uncorrected CRDS reading and the tank's assigned value on the WMO scales ($Xassign_{cal}$):

$$S = X'_{cal} / Xassign_{cal} \qquad (1)$$

where X'_{cal} is the uncorrected CRDS reading (the dry mole fraction of the species of interest, in units ppm or ppb for CO_2 and CH_4, respectively) of the calibration standard. The sensitivity of the calibration tank is used to correct the air sample data, as described below. Sensitivities for the target tank (and high-concentration tank, where available) are also tracked over time, however these tanks are not used in the calibration of the air data.

The CRDS analyzer provides a nominal mole fraction value, which we take as an uncalibrated measurement. We then calibrate the uncorrected dry air sample mole fraction readings from the CRDS analyzer (X'_{air}) using the single point drift-correction method:

$$\begin{aligned} Xcorr &= X'_{air} * (Xassign_{cal} / X'_{cal}) \qquad (2) \\ &= X'_{air} / S \end{aligned}$$

where $Xcorr$ is the calibrated data, X'_{cal} is the dry mole fraction measurement of the calibration tank, and $Xassign_{cal}$ is the assigned value of the calibration standard on the WMO scales (which is constant in time). For each instrument, we interpolate the daily runs of the field calibration gas standard in time to provide a time stamp for X'_{cal} at the time of the air sample measurement. The units of $Xcorr$ are in ppm CO_2 or ppb CH_4.

The sensitivity (S) of the high mole fraction tank is also tracked over time, providing a check on the analyzer stability at higher mole fractions. For the purposes of this study, we treat the high mole-fraction tanks as an unknown target tank and use them to estimate the uncertainty associated with our single-point calibration strategy by calculating the residual of repeated measurement of the high mole fraction tank from its assigned value. In Section 6.1 we discuss the individual components of uncertainty in the air measurements, including the extrapolation uncertainty, which is the uncertainty due to

Deleted: air

Moved up [4]: In addition to the ambient-level calibration and target tanks, the VIC and LJO sites had high mole-fraction standard tanks installed at the time of this study. These tanks were prepared by NOAA/ESRL and calibration assignments were provided prior to deployment (roughly 500 ppm CO_2 and 2600 ppb CH_4).

Deleted: We treat the high mole-fraction tanks as an unknown target tank.

Deleted: We use the high mole fraction tanks at these sites our assumption that S is not dependent on the mole fraction (see Section 6.1.1). In the Supplementary materials, we discuss an "Alternative calibration method" using limited measurements of a high mole fraction tank installed at the LJO and VIC sites in 2016 (see also Figures S2 and S3).

Deleted: Appendix A2… we discuss an "Alternative calibra ... [1]

3 Results

3.1 CO$_2$ and CH$_4$ observations

Figure 2 shows the 1 hour average observations collected from nine sites in the Los Angeles surface network between January 1, 2013 and December 31, 2015. Tables 2 and 3 show the statistics on the CO$_2$ and CH$_4$ mole fractions collected during 2015 based on one hour observations collected during all hours and mid-afternoon hours (i.e., hourly observations collected between 12-16:00 LT or UTC-8, with no local adjustment for daylight savings time). Generally, each site exhibits the expected seasonal cycle for CO$_2$ and CH$_4$, with wintertime maxima and summertime minima. The Downtown LA (USC), Compton (COM), and Fullerton (FUL) sites exhibit the highest average mid-afternoon CO$_2$ mole fractions during 2015 (Table 2). The annual average CO$_2$ mole fraction was 421.6 ppm (USC), 418.6 ppm (FUL), and 418.0 ppm (COM) based on one hour average data collected during mid-afternoon hours in 2015 (Table 2). For CH$_4$, the annual average mole fraction was 2009.9 ppb (USC), 1985.6 ppb (GRA) 1978.2 ppb (FUL) and 1977.2 ppb CH$_4$ (COM), based on data collected during mid-afternoon hours in 2015 (Table 3). While USC exhibits the highest CO$_2$ and CH$_4$ mole fractions on average, CH$_4$ exhibits a somewhat different spatial pattern relative to CO$_2$, with the GRA site showing the second largest CH$_4$ mid-afternoon enhancements.

Deleted: Atmospheric CO$_2$ and CH$_4$ mole fractions can vary on timescales ranging from less than 1 hour, to annual, and inter-annual cycles. …igure 2 shows the 1 hour average observations coll ... [2]

Victorville and San Clemente Island (VIC and SCI) show less variability in CO$_2$ and CH$_4$ mole fractions compared to the other sites within the SCB (Figure 2). During 2015, CO$_2$ mole fractions at SCI ranged from 391.2 ppm to 425.2 ppm CO$_2$, with an average mole fraction of 402.4 ppm CO$_2$ during mid-afternoon hours. Similarly, CH$_4$ mole fractions ranged from 1824.7 ppb to 2231.4 ppb CH$_4$, with an average of 1900.9 ppb CH$_4$ during mid-afternoon hours. At VIC, CO$_2$ mole fractions ranged from 395.9 ppm to 442.6 ppm CO$_2$, with an average of 404.4 ppm CO$_2$, while CH$_4$ mole fractions ranged from 1832.7 ppb to 2105.3 ppb CH$_4$, with an average of 1898.6 ppb CH$_4$ during mid-afternoon. We find that SCI and VIC are the cleanest sites due to their small annual average variability. A third "extra domain" site is located outside the SCB boundary, at La Jolla (LJO). On average, LJO exhibits more variability and higher CO$_2$ and CH$_4$ mole fractions compared to the SCI and VIC sites.

Deleted: in their annual average …n CO$_2$ and CH$_4$ level…c ... [3]

Feng et al. (2016) used a forward modelling framework to explore variability in modelled CO$_2$ mole fractions during the CalNex period (May-June 2010). Their results, based on modelled CO$_2$ pseudo-data, are generally in agreement with the observations from the SCI and VIC sites. Feng et al. (2016) also showed that the IRV site was relatively clean with respect the modelled pseudo-CO$_2$ data. As shown in Figure 2, during spring/summer months, sites such as IRV and LJO typically show less trace gas variability relative to winter months due to more persistent onshore flow. However, during the

Deleted:

The heterogeneous mixture of sources in urban LA complicates sectoral attribution of CO$_2$ and CH$_4$ sources. The variability at each site is likely a reflection of the site's footprint, or its sensitivity to sources in the area. Measurement footprints are typically variable and generally larger during the daytime than at night, and as such footprints are also more difficult to quantify during stable night-time conditions (Djuricin et al., 2010; Turnbull et al., 2015).

rest of the year, the IRV site shows CO_2 and CH_4 mole fractions in the same range as other suburban sites, such as GRA and FUL (Figure 2, Tables 2 and 3). The LJO site is outside the innermost model domain used Feng et al. (2016) and was not discussed as part of that study. Future work should focus on comparing modelled and observed CO_2 and CH_4 mole fractions during different meteorological conditions, but using periods with overlapping model and measurement results from the same time period.

Tables 2 and 3 also show the median and interquartile ranges for the CO_2 and CH_4 observations. At most sites, the data distributions are skewed and have long-tails, where a relatively small fraction of observations exhibit significantly elevated CO_2 and/or CH_4 mole fractions (see also Section 5, where we discuss the long-tail distribution with regards to the enhancement above background). Generally, high concentration spikes can occur at night and in the early morning, when the atmosphere is more stable, and when the site is more sensitive to nearby sources. One example is the suburban GRA site, which shows many high concentration CH_4 spikes since data collection began in 2013 (Figure 2, right panels, note scale difference on the y-axis). Many of the CH_4 spikes throughout the GRA record occur at night, suggesting contributions from a nearby source. Shallower PBL heights at night will lead to higher trace gas enhancements and higher sensitivity to local surface emissions (e.g., Djuricin et al., 2010; Turnbull et al., 2015).

In addition to emissions, it has been demonstrated previously that meteorology plays an important role in controlling the variability of trace gas observations within the planetary boundary layer (PBL) (e.g., Feng et al., 2016; Newman et al., 2013; Xueref-Remy et al., 2016). Diurnal variations in trace gases are driven in part by changes in the height of the PBL. A stable PBL prevents surface emissions from mixing with the atmosphere above. Given a constant flux, and assuming that transport in and out of the boundary layer remains approximately constant, the trace gas mole fraction observed within the PBL will increase or decrease as the PBL height falls or rises, respectively. Newman et al. (2013) demonstrated this for CO_2 using observations from Pasadena, CA (the CIT-1 site in Table 1). The LA surface observations from mid-afternoon hours show less variance in the within-hour CO_2 and CH_4 values and a smaller inter-quartile range relative to all hours (Table 2). The reduced variability in the CO_2 and CH_4 observations during mid-afternoon hours is in part due to the larger height of the PBL during the mid/late afternoon. Rahn and Mitchell (2016) evaluated Aircraft Meteorological Data Relay (AMDAR) automated weather reports from three major international airports in Southern California (LA, Ontario, and San Diego) between 2001 and 2014. Overall, they found that PBL depth observations from LA (in the western LA Basin) showed the least variability (smallest interquartile range) during the hours just before sunset (~21:00 UTC to 03:00 UTC) indicating a fairly regular range of boundary layer height at this time (Rahn and Mitchell, 2016). CO_2 and CH_4 observations are also more likely to be sensitive to local sources when the PBL is shallow and the atmosphere is less well mixed (and at low wind speeds). The PBL height may also vary with season. Southern California is characterized by a well-defined boundary layer during the spring and summer months due to strong temperature inversions associated with large-scale subsidence. During the autumn and winter, the large-scale subsidence is less prominent and the presence of a weak temperature inversion (or one that extends down to near the surface) makes it more difficult to identify a

Deleted: The heterogeneous mixture of sources in urban LA sectoral attribution of CO_2 and CH_4 sources. The variability at each site is likely a reflection of the site's footprint, or its sensitivity to sources in the area. Measurement footprints are typically variable and generally larger during the daytime than at night, and as such footprints are also more difficult to quantify during stable night-time conditions (Djuricin et al., 2010; Turnbull et al., 2015).

Deleted: , respectively

Deleted: level

Deleted: that the other measurement sites are not sensitive to

Moved up [3]: In general, we do not expect the surface sites to be equally sensitive to CO_2 and CH_4, as the network design was only optimized for detection of fossil-fuel CO_2 emissions (Kort et al., 2013).

Deleted: Resolving the fine-scale structure of CO_2 and CH_4 emissions at the sectoral level will likely require footprint analysis and additional tracer measurements, which are planned as part of future work

Deleted: CO_2 (and CH_4)

Deleted: e.g.

Moved down [2]: Newman et al. (2013) demonstrated this for CO_2 using observations from the CIT site.

Deleted: Therefore, g

Deleted: CO_2 and CH_4

Moved (insertion) [2]

Deleted: the CIT site

Deleted: O

Deleted: day

Deleted: midday

Deleted: stability of the PBL depth

Deleted: stability of the

boundary layer (Rahn and Mitchell 2016). As part of future work, we plan to evaluate the diurnal and seasonal variability in the CO_2 and CH_4 signals with PBL depth measurements from a Mini Micropulse Lidar (MiniMPL) instrument located in Pasadena near the CIT measurement sites (Ware et al., 2016).

Wind speed is also an important factor controlling variability in observed trace gas mole fractions, as has been demonstrated previously for CO_2 (e.g., Newman et al., 2013; Xueref-Remy et al., 2016). This is also related to the measurement footprint, as discussed earlier. For example, at low wind speeds, observations within the PBL are more likely to reflect sources and sinks in close proximity to the site (with distances of roughly 10 km or less), while at higher wind speeds, the observation site will become more sensitive to transported emissions from more distant sources (d ~ 10 km to 100 km), while the influences from nearby sources will appear more diluted. We do not go into further detail on the impacts of meteorology on the CO_2 and CH_4 signals as part of this analysis. Future work will explore the impacts of meteorology and PBL height on the CO_2 and CH_4 (and CO) signals observed by the network using footprint analysis, and weather reanalysis products.

There are three potential signals of interest for urban and regional greenhouse gas studies. All may be potentially relevant for utilizing greenhouse gas measurements in local or regional inverse modelling studies: (1) diurnal changes in the measured mole fraction at one location over a 24-hour period; (2) gradients in the measured mole fraction between locations; and (3) the local enhancement, which is the difference between an observed mole fraction at one location and a defined background mole fraction and is referred to here as CO_2xs and CH_4xs (see below). In the remainder of this paper, we focus on the third type of signal discussed above, the enhancement above background.

3.2 Calculating CO_2 and CH_4 enhancements

The enhancement relative to the background mole fraction can be useful for evaluating local additions of CO_2 and CH_4 from urban regions. We define the enhancement or excess signal (X_{XS}) as follows:

$$X_{XS} = X_{OBS} - X_{BG} \qquad (3)$$

where X_{OBS} is the calibrated CO_2 or CH_4 mole fraction at the site of interest, and X_{BG} is the background mole fraction (i.e., the mole fraction from an air mass entering the domain or region of interest), all with units of ppm CO_2 or ppb CH_4.

4 Estimating background mole fractions

A critical goal for the LA Megacity Carbon Project is to identify an optimized background measurement location (or locations). Prior studies in the LA region have used either a coastal marine boundary layer background derived from observations from La Jolla, CA (LJO, 32.87°N; 117.25°W, 0 m asl; Graven et al., 2012), or Palos Verdes Peninsula (PVP, 33.74 °N; 118.35°W, 116 m asl; Newman et al., 2013, 2016), or a continental, free-troposphere background based on night-

Deleted: mini

Deleted: m

Deleted: lidar

Deleted: installed near the location

Deleted: of the

Deleted: CO_2 (and CH_4)

Deleted: e.g.

Deleted: -

Deleted: (referred to here as ΔCO_2 and ΔCH_4)

Deleted: n

Deleted: ΔX

Deleted: $\Delta X = X_{obs} - X_{bg}$

Deleted: X_{OBS}

Deleted: mixing ratio

Deleted: X_{BG}

time flask measurements from the mountaintop site at Mt Wilson, CA in the San Gabriel mountains bordering the northern edge of the LA Basin (MWO, 34.22°N; 118.06°W, 1670 m asl; Figure 1). Prior studies attempting to constrain CH_4 emissions in California have also estimated background mole fractions along their model domain boundary using particle trajectory endpoints from WRF-STILT footprint simulations as a look-up for a latitudinally averaged, 3-D marine boundary layer (MBL) "curtain" product (Jeong et al., 2012, 2013; Zhao et al., 2009).

Deleted: mixing ratios

Evaluating the composition of a background air mass depends in part on the application. For example, in forward and inverse modelling studies, the location and scale of the domain of interest will determine the background requirements. A model that is used to estimate the enhancement due to local emissions should account for influences from sources both within and outside the domain of interest, as well as recirculation effects (i.e., when air exits the domain and returns a short while later). There is obviously no single background that is representative for all cases. There may also be cases when a single background site is not appropriate for estimating enhancements throughout the Basin. Out-of-domain sites may help resolve within-domain emissions under some conditions, however the appropriate background site will also depend on the prevailing meteorological conditions. For Los Angeles, if the prevailing wind is from the land (offshore), then a continental background may be most appropriate, whereas if the wind is from the western coastal boundary (onshore), then a marine background may be most appropriate. Out-of-domain influences can also lead to spatial gradients that are independent of within-domain emissions, and will be more difficult to discern or characterize. In such cases, within domain sites may occasionally be useful for characterizing background conditions.

In this study, the domain of interest is defined by the South Coast Air Basin boundary (Figure 1). The sites most suitable for characterizing background (or upwind) conditions are SCI, LJO, VIC, and MWO, which are all located outside this SCB domain. Overall, SCI, VIC, and LJO are most similar to the mole fractions of the remote MBL in terms of their annual average CO_2 and CH_4 mole fractions (Table 2). LJO is a coastal, suburban site in La Jolla, CA (as described above); SCI is an offshore island site located on San Clemente Island, CA, just southwest of LA (32.92°N; 118.49°W, 480 m asl). VIC is a rural, desert site located outside the city of Victorville, CA (34.61°N; 117.29°W, 1370 m asl); and MWO is a mountaintop site, as described above. LJO and SCI are potentially useful for characterizing the Pacific marine boundary layer background values; VIC for characterizing a continental background; and MWO for characterizing a continental, mid-tropospheric background. At best, background conditions may only be observed intermittently from any of these sites because each site can also be influenced by local and within-domain emissions under certain meteorological conditions. In Section 4.1, we use an observation-based method to select background observations at the LJO, SCI, VIC, and MWO sites and in Section 4.2 we compare these estimates. In Section 4.3, we discuss some air mass back trajectories and the implications for background estimates for the LJO, SCI, VIC, and MWO sites.

4.1 Background methods

Estimating greenhouse gas enhancements at the local scale requires measurements that resolve variability in background air masses (e.g., Graven et al., 2012; Turnbull et al., 2015). In the literature, several methods have been demonstrated for identifying background observations, including applying statistical filters to look for periods with stable measurements, filtering for meteorological conditions and/or chemical parameters, or using modelled and/or reanalysis products in combination with observations to estimate gradients (e.g., Alden et al., 2016; Ruckstuhl et al., 2012; Thoning et al., 1989). Methods relying on chemical filtering techniques involve monitoring multiple species to identify pollution events or to inform about the sensitivity of a site to local pollution, while methods relying on meteorological filters assume some prior knowledge about the transport of polluted air masses to the site.

In this study, we used a data selection approach based on simple statistical filtering criteria, where the stability of the observed CO_2 and CH_4 mole fractions is used as an indicator of background air. Using this approach, we aim to estimate a local continental and marine background that can be used to estimate CO_2 and CH_4 enhancements in Los Angeles with relatively low-latency (i.e., with reduced delays such that near-real time atmospheric monitoring of the enhancement signal will be possible). Our data selection approach relies on several criteria: (1) a small degree of variability within a one hour period, and 2) small hour-to-hour variability, and (3) persistence of the first two conditions for several hours. Based on these criteria, we exclude observations that are impacted by local emissions or recirculation effects at the continuous observation sites. This data filtering approach does not rely on the availability of any other observations (i.e., winds, boundary layer height, etc.). In this sense, we consider this background selection algorithm to be operational in that it can be used to estimate background mole fractions in real time or near-real time.

LJO and SCI "Marine" Background and VIC "Continental" Background Estimates: The LJO, SCI, and VIC air observations were filtered according to statistical criteria based on the variability in the hourly average data (see Supplementary materials). As shown in Figure 3, the CO_2 and CH_4 observations from SCI exhibit much less variability compared to VIC and LJO. Figure S4 shows histograms of the hourly standard deviations for the SCI, VIC, and LJO observations. As discussed earlier, the variability in the LJO record is more like an urban/suburban site than a background site. This is primarily due to along-shore transport from the north and the proximity to other local sources (including a large landfill immediately to the east). After applying the selection criteria respective to each site, the CCGCRV curve fitting software was used to estimate a "smooth curve" fit to the selected observations (Thoning et al., 1989; http://www.esrl.noaa.gov/gmd/ccgg/mbl/crvfit/crvfit.html). The curve-fitting parameters are described further in the Supplementary materials. The full time series, selected data and "smooth curve" results are shown in Figure 3 and the final smooth curve results for each site are shown in Figure 4 (panels *a-b*). We discuss the uncertainty in the smooth curve estimates in Section 6.2 (see also, Figure S10).

Deleted: steady

Deleted: are

Deleted: 1

Deleted: should be able to

Deleted: very

Deleted: –

Deleted: the same criteria.

Deleted: Our data filtering criteria loosely follow the preliminary selection criteria discussed by Thoning et al. (1989) and were as follows: (1) Check for stability of the CO_2 and CH_4 observations within 1-hour and only retain measurements if the 1-hour SD is <0.3 ppm CO_2 and <5 ppb CH_4; (2) Check for large hour-to-hour changes in CO_2 concentration and retain measurements if the hour-to-hour difference is less than 0.25 ppm CO_2 (no hour-to-hour criteria were used for CH_4); (3) Retain only those observations with six or more consecutive hours that meet criteria 1 and 2.

Deleted: remaining

Field Code Changed

Deleted: given

Deleted: Appendix A3

Deleted: top

MWO "Continental, Mid-Troposphere" Background Estimate: Mt. Wilson (MWO) is a mountaintop observatory overlooking the South Coast Air Basin, approximately 1670 m asl (Figure 1). At night, the PBL is shallow and the MWO site is more likely to be influenced by air from the free-troposphere. During the daytime, the MWO CO$_2$ and CH$_4$ mole fractions can be influenced by emissions from the Basin either due to upslope winds or due to the rising of the PBL above MWO. Calibrated continuous in situ observations from MWO were not available at the time of this study. Instead, we used the MWO night-time flask record from NOAA/ESRL to produce a smooth curve background estimate using a similar approach to that described above for the SCI, LJO, and VIC sites. Flask samples have been collected at MWO approximately every 3-4 days since 2010. Only flask samples collected between 23:00 and 05:00 hours LST (local standard time) were used in the smooth curve fit because only night-time samples are likely to be representative of background conditions. The curve fitting parameters are described in the Supplementary materials. The final smooth curve results are shown in Figure 4 (panels *a-b*).

Pacific Marine Boundary Layer (MBL) Background: The Pacific MBL reference surface was developed using weekly flask air samples from the NOAA's Global Greenhouse Gas Reference Network (GGGRN, see http://www.esrl.noaa.gov/gmd/ccgg/mbl/ and Masarie and Tans, 1995). The MBL reference surface is a data product smoothed in time and over latitude that uses NOAA measurements from samples that are predominantly influenced by well-mixed MBL air (typically remote, marine sea level locations with prevailing onshore winds). The Pacific MBL product provides a 2-D (latitude and time) representation of CO$_2$ and CH$_4$ mole fractions along the Pacific boundary of North America based on the subset of GGGRN MBL sites in the Pacific Basin. We compare the results from SCI, LJO, VIC, and MWO to the Pacific MBL reference surface in Figure 4.

We note that the method used to estimate background would fail to give a measure of influences from outside the domain under some conditions. Below we compare the background estimates described above (Section 4.2) and discuss some meteorological considerations for background estimation (Section 4.3).

4.2 Comparison of background estimates

We compared the background estimates derived from the SCI, LJO, VIC, and MWO sites from January 2014 to June 2016 with the 2-D Pacific marine boundary layer (MBL) reference from 33.4°, 36.9°, and 40.5° N (Figure 4, panels *a-b*). There are small but systematic differences in the background estimates determined for each site. Next, we subtracted each background reference curve and the Pacific MBL background estimate from 33.4° N (Figure 4, panels *c-d*). For CO$_2$, the background estimates from SCI and LJO are both more similar to the Pacific MBL estimate from 33.4° N and show a more pronounced CO$_2$ minima in the summer compared to the MWO and VIC background estimates. The average absolute difference between the Pacific MBL estimate at 33.4° N and each background estimate from SCI, LJO, VIC, and MWO for the period shown in Figure 4 is: 0.8, 0.7, 1.7 and 1.5 ppm CO$_2$, and 8.0, 8.9, 10.1, and 13.7 ppb CH$_4$, respectively. For CH$_4$ the background curve from SCI is most similar to the Pacific MBL estimate. The average absolute differences between the

Deleted: g

Deleted: Mt Wilson

Deleted: given in Appendix A3

Deleted: top

Deleted: mixing ratios

Deleted: during

Deleted: -2015

Deleted: roughly

Deleted: curves

Deleted: For CO$_2$, the seasonal cycle at SCI and LJO is more similar to the Pacific MBL estimates than the MWO and VIC results. The SCI and LJO background estimates show more pronounced CO$_2$ minima in the summer relative to , similar to the MBL estimate from 33.4° N. This suggest that under the appropriate filtering criteria, LJO and SCI observations can be used to derive a marine background estimate for CO$_2$. During summer months, the background derived from VIC and MWO are differ from the MBL estimates by up t

Deleted: Overall, the differences from the Pacific MBL estimate from 40.5° N range from -20 and +60 ppb CH$_4$ during summer months and ±30 ppb CH$_4$ during all other months. he SCI and LJO background estimates are more similar to the Pacific MBL background during almost all times of year compared to VIC and MWO. For SCI, the differences from the Pacific MBL estimate ranging from -31 to +2 ppb CH$_4$ during summer and from -35 to +10 ppb CH$_4$ during the rest of the year. During summer 2015, the CH$_4$ background derived from LJO is very different from the other marine background estimate. A landfill near the LJO site could influence the observations at this site. This hypothesis could be confirmed using footprint analysis. Further refinement of the data selection algorithm could also provide better agreement between the CH$_4$ background estimates.

... [4]

background estimates from SCI and LJO and the Pacific MBL estimate from 33.4° N are <1 ppm CO_2 and <10 ppb CH_4, suggesting that both sites are useful for deriving marine background estimates for CO_2 and CH_4 when the appropriate filtering criteria are used. The cause of the larger differences between the continental (i.e., VIC and MWO) and marine (i.e., SCI, LJO, and Pacific MBL) background estimates is not clear. Future modelling studies could investigate whether a time-dependent background selection method – e.g., based meteorological information and the origin of incoming air mass – can be used to determine the appropriate background site under some of the more common meteorological regimes in the SCB. In Section 4.3 we discuss some additional considerations regarding atmospheric transport. In Section 5 we estimate CO_2 and CH_4 enhancements using the SCI background estimate and in Section 6.2, we assess the uncertainty in the SCI background estimates relative to the enhancements near Downtown LA.

4.3 Back-trajectory analysis

Our approach for estimating background mole fractions thus far has ignored variations in atmospheric transport. In reality, winds transport air masses in and through the SCB on various timescales. Therefore, the optimal background site for selecting observations could vary diurnally, weekly, monthly, and/or seasonally. Wind back trajectories can be useful for selecting a primary background site, based on the prevailing winds. We performed a simple back trajectory analysis and below discuss some preliminary conclusions based on that analysis. Results in Figure 5 are shown for 14:00 LST (local standard time), however, in general, the back trajectories computed for 12:00 and 16:00 LST show similar results.

We computed twenty-four hour back trajectories for winds arriving at the CIT site in Pasadena at 14:00 LST using NOAA's HYSPLIT model (Figure 5; Stein et al., 2015; Rolph, 2016). During the warmer months (spring/summer, or roughly May through September), winds enter the Basin almost exclusively on-shore, originating over the ocean. These air masses generally travel south along the coast before being directed inland. Conversely, during the cooler months (fall/winter months, roughly November to March), there is much more variety in the provenance of the air masses (Figure 5). During November to March, a significant fraction of days have off-shore winds (i.e., from the north to northeast, and originating from the Mojave desert region over the mountains), which could indicate Santa Ana conditions, a typical mode of variability in the Los Angeles climatology (e.g., Conil and Hall, 2006). During off-shore wind conditions, coastal sites such as La Jolla or San Clemente Island may not be relevant choices for selecting background observations as these sites may be subject to outflow and recirculation of an air mass from over land. Coastal ("Catalina") eddies are also a common occurrence along the CA bight, which is the mostly convex part of the Southern California coastline (Figures 1 and 5). Conditions that favor coastal eddies are most common between April and September, though they develop at almost any time of the year (Rahn and Mitchell, 2016). During such conditions, a site northwest of the Los Angeles Basin may be a more relevant choice for background. However, as shown in Section 4.3, the MBL background derived using the SCI and LJO sites was very similar to the Pacific MBL reference curves between ~33° N and 40° N.

At least some of the differences in our background estimates from the LA sites can be explained by differences in

Deleted: median difference between the Pacific MBL estimate from 40.5° N and the other background estimate from SCI, LJO, VIC, and MWOare: , 0., and ppm CO_2 and -3.5, , , and ppb CH_4.

Deleted: As shown below in Sections 5 and 6, this is ~15-1% of the median enhancement and ~10-13% of the median CH_4 enhancement at the USC and FUL sites

Deleted: LA Basin

Deleted: A

Deleted: i.e.

Deleted: or could have

Deleted: -like

Deleted: which are

Deleted: for

Deleted: area during November to March

Deleted: e.g.

Deleted: we

Deleted: ed

Deleted: or

Deleted: surface

Deleted: roughly

Deleted: -

the prevailing meteorological conditions and a lag in the transport of air masses between the sites. The VIC and MWO sites show larger differences from the marine background estimates during summer months for both CO_2 and CH_4. During summer months, the marine CO_2 background estimates (from SCI, LJO, and the MBL estimates) all show a more pronounced CO_2 minima in the summer compared to the MWO and VIC background estimates. This is consistent with the back-trajectory analysis in Figure 5, which shows that onshore flow conditions are more persistent from May to September. Overall, the CO_2 background estimates from VIC and MWO are most similar to one another. The total inlet elevation at VIC (1370 m asl + 100 m agl inlet height) is only about 200 m lower than at MWO (1670 m asl), suggesting these two sites may be sensitive to similar air masses under some meteorological conditions. Overall, the VIC and MWO sites may not be relevant choices for background during summer, when onshore flow patterns dominate. Conversely, SCI and LJO may not be relevant choices for background when flow is from the continent. In future studies, background data could also be selected based on the prevailing flow patterns in the region of interest (e.g., McKain et al., 2015).

Our back-trajectory analysis does not have the temporal resolution necessary to evaluate diurnal land-sea breezes. The spatial resolution of the NAM12 meteorological data used by HYSPLIT is 12 km. From this analysis, we can certainly see seasonal variations of the wind direction and the incoming air masses for the LA basin. We do not compare the day/night differences in meteorology, such as land/sea breezes, in our analysis, though we note that these circulation patterns could be important for understanding the greenhouse gas variability (especially at coastal sites such as SCI, LJO, and possibly IRV). Such analysis would require a higher resolution model, such as the 1.3 km resolution WRF-Chem model discussed by Feng et al. (2016), which is beyond the scope of this study. Feng et al. (2016) found that sea breeze prevailed over the LA megacity at ~14:00 LST during the May/June 2010 (CalNex) study. Furthermore, the modelled topography of the Palos Verdes Peninsula was found to divide the sea breeze into west and southwest onshore flows that later converged in the Central Basin. In general, transport models do not do well overnight (Feng et al., 2016), which makes evaluation of diurnal variations challenging using modelled CO_2 or CH_4 output. Future modelling studies that overlap with the CO_2 and CH_4 records will be needed to evaluate the impact of land/sea-breezes on CO_2 and CH_4 observations from coastal sites and could also improve our understanding of the impacts winds induced by topography on the greenhouse gas observations.

Feng et al. (2016) used results from a forward model simulation to explore correlations in CO_2 concentrations in a model framework. They showed that CO_2 is trapped and accumulates due to the mountain barrier, leading to CO_2 enhancements at in-basin sites relative to the desert site at VIC. Feng et al. also found that while the modelled CO_2 levels at the VIC desert site were mainly anti-correlated with the LA Basin sites, CO_2 that accumulated in the Basin could occasionally be pushed over the mountains and into the desert due to episodic strong sea breezes and onshore flow conditions. This supports our conclusions that VIC and MWO (night-time) observations may not always provide representative background mole fractions, particularly during summer months when onshore flow conditions prevail. It is important to note that our approach for evaluating background mole fractions from MWO relied on night-time flask

Deleted: For VIC, there is virtually no CO_2 or CH_4 data meeting the selection criteria during the summer and early fall months (Figure 3). The

Deleted: back trajectory

Deleted: ed

Deleted: we

Deleted: consis

Deleted: tent

Deleted: roughly

Deleted: , d

Deleted: uring the same period when our background algorithm failed to find VIC observations meeting the stability criteria (Figures 3 and 4). The VIC inlet elevation (1370 m asl 100 m agl inlet height) is only roughly 200 m lower than MWO (1670 m asl). T

Formatted: Subscript

Deleted: smooth curve

Deleted: is

Deleted: to that of MWO,

Deleted: suggesting these two sites may be sensitive to similar air masses.

Deleted: T

Deleted: refore, we conclude that the

Deleted: back trajectory

Deleted: (

observations only, which were collected between 23:00 and 05:00 hours LST. Feng et al. refer to MWO as a "western basin" site, exhibiting spatial CO_2 correlations similar to the GRA, CIT, USC, and COM sites. Feng et al. (2016), but do not discuss day/night differences in the sensitivity of the MWO site. At night, when the PBL is shallower, there is reduced likelihood for air from the SCB to be transported to the MWO site. In the future, continuous observations from MWO should be analyzed in conjunction with the night-time flask record to evaluate diurnal variability in CO_2 and CH_4. While the simulations discussed by Feng et al., (2016) only cover a brief period during spring/summer 2010, future modelling studies over longer periods (e.g., one year) could improve our understanding of variations in the mesoscale circulation in the LA megacity and the impacts on the observed CO_2 and CH_4 mole fractions. The variety and complexity of meteorology in the South Coast Air Basin suggests that a more sophisticated background selection algorithm is needed to determine the site that is "upwind" during different prevailing wind conditions. Future model analyses could also help determine when our observation sites are most relevant for estimating background.

Deleted: we expect
Deleted: to be
Deleted: ing
Deleted: the
Deleted: that
Deleted: will
Deleted: work
Deleted: we plan to analyze
Deleted: from MWO
Deleted: the
Deleted: observations at this site

Overall, the LJO and SCI background estimates establish a marine sector background to within roughly 1 ppm CO_2 and 10 ppb CH_4 (excluding the period during summer 2015 discussed above). SCI is the most representative of local marine background conditions for both CO_2 and CH_4 throughout the year. The LJO background curve also helps confirm that the background estimate from SCI is reasonable. Therefore, we use SCI as the background reference site to calculate CO_2 and CH_4 enhancements for the LA surface sites (see Section 5).

Deleted: below

5 CO_2 and CH_4 enhancements

We calculated the average enhancement at each site using the SCI marine background reference. Moderate to large CO_2 and CH_4 enhancements (CO_2xs and CH_4xs) are observed above the background mole fractions. Tables 4 and 5 show statistics regarding the enhancement at each site estimated for all hours and mid-afternoon hours (12:00-16:00 LT, not including adjustment for daylight savings time) during 2015. Figure 6 shows the annual average CO_2xs and CH_4xs values at 9 sites for observations collected during all hours and mid-afternoon hours during 2015, with sites arranged by latitude. Overall, the results show that the CO_2 and CH_4 enhancements in LA are characterized by a large degree of spatial and temporal variability (Figures 2 and 6). During mid-afternoon hours – the period of the day that is most relevant for flux inversions – the median enhancement in 2015 was 13.9, 12.3 10.3, 10.4, 5.9 ppm CO_2xs and 82, 58.3, 52, 69, and 40.6 ppb CH_4xs at the USC, FUL, COM, GRA and IRV sites, respectively (Figure 6 and Table 5). During 2015, largest mid-afternoon median CO_2 were observed at the USC and FUL sites and the largest CH_4 enhancements were observed at the USC and GRA sites. We do not discuss the results from the Ontario site (ONT) in detail because measurements were only available from Sept-Dec 2015 and therefore are not representative of the annual average.

Deleted: Δ
Deleted: Δ
Deleted: day
Deleted: Δ
Deleted: Δ
Deleted: day

In general, the CO_2 and CH_4 enhancements are larger in winter relative to spring and summer months (Figure 2). Anthropogenic (fossil) CO_2 sources dominate in winter months due to increased emissions from the residential and electric

Deleted: of both gases are more pronounced
Deleted: Prior studies have shown
Deleted: that a

production sectors (Wong et al., 2015). Increased summertime insolation is expected to produce a deeper afternoon mixed layer depth in summer relative to winter, which in turn would result in larger trace gas enhancements within the PBL during winter relative to summer. As discussed earlier, Ware *et al.* (2016) used backscatter data from a MiniMPL instrument located in Pasadena, CA to estimate mixing heights over two years from 2012-2014. They found the mean afternoon maximum mixing depth was 770 m agl in summer (June and August) and 670 m agl in winter (December–February). However, seasonal differences in mixing depth should also be considered in the context of the daily and weekly variability. Ware *et al*. (2016) show that the maximum depth of the afternoon mixing layer may differ by a factor of 2 from day-to-day. Additionally, Ware *et al.* show that the within-season S.D. for the afternoon maximum mixing height is about 220 m, or approximately 30% of the mean afternoon maximum mixing depth in either summer or winter (which is larger than the observed average seasonal differences in mixing height). Overall, the large variability in mixing layer depth over different timescales suggests that the meteorological impacts on trace gas concentrations in the PBL can also be quite variable.

On average, the more urbanized areas, such as the USC site near Downtown LA, exhibit larger median CO$_2$xs values during 2015 (Figure 6 and Table 4). CH$_4$ shows a slightly different spatial distribution in the median enhancement relative to CO$_2$, with the second largest CH$_4$ enhancements observed at the GRA site, which is a suburban site located in the San Fernando Valley. CO$_2$xs and CH$_4$xs exhibit long-tail distributions, a reason we report the median and interquartile range in Tables 4 and 5 in addition to the other statistics. As mentioned earlier, relatively large CH$_4$ excursions, on the order of 4 ppm above background or more, are observed throughout the GRA time series (Figure 2). The GRA site also exhibits a long-tail distribution with respect to the CH$_4$ enhancements, which is more pronounced compared to the other sites, even during mid-afternoon hours (see Supplemental materials, Figure S11, which shows data outside the interquartile range). Many of the larger enhancements occur during night-time/early morning hours. The smaller enhancements during mid-afternoon hours relative to night suggest that GRA may be sensitive to a local CH$_4$ source at night, when the PBL becomes shallower and could be more stratified (Figures 2 and 6 and Tables 2–5). The long-tail distribution for CH$_4$ in Los Angeles and the prevalence of fugitive CH$_4$ emissions across the LA urban landscape was previously demonstrated by Hopkins et al. (2016), using extensive mobile surveys. Hopkins et al. (2016) identified 75% of methane hotspots to be of fossil origin, while 20% were biogenic, and of 5% of indeterminate source using the ratio of ethane to methane (C$_2$H$_6$/CH$_4$). They also found that fossil fuel sources accounted for 58% to 65% of methane emissions and suggested that there are widely distributed methane sources, primarily of fossil origin, that are not included in bottom-up inventories. In future work, detailed analysis of winds, measurement footprints, and tracer/tracer analyses will be used to evaluate the origin of the anomalous CH$_4$ enhancements.

Deleted: Δ

Deleted: and ΔCH$_4$

Deleted: s

Deleted: and 5

Deleted: ... [5]

Deleted: enhancements also

Deleted: day

Deleted: m

Deleted: 6

Deleted: the outliers

Deleted: in addition to

Deleted: median and

Deleted: midday

6 Uncertainty in the CO_2 and CH_4 enhancements (U_{excess})

Both measurement uncertainty and imperfect knowledge of the composition of background air limit the precision of observation-based estimates of local- or regional-scale greenhouse gas enhancements (e.g., Graven et al., 2009; 2012a; 2012b; Turnbull et al., 2009; 2015). We estimate the uncertainty in the enhancement as follows:

$$(U_{excess})^2 = (U_{air})^2 + (U_{BG})^2 \quad (4)$$

where U_{excess} is the total uncertainty in the enhancement of CO_2 or CH_4 and is defined as the quadrature sum of the uncertainty in the air measurement (U_{air}) and the uncertainty in the background mole fraction (U_{BG}). We note that U_{BG} is not statistically independent of U_{air} because U_{BG} is derived from measured values. In the remainder of this study, we explore the measurement uncertainty in our approach and calibration strategy (U_{air}) using data from the LJO site (Section 6.1) and the uncertainty in the background mole fraction using the marine reference background from SCI (Section 6.2).

6.1 Measurement uncertainty analysis (U_{air})

We model the uncertainty in the air measurements following the general methods outlined in Andrews et al. (2014), using the quadrature sum of multiple uncertainty components:

$$(U_{air})^2 = (U_{extrap})^2 + (U_{h20})^2 + (U_M)^2 \quad (5)$$

where

$$U_M = U_{TGT} \quad (6)$$

or

$$(U_M)^2 = (U_p)^2 + (U_b)^2 + (U_{scale})^2 \quad (7)$$

(whichever is greater).

Equation 5 describes U_{air}, the total uncertainty in the reported air mole fractions, and its individual components, which have units in mole fraction CO_2 or CH_4 (ppm or ppb). In Eq. 5, U_{extrap} is the extrapolation uncertainty, or the uncertainty introduced because the measured mole fraction of the air sample differs from the value of the calibration standard (Section 6.1.1), and U_{h2o} is uncertainty from the treatment of water vapor (Section 6.1.2). In Eqs. 6-7, U_M is the greater of two terms, defined by either U_{TGT} the uncertainty determined by the target tank measurements or the quadrature sum of several terms: U_p, the analyzer precision (Section 6.1.4), U_b, the analyzer calibration baseline uncertainty (6.1.5), and U_{scale} the scale reproducibility (Section 6.1.6). In Eq. 6, U_{TGT} is equivalent to a Root Mean Square Error (RMSE), and is

Deleted: $U_{Enhancement}$

Deleted: $(U_{Enhancement})^2 = (U_{air})^2 + (U_{BG})^2$

Deleted: $U_{Enhancement}$

Deleted: proportional to

Deleted: U_{air}

Deleted: U_{BG}

Deleted: U_{BG}

Deleted: U_{air}

Deleted: U_{BG}

Deleted: U_{air}

Deleted: $(U_{air})^2 = (u_{extrap})^2 + (u_{h2o})^2 + (u_M)^2$

Deleted: $u_M = u_{TGT}$

Deleted: $(u_M)^2 = (u_p)^2 + (u_b)^2 + (u_{scale})^2$

Deleted: U_{air}

Deleted: u_{extrap}

Deleted: u_{h2o}

Deleted: u_M

Deleted: u_{TGT}

Deleted: u_p

Deleted: u_b

Deleted: u_{scale}

Deleted: u_{TGT}

estimated using the corrected target tank residual over 10 days, similar to Andrews et al. (Section 6.1.3).

Overall, Eqs. 5 to 7 describe a generic algorithm that can be applied to other analyzers, as well as for CO measurements. Time-dependent monitoring of U_b, U_p and U_{TGT} is useful when tracking analyzer performance. Although the overall measurement uncertainty is typically small, an increase in any of these values (U_b, U_p and U_{TGT}) may indicate problems with a specific analyzer. Thus, this system could be used to generate alerts for the data user to identify periods when an analyzer is performing poorly or to indicate periods when the measurements may not be useful for atmospheric inverse modelling studies.

Deleted: u_b, u_p

Deleted: u_{TGT}

Deleted: u

Deleted: $_b$, u_p and u_{TGT}

6.1.1 Extrapolation uncertainty (U_{extrap})

Deleted: u_{extrap}

We corrected the air measurements in Figure 2 using a single-point calibration method. As a result, any air measurement that is different from the value of the calibration standard is subject to an extrapolation uncertainty, U_{extrap}, which is the uncertainty introduced because the measured mole fraction of the air sample differs from (and in many cases is larger than) the value of the calibration standard (around 400 ppm CO_2 and 1850 ppb CH_4). We estimate U_{extrap} as follows:

Deleted: one

Deleted: u_{extrap}

Deleted: u

$$U_{extrap} = |\varepsilon| * |X_{corr} - X_{assign_{cal}}| \qquad (8)$$

Deleted: $u_{extrap} = |\varepsilon| \times |Xcorr - Xassign_{cal}|$

where ε (described below) has units of ppm/ppm or ppb/ppb and is multiplied by the absolute value of the difference between the sampled air concentration and the assigned calibration tank value ($|X_{corr} - X_{assign_{cal}}|$). We estimate this uncertainty as a linear function of $|X_{corr} - X_{assign_{cal}}|$ based on calibration analysis of multiple similar model CDRS units in the laboratory that show a linear relationship in the error (discussed further below and shown in Figures S5 and S6).

Deleted: and

Deleted: $|Xcorr - Xassign_{cal}|$

Our approach relies on independent estimates of ε, the slope parameter, to determine the magnitude of the systematic and random components of the error in our calibration method. Ideally, initial estimates of ε would be determined empirically via testing each analyzer in a laboratory prior to deployment in the field to provide estimates of the magnitude of the extrapolation uncertainty (e.g., Andrews et al., 2014; Richardson et al., 2012). At the time of this study, it was not possible to test many of the CRDS analyzers in a laboratory prior to deployment in the field because high mole fraction standards spanning the range of CO_2 and CH_4 measurements expected in LA were not available.

Deleted: error due to the single-point calibration method

Since a suite of calibration standards was not available at the time of this study, we determined ε using the average "correction" slope determined from analysis of a series of standard tanks at different mole fraction tanks on a suite of CRDS analyzers. Within the LA network, only the LJO and VIC analyzers had field calibration data from high mole fraction tanks available at the time of this study. We used the limited measurements of these high mole fraction tanks (approximately 500 ppm CO_2 and 2600 ppb CH_4) to compute an average ε over the period when the tank was available. We also investigated laboratory calibration data from the seven additional Picarro CRDS model G2401 and G2401-m analyzers, as described

Deleted: a

Deleted: high mole fraction

below. These analyzers are not part of the network, but are similar to the CRDS analyzers used in the field in the LA network.

Calibration analyses for the seven independent analyzers were performed at NOAA/ESRL during 2014 to 2015 with between 3 and 7 reference tanks calibrated on the WMO scales for each gas (up to approximately 470 ppm CO_2 and 3060 ppb CH_4). A single standard tank (the tank with a CO_2 value closest to 400 ppm) was set as the calibration standard ($X_{assign_{cal}}$) and was used to correct the CRDS reading for the other standard gases using Eq. 2. Next, we plotted the residual of the corrected mole fraction for each tank measurement and its assigned value ($X_{corr} - X_{assign}$) as a function of the difference in the assigned mole fraction between a given tank and the calibration tank ($X_{assign_{span}} - X_{assign_{cal}}$). The slope of this relationship is equivalent to ε for a given analyzer. Estimates of the correction factor, ε, and regression statistics for these seven analyzers are summarized in Tables S2 and S3 and the data are shown in Figures S5 and S6 (see Supplemental materials).

The values of the slope correction (ε) are 0.0027 and 0.0018 ppm/ppm for CO_2 and 0.0012 and 0.0060 ppb/ppb for CH_4, for the LJO and VIC analyzers respectively. These results are compared with the other analyzers in Table S2. For CH_4, all analyzers show a clear linear relationship between the error and the mole fraction of the tank, and there is very little difference in the slope between different analyzer units (see Supplementary materials, Figure S6). Interestingly, for CO_2, we find that the two older analyzers (CFKBDS-2007 and -2008) have larger slopes, while the majority of the analyzers have very little dependence on the mole fraction and have errors close to zero (see Figure S5). The results in Table S2 are used to estimate the magnitude of the error in the corrected air sample mole fractions caused by assuming a constant analyzer sensitivity, or slope correction. The average value of ε from all 9 analyzers was used in Eq. 8 to estimate the uncertainty in this correction (U_{extrap}). The slope from these calibration experiments (ε) gives an estimate of the error in the single point calibration and how it increases when the measurement is farther from the value of the single calibration point. Overall, U_{extrap} is proportional to the fractional difference between the mole fraction of the air sample and that of the ambient-level calibration tank. The average and standard deviation of ε also provide estimates of the systematic and random components of the error in the single-point calibration method (Table S3).

We also estimated the error associated with the single-point calibration strategy using Eq. 8 and various estimates of ε for 3 cases: (1) the average and standard deviation of ε from all 9 analyzers, (2) the average ε from 7 analyzers (excluding LJO and VIC), and (3) an instrument specific estimate of ε from the LJO site (Table 5). Next, we estimated the error assuming an hourly average air measurement of 500 ppm CO_2 and 6000 ppb CH_4 (i.e., roughly 100 ppm CO_2 and 4000 ppb CH_4 enhancement above the "near ambient" calibration standard). Finally, we corrected air data from the LJO and VIC sites using an "Alternate Calibration Method," during times when a limited number of measurements of a high mole-fraction CO_2 and/or CH_4 standard were available for analysis (see Supplementary materials, Figures S2 and S3). Overall, the difference

Deleted: $Xassign_{cal}$

Deleted: $Xcorr - Xassign$

Deleted: $Xassign_{span} - Xassign_{cal}$

Deleted: 6

Deleted: 7

Deleted: (the data are shown in the Supplemental materials,

Deleted: 1

Deleted: 2

Deleted: 6

Deleted: materials

Deleted: 2

Deleted: 1

Deleted: 6

Deleted: an extrapolation to our single-point calibration and

Deleted: u_{extrap}

Deleted: u

Deleted: $_{extrap}$

Deleted: 7

Deleted: Appendix

Deleted: A

Deleted: A

between the single-point (default) calibration method and the "Alternate Calibration Method" are <0.2 ppm CO_2 and <5 ppb CH_4 for the majority of air measurements. We also estimated the maximum correction using both approaches (the "Alternate Calibration Method" and a correction and error based on U_{extrap}), and the results are summarized in Table S2.

Deleted: u_{extrap}

Deleted: 6

While the initial results are very promising, and the corrections tend to be small, there is a large degree of variability in the estimates of *ε* for individual analyzers. The value of *ε* can be different for different analyzers and can also change over time for a single analyzer (Table S2 and S3 and Figures S5 and S6). Based on the experiments discussed here, our current calibration strategy could be modified to correct the concentration data using the mean value of *ε* found from all the analyzers and estimating an uncertainty in that correction. However, our approach for estimating *ε* is based on relatively small statistical sample of analyzers. Furthermore, the two estimates we do have from the LJO and VIC field sites only rely on one additional calibration point other than the calibration tank, making it difficult to estimate a robust fit for these analyzers. An estimate of *ε* for each analyzer in the field (or from a larger statistical sample of analyzers) is needed to provide a robust estimate of the mean *ε* to correct the air sample data. Values of *ε* could also be estimated for the analyzers deployed in the field, for example, by deploying a suite of calibration standards with varying concentrations of CO_2 and CH_4 (e.g., a round-robin). We have chosen not to correct the data and keep it tied to the single-point calibration until more experimental evidence can be obtained. In the future, the surface network will move to a 2-point calibration strategy. This will rely on the availability of high-mole fraction tanks for deployment in the field, and a calibration uncertainty that is lower than our current estimates for U_{extrap}.

Deleted: s 6

Deleted: 7

Deleted: 1

Deleted: 2

Deleted: e.g.

Deleted: uncertainty

Deleted: u_{extrap}

6.1.2 Uncertainty associated with water vapor (U_{h2o})

Deleted: u_{h2o}

The presence of water vapor in the sample air contributes to the uncertainty in the CRDS measurements. Below we describe three potential sources of uncertainty in the measurements due to water vapor: 1) the coefficients used to determine the water vapor correction, which can vary from instrument to instrument, 2) bias due to imperfect drying, and 3) random noise in the H_2O measurement reported by the CRDS analyzer, which ultimately gets incorporated in the water vapor correction (Rella et al., 2013).

The Picarro CRDS analyzers use a factory default water vapor correction model that relies on the parameters derived by Chen et al. (2010):

$$\frac{CO_{2_{wet}}}{CO_{2_{dry}}} = 1 + aH_{rep} + bH_{rep}^2 \qquad (9)$$

$$\frac{CH_{4_{wet}}}{CH_{4_{dry}}} = 1 + cH_{rep} + dH_{rep}^2 \qquad (10)$$

where H_{rep} is the water vapor mole fraction reported by the analyzer, $(CO_2)_{wet}$ and $(CH_4)_{wet}$ are the uncorrected CRDS, wet-

Deleted: mixing ratio

gas mole fractions reported by the analyzer, $(CO_2)_{dry}$ and $(CH_4)_{dry}$ are the dry-gas mole fractions, while a, b, c, and d are experimentally determined parameters (where a = -0.012000, b = -0.0002674, c = -0.00982, and d = -0.000239). This correction is currently being applied to the analyzers in the LA network. Users are free to design and perform their own experiments and derive parameters specific to each instrument (Nara et al., 2012; Rella et al., 2013; Welp et al., 2013). However, while an instrument specific correction of water vapor could potentially lead to reduced uncertainty, prior laboratory studies have also found that the benefits of an instrument specific correction are small at low water vapor levels (Nara et al., 2012; Rella et al., 2013).

The Nafion drying system described in Section 2.3 and by Welp et al. (2013) allows us to stabilize the water vapor concentrations in the sample gas stream (H_{rep} in Eqs. 9-10) to 0.1±0.01%. With this drying system, the uncertainty in the water vapor correction drops to 0.015 ppm for CO_2 and 0.21 ppb for CH_4 when using the factory parameters described above (Rella et al., 2013; Welp et al., 2013).

The use of a Nafion dryer could also potentially introduce a bias due to imperfect drying. A slight permeation of CO_2 and CH_4 can occur across the membrane, especially when the Nafion membrane is wet (e.g., Ma and Skou, 2007; Welp et al., 2013). In our measurement setup, running the dry standard gases through the Nafion dryer significantly reduces this bias effect. The water vapor concentration from the dry standard gas runs is similar to that of the preceding air measurements. We find that the water vapor mole fraction in the air measurements after a standard is run drops by 0.01% (from 0.10% to 0.09%). A similar effect has been described by Rella et al. (2013). We estimate the Nafion bias in our system based on this 0.01% variability in water vapor to be -0.011 ppm for CO_2 and 0.00028 ppb for CH_4 based on laboratory experiments performed at the SIO laboratories with the same Nafion drying system used in the field. Details about the laboratory experiments are available in the Supplementary materials (Figure S7).

Deleted: see

Deleted: 3

A final source of uncertainty regarding water vapor correction comes from the variability of the water vapor measurement on the CRDS analyzers. We estimate this to be 0.014 ppm for CO_2 and 0.069 ppb for CH_4 at the water vapor concentrations of our measurements (Rella et al., 2013; Welp et al., 2013).

The total uncertainty due to water vapor (U_{h2o}) is the quadrature sum of the water vapor correction uncertainty, the Nafion-induced bias due to changes in water vapor, and the variability (noise) of the water vapor measurements. Therefore, we estimate U_{h2o} is 0.0233 ppm for CO_2 and 0.221 ppb for CH_4 across the network and it is assumed to be constant at all times.

Deleted: u_{h2o}

Deleted: u_{h2o}

6.1.3 Uncertainty derived from target tank measurements (U_{TGT})

We define U_{TGT} in Eq. 6, where the target tank is treated as an unknown and the measured value is compared to the tank assignment to calculate the root mean square error (RMSE):

Deleted: u

Deleted: $_{TGT}$

Deleted: u_{TGT}

$$U_{TGT} = \sqrt{(Xcorr_{TGT} - Xassign_{TGT})^2} \qquad (11)$$

where, $Xcorr_{TGT}$ is the corrected target tank measurements and $Xassign_{TGT}$ is the assigned value of the target tank by the calibration laboratory (NOAA/ESRL or SIO). The assigned values are constant over the lifetime of the cylinder and are determined based on laboratory measurements traceable to the WMO scales. Errors in the tank assignments are typically small and would result in a bias in the measurement, rather than a random error (see Section 6.1.6). To calculate $Xcorr_{TGT}$, the uncorrected CRDS target tank concentration readings are treated as an unknown sample and are corrected using Eq. 2. For each target tank measurement, U_{TGT} is calculated as the RMSE (Eq. 11) over 11 target measurements centered on the measurement time (this is usually a 10-day period). Then, this time-dependent U_{TGT} is interpolated in time onto all the air measurements. Overall, U_{TGT} includes errors in the assigned value of the calibration tank and the target tank, and also encompasses other errors (e.g., the instrument precision and the calibration standard baseline uncertainty), as well as additional and possibly unknown errors due to delivery of air to the analyzer downstream of the Valco valve. Drift in either the calibration or target cylinders will also manifest as an increasing U_{TGT}. In this way, U_{TGT} is useful as a diagnostic of instrument performance.

6.1.4 Analyzer precision (U_p)

The analyzer precision (U_p) is defined as the standard deviation of the 10-minute daily calibration standard tank measurement:

$$U_p = \sigma_{cal} \qquad (12)$$

where σ_{cal} is the standard deviation of the uncorrected CRDS, dry mole fraction measurements for the calibration tank at roughly 2.5-second resolution. Our definition of U_p is different from that described by Andrews et al., (2014), where the analyzer precision was defined as the standard error of the calibration measurements. To use the standard error, we must assume statistical independence of the measurements and estimate a maximum value for N, the number of samples in the average that reduce the uncertainty.

We performed an Allan deviation analysis to estimate stability of the Picarro CRDS analyzer due to noise processes. The Allan deviation is the square root of the Allan variance (Allan, 1966, 1987) and was plotted as a function of averaging time for calibration runs at the LJO site during January 2016 (Figure S8). During this month, the calibration tank was run 28 times through the CRDS analyzer for 30 minutes at each time (10 minutes longer than the normal calibration run period, for quality check purposes). We omitted the first 10 minutes of data and performed the Allan deviation analysis on the next 20 minutes of data for each of the 28 calibration runs. We found that the instrument variability does not decrease with averaging as would be expected (with a slope of -1/2) for a white noise profile, indicating correlation in the noise at various longer time scales. In other words, the deviation (noise) therefore does not decrease as the inverse square root of the

Deleted: u

Deleted: $\overline{(Xcorr_{TGT} - Xassign_{TGT})^2}$

Deleted: $Xassign_{TGT}$

Deleted: u_{TGT}

Deleted: u_{TGT}

Deleted: u_{TGT} is equivalent to a RMSE and

Deleted: e.g.

Deleted: $_{TGT}$

Deleted: $_{TGT}$

Deleted: u

Deleted: $_p$

Deleted: u_p

Deleted: σ_{cal}

Deleted: u

Deleted: $_p$

Deleted: 4

averaging time ($\sqrt{N}$), as it would for white noise. Filges et al. (2015) found a comparable result using similar CRDS units. Figure S8 shows the Allan deviation analysis for a subset of six (for figure clarity) of these calibration runs over the course of the month, also indicating that the characteristics of the noise in the analyzer may vary. The deviation does decrease with averaging time, but not in a consistent manner. Therefore, we have chosen not to compute the standard error in the mean by dividing the standard deviation by the square root of the number of measurements, because the characteristics of the noise in the analyzer vary with time and the data does not fit the criterion of the measurements being truly independent. We therefore quantify the precision of the analyzers as the 2.5-second standard deviation independent of averaging time, recognizing that it is likely an overestimate of the analyzer precision. This uncertainty for CO_2 and CH_4 is small compared to other sources, so we chose to retain it, and in the future (or for other species, such as CO), the precision could be modelled in a more robust manner.

6.1.5 Calibration baseline uncertainty (U_b)

To estimate the calibration baseline uncertainty (U_b) we follow a process similar to that described by Andrews et al. (2014). First, we calculate three different possible time series of the calibration tank measurement (X') to estimate S (in this case, the instrument sensitivity measured for the calibration tank). The first is an interpolation onto air data using every calibration run. The second and third time series use alternate sampling of the calibration tank time series (i.e., by either odd or even sampling of every other daily calibration run) to interpolate X' onto the time series of the air sample data (Figure S9). Next, we calculate the dry air mole fraction corrected at each point using each of these three different time series. The maximum uncertainty, $U_{b_{max}}$ is estimated as the standard deviation of the three corrected mole fractions (black solid line, Figure S9). The actual baseline uncertainty, U_b, is equal to this maximum value ($U_{b_{max}}$) at the halfway point in time between subsequent calibration runs, and goes to zero at the time of a calibration run, since that that time the calibration value is known exactly. Thus, U_b is equal to $U_{b_{max}}$ weighted by the time difference between an air sample measurement and the adjacent calibration run (dashed line, Figure S9).

6.1.6 Uncertainty in calibration tank assignments (U_{scale})

Absolute scale accuracy includes uncertainties in the values assigned to the primary calibration standards, as well as scale propagation errors (Andrews et al., 2014). Here we report an expanded uncertainty (95% C.L., approximately 2σ): 0.20 ppm at 400 ppm CO_2 (WMO X2007 scale) and 3.5 ppb at 1850 ppb CH_4 (WMO X2004A scale), where the total uncertainty is a relatively small function of the measured mole fraction. However, in our case, all measurements are calibrated relative to the same (WMO) scale, so scale reproducibility is the relevant metric for assessing measurement compatibility over time and between sites. Similar to Andrews et al. (2014), the reported scale reproducibility is 0.06 ppm for CO_2, and 1.0 ppb for CH_4 (2σ) (*B. Hall, personal communication*). We use the 1σ scale reproducibility (U_{scale}) in the calculation of U_{air} (0.03 ppm CO_2, and 0.31 ppb CH_4)

Deleted: 4

Deleted: considering that

Deleted: we will model

Deleted: u_b

Deleted: u_b

Deleted: $_{cal}$

Deleted: (S_{cal})

Deleted: see

Deleted: u_{bmax}

Deleted: u_b

Deleted: u_{bmax}

Deleted: u_b

Deleted: u_{bmax}

Deleted: u_{scale}

Deleted: U_{air}

Deleted: ppm CO_2

Cylinder drift has not been discussed and could also impact the measurement uncertainty. Andrews et al. (2014) report a mean difference between pre- and post-deployment tank calibrations of CO_2 and CH_4 for tanks prepared by the NOAA/ESRL laboratories. CO_2 has rarely been observed to drift in cylinders. Andrews et al. (2014) report a mean difference between pre- and post-deployment tank calibrations of 0.02±0.05 ppm CO_2 (post- minus pre-deployment from 177 tanks analyzed over approximately 10 years). CH_4 standards are generally very stable and field calibration residuals reported for CH_4 had not indicated any drift in the tanks (for CH_4 absolute stability is reported as 0±0.1 ppb yr^{-1} (Dlugokencky, 2005; Dlugokencky et al., 1994). CH_4 standards were generally stable, (Andrews et al., 2014; Dlugokencky, 2005). At the time of this study, none of our field calibration cylinders for the LA surface network had final calibrations; however routine field measurements of standard tanks to date do not indicate significant drift in either gas.

6.2 Uncertainty in the background estimates

We define the time-varying uncertainty in the background estimate as follows:

$$U_{BG} = \bar{X}_{RMSE} \qquad (13)$$

where $\bar{X}_{RMSE}$ is the absolute value of the monthly average residual of the selected background observations (red points, Figure 3) from the smooth curve result. Due to the method used to filter the observations, there are some gaps in the background observations. The background reference curves interpolate over observation gaps, however, the portions of the curve that are not constrained by observations are more uncertain relative to other periods. For data gaps longer than one month, it is not possible to estimate $\bar{X}_{RMSE}$. Since there are no observations to constrain the curve, we assign an interpolation uncertainty based on the maximum annual average residual. In other words, if there are long observation gaps, the interpolation uncertainty will default to the maximum residual based on periods when observations were available. The time-varying uncertainty estimates for the SCI, VIC, and LJO reference curves are shown in Figure S10. During 2015, the annual average uncertainty in the SCI smooth curve estimate is 1.4 ppm CO_2 and 11.9 ppb CH_4 (Table 6). This amounts to roughly 10% and 15% of the median mid-afternoon enhancement near Downtown LA (i.e., at the USC site) for CO_2 and CH_4, respectively.

6.3 Comparison of uncertainty estimates

Figure 7 shows the time-dependent measurement uncertainty estimates for the LJO site and Table 6 gives the average values for each uncertainty term during 2015. We assigned fixed values for U_{scale} (0.03 ppm CO_2 and 0.31 ppb CH_4) and U_{h2o} (0.0233 ppm CO_2, 0.221 ppb CH_4). Overall, U_{h2o} and U_{scale} are small components of U_{air}, the overall measurement uncertainty. We do not have time dependent estimates of all the uncertainty terms used in calculating U_{air} for every analyzer.

Deleted: this component of

Deleted: , while CH_4 standards are very stable

Deleted: **due to**

Deleted: We used the standard deviation of the fit residuals to define an uncertainty in the background mole fraction as follo ... [6]

Deleted: reference

Deleted: curve fit, U_{BG}

Deleted: analytical

Deleted: during 2015

Deleted: 7

Deleted: u_{scale}

Deleted: u_{h2o}

Deleted: u_{h2o}

Deleted: u_{scale}

Deleted: U_{air}

Deleted: U_{air}

Under normal operating conditions, the calibration baseline uncertainty (U_b) and the analyzer precision (U_p), are also negligible. The average U_b is 0.0042 ppm and 0.054 ppb for CO_2 and CH_4 respectively, with no significant outliers (based on the average for 11 analyzers deployed in the field). Similarly, U_p is a very small component of the overall uncertainty. Similarly, the values for analyzer precision across the network are similar to those derived from the LJO analyzer under normal operating conditions (roughly 0.024 ppm CO_2, 0.22 ppb CH_4 for the 20-minute average air observations, and 0.011 ppm CO_2 and 0.12 ppb CH_4 for the 1-minute average air observations). Both U_b and U_p can become non-negligible components of the uncertainty if there are problems with either the CRDS analyzer, or the delivery of calibration gas to the analyzer. For example, the standard deviation of some calibration runs may be higher than the values reported for the LJO analyzer suggest, either because of analyzer noise increasing due to hardware or software problems, analyzer drift during a calibration run, or because a limited number of calibration measurements were available to calculate an average due to analyzer problems. Therefore, the values derived from the LJO analysis represent the minimum quantities we expect for U_p, which is representative of the precision from a well-performing analyzer.

Deleted: u_b

Deleted: u_p

Deleted: u_b

Deleted: *u*

Deleted: $_p$

Deleted: *u*

Deleted: $_b$

Deleted: *u*

Deleted: $_p$

Overall, U_{extrap} provides an estimate of the uncertainty due to the single-point calibration method, which is the largest component of uncertainty in the air measurements (Figure 7 and Table S3). We find that U_{extrap} is linearly dependent on the difference between the mole fraction of the air sample and that of the ambient-level calibration tank, at least over the range of mole fractions tested (see Supplementary materials, Figures S5 and S6). As described earlier, we do not have instrument-specific estimates of ε for every analyzer to use in estimating U_{extrap}. Therefore, we assumed constant values for ε based on the average of the 9 analyzers shown in Table S2. During 2015, the average U_{extrap} value estimated for the LJO analyzer is 0.047 ppm CO_2 and 0.46 ppb CH_4. The magnitude of U_{extrap} is larger for air data with higher mole fractions, and scales as a percentage of the difference in the mole fraction of the air sample above the assigned value of the calibration tank. On average, the uncertainty due to U_{extrap} results in an uncertainty in the enhancement on the order of 0.0025 ppm/ppm (0.25%, or 0.25 ppm for a 100 ppm enhancement) for CO_2 and 0.003 ppb/ppb (0.3% or 0.30 ppb for a 100 ppb enhancement) for CH_4. Based on analysis of the LJO data during 2015, the average value of U_{air} is 0.070 ppm CO_2 and 0.72 ppb CH_4 (Table 6).   Overall, these experiments show that the single-point calibration introduces rather small errors in the final mole fraction assignments for CO_2 or CH_4, and especially relative to the enhancement above background (Figure 7 and Tables 4–5).

Deleted: u_{extrap}

Deleted: 7

Deleted: u_{extrap}

Deleted: 1

Deleted: 2

Deleted: u_{extrap}

Deleted: 6

Deleted: u_{extrap}

Deleted: u_{extrap}

Deleted: u_{extrap}

Deleted: U_{air}

Deleted: 8

Deleted: 8

We used Eq. 4 to estimate the uncertainty in the enhancement signal using the estimates of U_{air} and U_{BG} for the LJO analyzer and the SCI background estimate, respectively. Since U_{air} is time varying, the uncertainty in the enhancement is also time-dependent. On average, uncertainty in the enhancement is roughly 1.1 ppm and 11.7 ppb, for CO_2 and CH_4, respectively for the LJO air data. Overall, the uncertainty due to the assumptions about the background condition is the largest component of the error in the enhancement. However, on an annual average basis, the total uncertainty is generally

Deleted: U_{air}

Deleted: U_{BG}

Deleted: U_{air}

less than roughly 5 and 15% of the enhancement in downtown LA for CO_2 and CH_4, respectively.

7 Summary and Conclusions

Concerns about rising greenhouse gas levels have motivated many nations to begin monitoring or mitigating emissions, motivating the need for robust, consistent, traceable greenhouse gas observation methods in complex urban domains. Observations from organized urban greenhouse gas monitoring networks such as the LA surface network are emerging elsewhere (e.g., Shusterman et al., 2016; Turnbull et al., 2015; Xueref-Remy et al., 2016). To date, most of these research efforts have been largely disconnected. More information flow between existing urban observational networks and the science and applications communities is needed to understand greenhouse gas emissions from cities. Data and methods for greenhouse gas monitoring in urban regions should be fully disclosed and documented with a small degree of latency to make the best use of these atmospheric data for emissions verification and/or for informing policies more generally.

In this study, we describe the instrumentation and calibration methods used for the Los Angeles Megacity surface network. The measurement and sample module system described here provide robust, near-continuous and unattended measurement of CO_2 and CH_4 at urban and suburban monitoring stations in the South Coast Air Basin. A total of eleven analyzers have been deployed thus far, and most have been operational for more than 1.5 yrs. We reported the sampling configuration, algorithms to compute calibrated CO_2 and CH_4 mole fractions, and methods for estimating the local enhancement above background and uncertainties.

We presented an observation-based method for estimating background mole fractions using measurements from four remote, “extra-domain” sites. Our approach to background determination is useful for exploring variability in the enhancement signals. Relative to the enhancements observed at most sites, there is near equivalence of continental and MBL background estimates, except during summer months, when continental sites may not be relevant for estimating background due to prevailing on-shore flow conditions in the LA Basin. One strength of our observation-based strategy for background determination is the relatively short latency with which background observations can be evaluated (hours to days). This will be important as greenhouse gas research networks such as the LA network transition from research networks into monitoring networks and will allow near real-time estimation of local greenhouse gas enhancements. The stability criteria discussed here could also be used to identify periods that are optimal for flux inversion. For example, it may not be useful to select background observations when influences from outside the domain cause large gradients or fluctuations within the domain. Similarly, periods that are impacted by recirculation effects are not ideal for identifying background and thus are also not useful for estimating fluxes, and the measurement stability criteria may also be useful for identifying such periods.

Deleted: marine boundary layer

Deleted: conditions

Deleted: basin

We calculated CO_2 and CH_4 enhancements in the LA megacity from during 2015 using a marine background estimate. An urban site near Downtown LA has a median enhancement of roughly 20 ppm CO_2 and 150 ppb CH_4 during all hours, and roughly 15 ppm CO_2 and 80 ppb CH_4 during mid-afternoon hours (12-16:00 LT, local time), which is the typical

Deleted: midday

Deleted: roughly

period of focus for flux inversions. "Suburban" sites show moderate, but slightly smaller enhancements, with median values of 5 ppm to 10 ppm CO_2 and 30 ppb to 70 ppb CH_4 during mid-afternoon hours. Overall, the largest CO_2 and CH_4 enhancements were observed at the USC site near Downtown Los Angeles.

We also described the components of the analytical uncertainty that we believe to be most important for urban studies. The uncertainty in the enhancement was estimated using both the uncertainty in the air sample data collected form the measurement system and the uncertainty in the background mole fraction. The algorithm discussed here can also help determine periods when uncertainties in the observations are small and are therefore most useful for atmospheric inversion studies. The acceptable threshold for the measurement uncertainty depends in part on the question of interest, and how large the signal is relative to a local background.

Our analysis shows that the uncertainty in the single-point calibration method (U_{extrap}) is the largest component of the measurement uncertainty. Overall, U_{extrap}, the uncertainty in the single-point calibration strategy, scales as a function of the enhancement in the air data (roughly 0.3% of the enhancement for both CO_2 and CH_4). Based on our error analysis, U_{extrap} depends on the response, or sensitivity, of the individual analyzer, which is time varying. Our assessment of U_{extrap} could be further improved with more estimates of the correction factor (ε) from a larger statistical sample of analyzers. Currently, our ability to fully evaluate the magnitude of the correction to the air data is limited by the availability of high concentration standards in the field. In the near future, the LA measurement network will begin using analyzer specific estimates of the correction factor based on periodic measurements with high mole fraction tanks, which will allow correction of the random and systematic components of the uncertainty associated with the single-point calibration strategy.

While measurement uncertainty is important for estimating gradients between sites, accurate background determination and uncertainties in atmospheric transport will likely be more important for estimating urban enhancements and using observations in flux inversions. Overall, the uncertainty associated with background is larger than the analytical uncertainty. We find that a local marine background can be established to within ~1 ppm CO_2 and ~10 ppb CH_4 using local measurement sites. Overall, the background uncertainty is ~10% and ~15% of the mid-afternoon enhancement near Downtown LA for CO_2 and CH_4, respectively, based on the marine background estimate from SCI. However, both the analytical and background uncertainty are likely to be much smaller than the uncertainty due to atmospheric transport, a topic that we have only discussed briefly to provide context for the observations presented in this study. Our results suggest that reducing the uncertainty to less than 5% of the enhancement will require detailed assessment of the impact of meteorology on background conditions over a range of conditions (e.g., following Feng et al., 2016). Future modelling efforts for the LA Megacity Carbon Project may require equivalent attention to meteorological validation, as has been demonstrated here for the greenhouse gas observations, due to uncertainties in atmospheric transport.

Top down flux inversions relying on in situ greenhouse gas observations require accurate determination of urban enhancements relative to a local background. We calculated an expected atmospheric signal of Los Angeles carbon

Deleted: roughly and roughly

Deleted: -

Deleted: -

Deleted: midday

Deleted: in part

Deleted: (i.e. the enhancement)

Deleted: u_{extrap}

Deleted: u_{extrap}

Deleted: u_{extrap}

Deleted: u_{extrap}

Deleted: ; h

Deleted: "

Deleted: "

emissions assuming emissions are distributed evenly over the roughly 17,100 km^2 are of the South Coast Air Basin (SCB), an average wind speed of 2 m/s (based on annual average wind speed observed at the USC observation site) equivalent to a transit time of ~18 h), an average mixed layer depth of 1 km (Rahn and Mitchell, 2016; Ware et al., 2016) and estimated emissions, (Pacala et al., 2011). Estimated annual emissions of 144 Tg CO_2 y^{-1} would raise CO_2 mole fractions by roughly 10 ppm (based on Hestia-LA 2012, see e.g., Gurney et al., 2012, 2015). Assuming 0.4 Tg CH_4 y^{-1} annual emissions in the SCB based on a top-down study, CH_4 mole fractions would be enhanced by roughly 75 ppb (Wong et al., 2015). This is consistent with the mid-afternoon enhancements observed over downtown LA during 2015 (Figure 6 and Tables 4–5), and those reported in prior studies (Newman et al., 2013, 2016; Wong et al., 2015).

In the future, urban greenhouse gas monitoring networks such as the LA surface network could also be used to understand episodic sources or disturbance events such as fires, gas leaks, etc., which are difficult to capture with bottom-up approaches. This will also require background estimation in near real-time. Co-monitoring of tracers (e.g., CO_2 and CO enhancements, calibrated with ^{14}C measurements) is also planned as part of future work and will allow continuous or near-continuous estimation of fossil carbon signals in Los Angeles (Miller et al., 2015). Establishing greenhouse gas enhancements and emissions trends over a period of several years could help assist in determining the effectiveness of local control measures and mitigation strategies. As part of future work, forward and inverse modelling studies and tracer-tracer analyses should be used in conjunction with the calibrated CO_2 and CH_4 observations from the LA surface network to estimate fluxes, determine spatial and temporal emissions trends, and attribute those fluxes to specific sectors and/or sources.

Deleted: an annual emissions estimate of

Deleted: ese

Deleted: estimates ar

Deleted: e

Deleted: midday

Deleted: previously

Deleted: we plan to use

Deleted: presented here

Deleted: greenhouse gas emissions

Deleted: to

References

Alden, C. B., Miller, J. B., Gatti, L. V, Gloor, M. M., Guan, K., Michalak, A. M., van der Laan-Luijkx, I. T., Touma, D., Andrews, A., Basso, L. S., Correia, C. S. C., Domingues, L. G., Joiner, J., Krol, M. C., Lyapustin, A. I., Peters, W., Shiga, Y. P., Thoning, K., van der Velde, I. R., van Leeuwen, T. T., Yadav, V. and Diffenbaugh, N. S.: Regional atmospheric CO2 inversion reveals seasonal and geographic differences in Amazon net biome exchange, Glob. Chang. Biol., 3427–3443, doi:10.1111/gcb.13305, 2016.

Allan, D. W.: Statistics of Atomic Frequency Standards, Proc. IEEE, 54(2), 221–230, doi:10.1109/PROC.1966.4634, 1966.

Allan, D. W.: Time and frequency (time-domain) characterization estimation and prediction of precision clocks and oscillators, IEEE Trans. Ultrason. Ferroelectr., 34(6), 647–654, 1987.

Andrews, A. E., Kofler, J. D., Trudeau, M. E., Williams, J. C., Neff, D. H., Masarie, K. A., Chao, D. Y., Kitzis, D. R., Novelli, P. C., Zhao, C. L., Dlugokencky, E. J., Lang, P. M., Crotwell, M. J., Fischer, M. L., Parker, M. J., Lee, J. T., Baumann, D. D., Desai, A. R., Stanier, C. O., De Wekker, S. F. J., Wolfe, D. E., Munger, J. W. and Tans, P. P.: CO_2, CO, and CH4 measurements from tall towers in the NOAA Earth System Research Laboratory's Global Greenhouse Gas Reference Network: instrumentation, uncertainty analysis, and recommendations for future high-accuracy greenhouse gas monitoring efforts, Atmos. Meas. Tech., 7(2), 647–687, doi:10.5194/amt-7-647-2014, 2014.

Formatted: Subscript

Angevine, W. M., Eddington, L., Durkee, K., Fairall, C., Bianco, L. and Brioude, J.: Meteorological model evaluation for CalNex 2010, Mon. Weather Rev., 120530140005004, doi:10.1175/MWR-D-12-00042.1, 2012.

Asefi-Najafabady, S., Rayner, P. J., Gurney, K. R., McRobert, A., Song, Y., Coltin, K., Huang, J., Elvidge, C. and Baugh, K.: A multiyear, global gridded fossil fuel CO_2 emission data product: Evaluation and analysis of results, J. Geophys. Res. Atmos., 119, 10213–10231, doi:10.1002/2013JD021296, 2014.

Formatted: Subscript

Bréon, F. M., Broquet, G., Puygrenier, V., Chevallier, F., Xueref-Remy, I., Ramonet, M., Dieudonné, E., Lopez, M., Schmidt, M., Perrussel, O. and Ciais, P.: An attempt at estimating Paris area CO_2 emissions from atmospheric concentration measurements, Atmos. Chem. Phys., 15(4), 1707–1724, doi:10.5194/acp-15-1707-2015, 2015.

Formatted: Subscript

Brioude, J., Angevine, W. M., Ahmadov, R., Kim, S. W., Evan, S., McKeen, S. A., Hsie, E. Y., Frost, G. J., Neuman, J. A., Pollack, I. B., Peischl, J., Ryerson, T. B., Holloway, J., Brown, S. S., Nowak, J. B., Roberts, J. M., Wofsy, S. C., Santoni, G. W., Oda, T. and Trainer, M.: Top-down estimate of surface flux in the Los Angeles Basin using a mesoscale inverse modeling technique: Assessing anthropogenic emissions of CO, NOx and CO_2 and their impacts, Atmos. Chem. Phys., 13(7), 3661–3677, doi:10.5194/acp-13-3661-2013, 2013.

Formatted: Subscript

Conil, S. and Hall, A.: Local Modes of Atmospheric Variability: A Case Study of Southern California, J. Clim., 19, 4308–4325, 2006.

Conley, S., Franco, G., Faloona, I., Blake, D. R., Peischl, J. and Ryerson, T. B.: Methane emissions from the 2015 Aliso Canyon blowout in Los Angeles, CA, Science (80-.)., doi:10.1126/science.aaf2348, 2016.

Cui, Y. Y., Brioude, J., McKeen, S. A., Angevine, W. M., Kim, S.-W., Frost, G. J., Ahmadov, R., Peischl, J., Bousserez, N., Liu, Z., Ryerson, T. B., Wofsy, S. C., Santoni, G. W., Kort, E. A., Fischer, M. L. and Trainer, M.: Top-down estimate of methane emissions in California using a mesoscale inverse modeling technique: The South Coast Air Basin, J. Geophys. Res. Atmos., 120(13), 6698–6711, doi:10.1002/2014JD023002, 2015.

Djuricin, S., Pataki, D. E. and Xu, X.: A comparison of tracer methods for quantifying CO$_2$ sources in an urban region, J. Geophys. Res., 115, D11303, doi:10.1029/2009JD012236, 2010.

Formatted: Subscript

Djuricin, S., Xu, X. and Pataki, D. E.: The radiocarbon composition of tree rings as a tracer of local fossil fuel emissions in the Los Angeles basin: 1980-2008, J. Geophys. Res. Atmos., 117(12), 1–15, doi:10.1029/2011JD017284, 2012.

Dlugokencky, E. J.: Conversion of NOAA atmospheric dry air CH$_4$ mole fractions to a gravimetrically prepared standard scale, J. Geophys. Res., 110(D18), D18306, doi:10.1029/2005JD006035, 2005.

Formatted: Subscript

Dlugokencky, E. J., Lang, P. M. and Masade, K. A.: The growth rate and distribution of atmospheric methane, , 99(94), 1994.

Duren, R. M. and Miller, C. E.: Measuring the carbon emissions of megacities, Nat. Clim. Chang., 2(8), 560–562, doi:10.1038/nclimate1629, 2012.

Etiope, G. and Ciccioli, P.: Earth's degassing: A missing ethane and propane source, Science, 323, 478, doi:10.1126/science.1165904, 2009.

Feng, S., Lauvaux, T., Newman, S., Rao, P., Ahmadov, R., Deng, A., Díaz-Isaac, L. I., Duren, R. M., Fischer, M. L., Gerbig, C., Gurney, K. R., Huang, J., Jeong, S., Li, Z., Miller, C. E., O'Keeffe, D., Patarasuk, R., Sander, S. P., Song, Y., Wong, K. W. and Yung, Y. L.: LA Megacity: a High-Resolution Land-Atmosphere Modelling System for Urban CO$_2$ Emissions, Atmos. Chem. Phys., 16, 9019–9045, doi:10.5194/acp-16-9019-2016, 2016.

Formatted: Subscript

Filges, A., Gerbig, C., Chen, H., Franke, H., Klaus, C. and Jordan, A.: The IAGOS-core greenhouse gas package: a measurement system for continuous airborne observations of CO$_2$, CH$_4$, H$_2$O and CO, Tellus B, 67, 27989, doi:10.3402/tellusb.v67.27989, 2015.

Formatted: Subscript

Formatted: Subscript

Formatted: Subscript

Graven, H. D., Guilderson, T. P. and Keeling, R. F.: Observations of radiocarbon in CO$_2$ at La Jolla, California, USA 1992–2007: Analysis of the long-term trend, J. Geophys. Res., 117(D2), D02302, doi:10.1029/2011JD016533, 2012.

Formatted: Subscript

Gurney, K. R., Chen, Y. H., Maki, T., Kawa, S. R., Andrews, A. and Zhu, Z.: Sensitivity of atmospheric CO$_2$ inversions to seasonal and interannual variations in fossil fuel emissions, J. Geophys. Res. D Atmos., 110(10), 1–13, doi:10.1029/2004JD005373, 2005.

Formatted: Subscript

Gurney, K. R., Mendoza, D. L., Zhou, Y., Fischer, M. L., Miller, C. C., Geethakumar, S. and de la Rue du Can, S.: High Resolution Fossil Fuel Combustion CO$_2$ Emission Fluxes for the United States, Environ. Sci. Technol., 43(14), 5535–5541, doi:10.1021/es900806c, 2009.

Formatted: Subscript

Gurney, K. R., Razlivanov, I., Song, Y., Zhou, Y., Benes, B. and Abdul-Massih, M.: Quantification of Fossil Fuel CO$_2$ Emissions on the Building/Street Scale for a Large U.S. City, Environ. Sci. Technol., 46, 12194–12202, doi:/10.1021/es3011282, 2012.

Formatted: Subscript

Gurney, K. R., Romero-Lankao, P., Seto, K. C., Hutyra, L. R., Duren, R. M., Kennedy, C., Grimm, N. B., Ehleringer, J. R., Marcotullio, P., Hughes, S., Pincetl, S., Chester, M. V., Runfola, D. M., Feddema, J. J. and Sperling, J.: Track urban emissions on a human scale, Nature, 525(7568), 179–181, doi:10.1038/525179a, 2015.

Hopkins, F. M., Kort, E. A., Bush, S. E., Ehleringer, J. R., Lai, C.-T., Blake, D. R. and Randerson, J. T.: Spatial patterns and source attribution of urban methane in the Los Angeles Basin, J. Geophys. Res. Atmos., 121, 2490–2507, doi:10.1002/2015JD024429.Received, 2016.

Hsu, Y.-K., VanCuren, T., Park, S., Jakober, C., Herner, J., FitzGibbon, M., Blake, D. R. and Parrish, D. D.: Methane emissions inventory verification in southern California, Atmos. Environ., 44(1), 1–7, doi:10.1016/j.atmosenv.2009.10.002, 2010.

Hutyra, L. R., Duren, R., Gurney, K. R., Grimm, N., Kort, E. a., Larson, E. and Shrestha, G.: Urbanization and the carbon cycle: Current capabilities and research outlook from the natural sciences perspective, Earth's Futur., 2(10), 2014EF000255, doi:10.1002/2014EF000255, 2014.

IEA: World Energy Outlook 2008., 2008.

Jacob, D. J., Crawford, J. H., Maring, H., Clarke, A. D., Dibb, J. E., Emmons, L. K., Ferrare, R. A., Hostetler, C. A., Russell, P. B., Singh, H. B., Thompson, A. M., Shaw, G. E., McCauley, E., Pederson, J. R. and Fisher, J. A.: The arctic research of the composition of the troposphere from aircraft and satellites (ARCTAS) mission: Design, execution, and first results, Atmos. Chem. Phys., 10(11), 5191–5212, doi:10.5194/acp-10-5191-2010, 2010.

Jeong, S., Zhao, C., Andrews, A. E., Bianco, L., Wilczak, J. M. and Fischer, M. L.: Seasonal variation of CH_4 emissions from central California, J. Geophys. Res., 117(D11), D11306, doi:10.1029/2011JD016896, 2012.

Jeong, S., Hsu, Y. K., Andrews, A. E., Bianco, L., Vaca, P., Wilczak, J. M. and Fischer, M. L.: A multitower measurement network estimate of California's methane emissions, J. Geophys. Res. Atmos., 118(19), 11339–11351, doi:10.1002/jgrd.50854, 2013.

Kort, E. A., Frankenberg, C., Miller, C. E. and Oda, T.: Space-based observations of megacity carbon dioxide, Geophys. Res. Lett., 39(17), L17806, doi:10.1029/2012GL052738, 2012.

Kort, E. A., Angevine, W. M., Duren, R. and Miller, C. E.: Surface observations for monitoring urban fossil fuel CO_2 emissions: Minimum site location requirements for the Los Angeles megacity, J. Geophys. Res. Atmos., 118(3), 1577–1584, doi:10.1002/jgrd.50135, 2013.

Lauvaux, T., Miles, N. L., Deng, A., Richardson, S. J., Cambaliza, M. O., Davis, K. J., Gaudet, B., Gurney, K. R., Huang, J., O'Keefe, D., Song, Y., Karion, A., Oda, T., Patarasuk, R., Razlivanov, I., Sarmiento, D., Shepson, P., Sweeney, C., Turnbull, J. and Wu, K.: High-resolution atmospheric inversion of urban CO_2 emissions during the dormant season of the Indianapolis Flux Experiment (INFLUX), J. Geophys. Res. Atmos., 121(10), 5213–5236, doi:10.1002/2015JD024473, 2016.

Ma, S. and Skou, E.: CO_2 permeability in Nafion ® EW1100 at elevated temperature, Solid State Ionics, 178, 615–619, doi:10.1016/j.ssi.2007.01.030, 2007.

Masarie, K. A. and Tans, P. P.: Extension and integration of atmospheric carbon dioxide data into a globally consistent measurement record, J. Geophys. Res., 100(D6), 11593–11610, doi:10.1029/95JD00859, 1995.

Formatted: Subscript

Formatted: Subscript

Deleted: (R)

Formatted: Subscript

McKain, K., Wofsy, S. C., Nehrkorn, T., Eluszkiewicz, J., Ehleringer, J. R. and Stephens, B. B.: Assessment of ground-based atmospheric observations for verification of greenhouse gas emissions from an urban region, Proc. Natl. Acad. Sci. U. S. A., 109(22), 8423–8, doi:10.1073/pnas.1116645109, 2012.

McKain, K., Down, A., Raciti, S. M., Budney, J., Hutyra, L. R., Floerchinger, C., Herndon, S. C., Nehrkorn, T., Zahniser, M. S., Jackson, R. B., Phillips, N. and Wofsy, S. C.: Methane emissions from natural gas infrastructure and use in the urban region of Boston, Massachusetts., 2015.

Miller, J. B., Lehman, S., Verhulst, K. R., Miller, C., Duren, R., Newman, S., Higgs, J. and Sloop, C.: Initial Atmospheric Fossil-fuel CO_2 Estimates from the Los Angeles Megacity Project, in 43rd Global Monitoring Annual Conference, 2015 Program and Abstracts Booklet, NOAA Earth System Research Laboratory, Global Monitoring Division., 2015.

Formatted: Subscript

Nara, H., Tanimoto, H., Tohjima, Y., Mukai, H., Nojiri, Y., Katsumata, K. and Rella, C. W.: Effect of air composition (N2, O2, Ar, and H2O) on CO_2 and CH_4 measurement by wavelength-scanned cavity ring-down spectroscopy: Calibration and measurement strategy, Atmos. Meas. Tech., 5(11), 2689–2701, doi:10.5194/amt-5-2689-2012, 2012.

Formatted: Subscript

Formatted: Subscript

Newman, S., Xu, X., Affek, H. P., Stolper, E. and Epstein, S.: Changes in mixing ratio and isotopic composition of CO_2 in urban air from the Los Angeles basin, California, between 1972 and 2003, J. Geophys. Res., 113(D23), D23304, doi:10.1029/2008JD009999, 2008.

Formatted: Subscript

Newman, S., Jeong, S., Fischer, M. L., Xu, X., Haman, C. L., Lefer, B., Alvarez, S., Rappenglueck, B., Kort, E. A., Andrews, A. E., Peischl, J., Gurney, K. R., Miller, C. E. and Yung, Y. L.: Diurnal tracking of anthropogenic CO_2 emissions in the Los Angeles basin megacity during spring 2010, Atmos. Chem. Phys., 13(8), 4359–4372, doi:10.5194/acp-13-4359-2013, 2013.

Formatted: Subscript

Newman, S., Xu, X., Gurney, K. R., Hsu, Y. K., Li, K. F., Jiang, X., Keeling, R., Feng, S., O'Keefe, D., Patarasuk, R., Wong, K. W., Rao, P., Fischer, M. L. and Yung, Y. L.: Toward consistency between trends in bottom-up CO_2 emissions and top-down atmospheric measurements in the Los Angeles megacity, Atmos. Chem. Phys., 16(6), 3843–3863, doi:10.5194/acp-16-3843-2016, 2016.

Formatted: Subscript

Pacala, S. W., Breidenich, C., Brewer, P. G., Fung, I., Gunson, M., Heddle, G., Law, B., Marland, G., Paustian, K., Prather, M., Randerson, J. T., Tans, P. and Wofsy, S. C.: Verifying greenhouse gas emissions: methods to support international climate agreements. [online] Available from: http://www.tandfonline.com/doi/full/10.1080/20430779.2011.579358 (Accessed 27 September 2014), 2011.

Peischl, J., Ryerson, T. B., Brioude, J., Aikin, K. C., Andrews, A. E., Atlas, E., Blake, D., Daube, B. C., de Gouw, J. A., Dlugokencky, E., Frost, G. J., Gentner, D. R., Gilman, J. B., Goldstein, A. H., Harley, R. A., Holloway, J. S., Kofler, J., Kuster, W. C., Lang, P. M., Novelli, P. C., Santoni, G. W., Trainer, M., Wofsy, S. C. and Parrish, D. D.: Quantifying sources of methane using light alkanes in the Los Angeles basin, California, J. Geophys. Res. Atmos., 118(10), 4974–4990, doi:10.1002/jgrd.50413, 2013.

Prasad, K., Bova, A., Whetstone, J. R. and Novakovskaia, E.: Greenhouse Gas Emissions and Dispersion: 1. Optimum Placement of Gas Inlets on a Building Rooftop for the Measurements of Greenhouse Gas Concentration., 2013.

Prinn, R. G., Huang, J., Weiss, R. F., Cunnold, D. M., Fraser, P. J., Simmonds, P. G., McCulloch, a, Harth, C., Salameh, P., O'Doherty, S., Wang, R. H., Porter, L. and Miller, B. R.: Evidence for substantial variations of atmospheric hydroxyl radicals in the past two decades., Science, 292(5523), 1882–8, doi:10.1126/science.1058673, 2001.

Rahn, D. A. and Mitchell, C. J.: Diurnal Climatology of the Boundary Layer in Southern California Using AMDAR Temperature and Wind Profiles, J. Appl. Meteorol. Climatol., 55(5), 1123–1137, doi:10.1175/JAMC-D-15-0234.1, 2016.

Rella, C. W., Chen, H., Andrews, A. E., Filges, A., Gerbig, C., Hatakka, J., Karion, A., Miles, N. L., Richardson, S. J., Steinbacher, M., Sweeney, C., Wastine, B. and Zellweger, C.: High accuracy measurements of dry mole fractions of carbon dioxide and methane in humid air, Atmos. Meas. Tech., 6(3), 837–860, doi:10.5194/amt-6-837-2013, 2013.

Richardson, S. J., Miles, N. L., Davis, K. J., Crosson, E. R., Rella, C. W. and Andrews, A. E.: Field testing of cavity ring-down spectroscopy analyzers measuring carbon dioxide and water vapor, J. Atmos. Ocean. Technol., 29(3), 397–406, doi:10.1175/JTECH-D-11-00063.1, 2012.

Riley, W. J., Hsueh, D. Y., Randerson, J. T., Fischer, M. L., Hatch, J. G., Pataki, D. E., Wang, W. and Goulden, M. L.: Where do fossil fuel carbon dioxide emissions from California go? An analysis based on radiocarbon observations and an atmospheric transport model, J. Geophys. Res. Biogeosciences, 113, 1–16, doi:10.1029/2007JG000625, 2008.

Ruckstuhl, A. F., Henne, S., Reimann, S., Steinbacher, M., Vollmer, M. K., O'Doherty, S., Buchmann, B. and Hueglin, C.: Robust extraction of baseline signal of atmospheric trace species using local regression, Atmos. Meas. Tech., 5(11), 2613–2624, doi:10.5194/amt-5-2613-2012, 2012.

Ryerson, T. B., Andrews, A. E., Angevine, W. M., Bates, T. S., Brock, C. A., Cairns, B., Cohen, R. C., Cooper, O. R., De Gouw, J. A., Fehsenfeld, F. C., Ferrare, R. A., Fischer, M. L., Flagan, R. C., Goldstein, A. H., Hair, J. W., Hardesty, R. M., Hostetler, C. A., Jimenez, J. L., Langford, A. O., McCauley, E., McKeen, S. A., Molina, L. T., Nenes, A., Oltmans, S. J., Parrish, D. D., Pederson, J. R., Pierce, R. B., Prather, K., Quinn, P. K., Seinfeld, J. H., Senff, C. J., Sorooshian, A., Stutz, J., Surratt, J. D., Trainer, M., Volkamer, R., Williams, E. J. and Wofsy, S. C.: The 2010 California Research at the Nexus of Air Quality and Climate Change (CalNex) field study, J. Geophys. Res. Atmos., 118(11), 5830–5866, doi:10.1002/jgrd.50331, 2013.

Shusterman, A. A., Teige, V., Turner, A. J., Newman, C., Kim, J. and Cohen, R. C.: The BErkeley Atmospheric CO_2 Observation Network : initial evaluation, , 1–23, doi:10.5194/acp-2016-530, 2016.

Stein, A. F., Draxler, R. R., Rolph, G. D., Stunder, B. J. B., Cohen, M. D. and Ngan, F.: NOAA's HYSPLIT atmospheric transport and dispersion modeling system, Bull. Am. Meteorol. Soc., 96(12), 2059–2077, doi:10.1175/BAMS-D-14-00110.1, 2015.

Thoning, K. W., Tans, P. P. and Komhyr, W. D.: Atmospheric carbon dioxide at Mauna Loa Observatory: 2. Analysis of the NOAA GMCC data, 1974–1985, J. Geophys. Res., 94(D6), 8549, doi:10.1029/JD094iD06p08549, 1989.

Turnbull, J. C., Sweeney, C., Karion, A., Newberger, T., Lehman, S. J., Tans, P. P., Davis, K. J., Lauvaux, T., Miles, N. L., Richardson, S. J., Cambaliza, M. O., Shepson, P. B., Gurney, K., Patarasuk, R. and Razlivanov, I.: Toward quantification and source sector identification of fossil fuel CO 2 emissions from an urban area: Results from the INFLUX experiment, J.

Formatted: Subscript

Geophys. Res. Atmos., 120(1), 292–312, doi:10.1002/2014JD022555, 2015.

United Nations: World Urbanization Prospects: The 2014 Revision, Highlights (ST/ESA/SER.A/352)., 2014.

Viatte, C., Lauvaux, T., Hedelius, J. K., Parker, H., Chen, J., Jones, T., Franklin, J. E., Deng, A. J., Gaudet, B., Verhulst, K., Duren, R., Wunch, D., Roehl, C., Dubey, M. K., Wofsy, S. and Wennberg, P. O.: Methane emissions from dairies in the Los Angeles Basin, Atmos. Chem. Phys. Discuss., 1–47, doi:10.5194/acp-2016-281, 2016.

Ware, J., Kort, E. A., Decola, P. and Duren, R.: Aerosol lidar observations of atmospheric mixing in Los Angeles: Climatology and implications for greenhouse gas observations, J. Geophys. Res. Atmos., 121(9862–9878), 1–17, doi:10.1002/2016JD024953, 2016.

Wecht, K. J., Jacob, D. J., Sulprizio, M. P., Santoni, G. W., Wofsy, S. C., Parker, R., Bösch, H. and Worden, J.: Spatially resolving methane emissions in California: Constraints from the CalNex aircraft campaign and from present (GOSAT, TES) and future (TROPOMI, geostationary) satellite observations, Atmos. Chem. Phys., 14(15), 8173–8184, doi:10.5194/acp-14-8173-2014, 2014.

Welp, L. R., Keeling, R. F., Weiss, R. F., Paplawsky, W. and Heckman, S.: Design and performance of a Nafion dryer for continuous operation at CO_2 and CH_4 air monitoring sites, Atmos. Meas. Tech., 6(5), 1217–1226, doi:10.5194/amt-6-1217-2013, 2013.

Wennberg, P. O., Mui, W., Wunch, D., Kort, E. A., Blake, D. R., Atlas, E. L., Santoni, G. W., Wofsy, S. C., Diskin, G. S., Jeong, S. and Fischer, M. L.: On the sources of methane to the Los Angeles atmosphere., Environ. Sci. Technol., 46(17), 9282–9, doi:10.1021/es301138y, 2012.

Wong, C. K., Pongetti, T. J., Oda, T., Rao, P., Gurney, K. R., Newman, S., Duren, R. M., Miller, C. E., Yung, Y. L. and Sander, S. P.: Monthly trends of methane emissions in Los Angeles from 2011 to 2015 inferred by CLARS-FTS observations, Atmos. Chem. Phys., 16(20), 13121–13130, doi:10.5194/acp-16-13121-2016, 2016.

Wong, K. W., Fu, D., Pongetti, T. J., Newman, S., Kort, E. A., Duren, R., Hsu, Y.-K., Miller, C. E., Yung, Y. L. and Sander, S. P.: Mapping $CH_4 : CO_2$ ratios in Los Angeles with CLARS-FTS from Mount Wilson, California, Atmos. Chem. Phys., 15(1), 241–252, doi:10.5194/acp-15-241-2015, 2015.

Wunch, D., Wennberg, P. O., Toon, G. C., Keppel-Aleks, G. and Yavin, Y. G.: Emissions of greenhouse gases from a North American megacity, Geophys. Res. Lett., 36(15), n/a-n/a, doi:10.1029/2009GL039825, 2009.

Wunch, D., Toon, G. C., Hedelius, J. K., Vizenor, N., Roehl, C. M., Saad, K. M., Blavier, J. F. L., Blake, D. R. and Wennberg, P. O.: Quantifying the loss of processed natural gas within California's South Coast Air Basin using long-term measurements of ethane and methane, Atmos. Chem. Phys., 16(22), 14091–14105, doi:10.5194/acp-16-14091-2016, 2016.

Xueref-Remy, I., Dieudonné, E., Vuillemin, C., Lopez, M., Lac, C., Schmidt, M., Delmotte, M., Chevallier, F., Ravetta, F., Perrussel, O., Ciais, P., Bréon, F.-M., Broquet, G., Ramonet, M., Spain, T. G. and Ampe, C.: Diurnal, synoptic and seasonal variability of atmospheric CO_2 in the Paris megacity area, Atmos. Chem. Phys. Discuss., doi:10.5194/acp-2016-218, in review, 2016.

Zhao, C., Andrews, A. E., Bianco, L., Eluszkiewicz, J., Hirsch, A., MacDonald, C., Nehrkorn, T. and Fischer, M. L.:

Deleted: (April), 1–51,

Atmospheric inverse estimates of methane emissions from Central California, J. Geophys. Res. Atmos., 114(16), 1–13, doi:10.1029/2008JD011671, 2009.

Zhao, C. L. and Tans, P. P.: Estimating uncertainty of the WMO mole fraction scale for carbon dioxide in air, J. Geophys. Res. Atmos., 111(8), 1–10, doi:10.1029/2005JD006003, 2006.

Acknowledgements

The authors are thankful for helpful discussions on the uncertainty analysis and comments on the manuscript from A. Pintar, A. Possolo, S. Ghosh, K. Mueller, and J. Whetstone. We are also thankful for valuable advice from A. Andrews on the background selection method and uncertainty analysis based on experience with the NOAA tall-tower network, and for comments that significantly improved the manuscript. We also thank E. Dlugokencky and A. Andrews for providing the Pacific Marine Boundary Layer Reference, which is constructed using measurements from the NOAA Global Greenhouse Gas Reference Network. We thank C. Sweeney and T. Newberger at NOAA/ESRL for calibration data on the series of Picarro G2401 analyzers presented in this study and B. Hall for providing calibration gases and for advice regarding uncertainty in the WMO/NOAA scales. We also thank A. Cox, W. Paplawsky, and T. Lueker at the SIO calibration laboratories for support regarding site operations and calibration tanks. Earth Networks provided invaluable support for installation of sample modules and calibration gases at many of the sites. We would like to thank several Earth Networks staff, including B. Angel and C. Fain for keeping sites maintained and online and for regular status updates throughout the course of this study, D. Bixler and B. Biggs for network support, and J. Aman for regular quality control checks. A portion of this research was carried out at the Jet Propulsion Laboratory, California Institute of Technology, under contract with the National Aeronautics and Space Administration. Additional support was provided by the NIST Greenhouse Gas and Climate Science Measurements Program and the NOAA Atmospheric Chemistry, Carbon Cycle, and Climate Program. FH's research was supported by an appointment to the NASA Postdoctoral Program at JPL, California Institute of Technology, administered by Universities Space Research Association under contract with NASA. Certain commercial equipment, instruments, or materials are identified in this paper in order to specify the experimental procedure adequately. Such identification is not intended to imply recommendation or endorsement by the National Institute of Standards and Technology, nor is it intended to imply that the materials or equipment identified are necessarily the best available for the purpose. © 2016 All Rights Reserved.

Figure captions

Figure 1. Map of the Los Angeles Megacity and locations of the greenhouse gas monitoring network sites. Site locations are shown by the black squares (see Table 1 for details). The South Coast Air Basin (perimeter of the black line) is a geopolitical boundary including non-desert portions of the Los Angeles, Riverside, San Bernardino Counties and all of Orange County (defined by the interior back lines). Background image shows surrounding topography plotted with the average monthly nightlight radiance data from VIIRS during March 2016 (units nW/cm^2/sr) as a proxy for population density (http://ngdc.noaa.gov/eog/viirs/download_monthly.html). Continuous measurements from the MWO, SBC, PVP, and CIT sites are not included as part of this study, however, MWO flask data are included as part of the background analysis.

Figure 2. Time series plots showing the calibrated one-hour average dry air mole fractions for CO_2 (left panels) and CH_4 (right panels) in units parts per million (ppm) from nine CRDS analyzers in the LA Megacity Network. Atmospheric CO_2 and CH_4 observations were corrected using the single-point calibration method. Site codes, from top:. University of Southern California/Downtown LA (USC), Compton (COM), California State University, Fullerton (FUL), Ontario (ONT), Granada Hills (GRA), University of California, Irvine (IRV), La Jolla (LJO), Victorville (VIC), and San Clemente Island (SCI). Data are shown for observations collected between January 2013 and June 2016. The length of each record reflects the commissioning date of each site. Data gaps in these records indicate periods when the instruments were non-operational or data quality was determined to be poor and was flagged (see Supplementary materials). Note that the y-axis scale is different for the VIC and SCI (CO_2 and CH_4) and GRA (CH_4 only) sites.

Figure 3. Time series of 1-hour average observations from the San Clemente Island (SCI, *upper panels*), Victorville (VIC, *middle panels*), and La Jolla (LJO, *lower panels*) sites between 2014 and 2015. Hourly average observations of CO_2 (left panels) and CH_4 (right panels) were filtered using stability criteria, as described in the text. The CCGCRV curve fitting algorithm was then used to fit the selected data in an iterative approach by removing CO_2 and CH_4 outliers >±2σ (see Supplementary materials for further information on the fitting parameters). The final filtered dataset (red points) and smooth curve fits (cyan lines) are also shown. Note: Values outside of the range plotted are not shown.

Figure 4. Comparison of background estimates for Los Angeles for CO_2 (panels *a* and *c*) and CH_4 (panels *b* and *d*) at various sites from January 2014 to June 2016. *Panels a-b:* Smooth curve results for Victorville (VIC, cyan); San Clemente Island (SCI, blue); La Jolla (LJO, magenta); Mt Wilson (MWO, black); and a 2-D Pacific marine boundary layer curtain estimate (Pac. MBL, light blue, red, and yellow dashed lines show results for at 33.4°, 36.9°, and 40.5° N, respectively). The SCI, VIC, and LJO curves were generated using data selected based on stability criteria. The MWO curve was generated using night-time flask data collected every 3-4 days. *Panels c-d:* Background estimates from each site plotted as a difference from the MBL curtain at 33.4° N.

Figure 5. HYSPLIT back trajectories estimated for the previous 24-hours, ending in Pasadena, CA (red circle, at the CIT measurement site) at 14:00 LST. Results are shown for January, March, May, July, September, and November 2015 (from top left to bottom right) using NAM12 hourly winds.

Figure 6. Boxplot of enhancements (CO_2xs and CH_4xs) in the LA megacity observed during 2015 relative to the San Clemente Island background estimate. Results are shown for CO_2xs (upper panels) and CH_4xs (lower panels) and for all hours (left panels) and mid-afternoon hours (12-16:00 LT, right panels). The sites are arranged by latitude from north to south (top to bottom): Victorville (VIC), Granada Hills (GRA), Ontario (ONT), Downtown LA (USC), California State University Fullerton (FUL), Compton (COM), University of California, Irvine (IRV), San Clemente Island (SCI) and La Jolla (LJO). Boxes outline the 25th and 75th percentiles of the sample data, respectively and red horizontal lines show the median values at each site. Values outside the 25th and 75th percentiles are not shown here, but are plotted in Figure S11. (Note: Only positive enhancements are shown. Results for the ONT site are for September to December 2015, while all other results are annual averages. Results from the USC site are shown for the G2401 analyzer only).

Figure 7. Time series of uncertainties in the La Jolla (LJO) air observations. U_p is the analyzer precision, U_{TGT} is the uncertainty derived from the target tank measurements, U_b is the calibration baseline uncertainty, and U_{extrap} (abbreviated U_{ex} in this figure) is the extrapolation uncertainty, or the uncertainty due to the single-point calibration strategy. U_{extrap} was estimated using a mean ε for 9 analyzers see text and Supplemental materials). The total analytical uncertainty in the air measurements (U_{air}) is calculated as described by Eqs. 5-7.

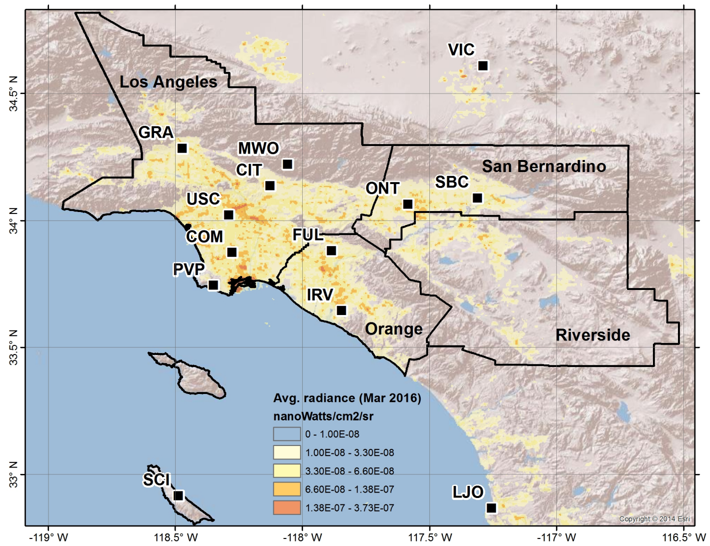

Figure 1. Map of the Los Angeles Megacity and locations of the greenhouse gas monitoring network sites. Site locations are shown by the black squares (see Table 1 for details). The South Coast Air Basin (perimeter of the black line) is a geopolitical boundary including non-desert portions of the Los Angeles, Riverside, San Bernardino Counties and all of Orange County (defined by the interior back lines). Background image shows surrounding topography plotted with the average monthly nightlight radiance data from VIIRS during March 2016 (units nW/cm^2/sr) as a proxy for population density (http://ngdc.noaa.gov/eog/viirs/download_monthly.html). Note: Continuous measurements from the MWO, SBC, PVP, and CIT sites are not included as part of this study, however, MWO flask data are included as part of the background analysis.

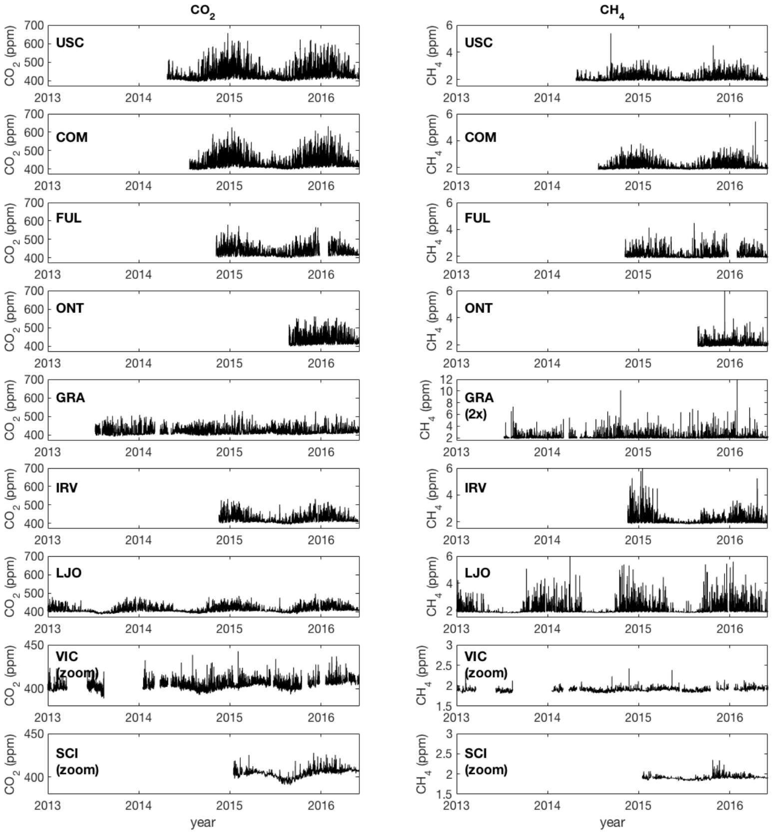

Figure 2. Time series plots showing the calibrated one-hour average dry air mole fractions for CO_2 (left panels) and CH_4 (right panels) in units parts per million (ppm) from nine CRDS analyzers in the LA Megacity Network. Atmospheric CO_2 and CH_4 observations were corrected using the single-point calibration method. Site codes, from top:. University of Southern California/Downtown LA (USC), Compton (COM), California State University, Fullerton (FUL), Ontario (ONT), Granada Hills (GRA), University of California, Irvine (IRV), La Jolla (LJO), Victorville (VIC), and San Clemente Island (SCI). Data are shown for observations collected between January 2013 and June 2016. The length of each record reflects the commissioning date of each site. Data gaps in these records indicate periods when the instruments were non-operational or data quality was determined to be poor and was flagged (see Supplementary materials). Note that the y-axis scale is different for the VIC and SCI (CO_2 and CH_4) and GRA (CH_4 only) sites.

Deleted: *<sp>*

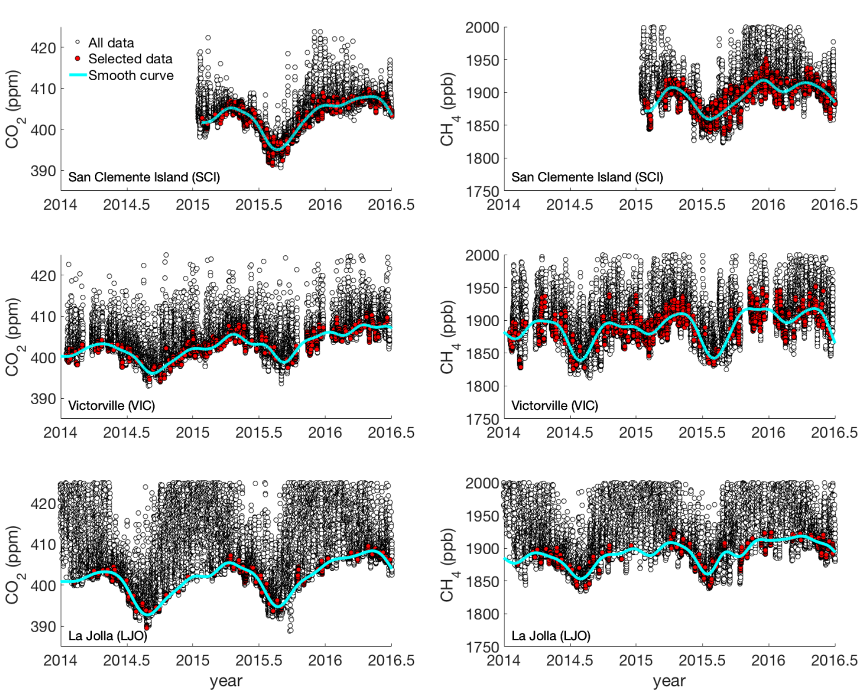

Figure 3. Time series of 1-hour average observations from the San Clemente Island (SCI, *upper panels*), Victorville (VIC, *middle panels*), and La Jolla (LJO, *lower panels*) sites between 2014 and 2015. Hourly average observations of CO_2 (left panels) and CH_4 (right panels) were filtered using stability criteria, as described in the text. The CCGCRV curve fitting algorithm was then used to fit the selected data in an iterative approach by removing CO_2 and CH_4 outliers >±2σ (see Supplementary materials for further information on the fitting parameters). The final filtered dataset (red points) and smooth curve fits (cyan lines) are also shown. Note: Values outside of the range plotted are not shown.

Deleted: measurements

Deleted: , roughly following the preliminary selection criteria described by Thoning et al., (1989).

Deleted: iteratively,

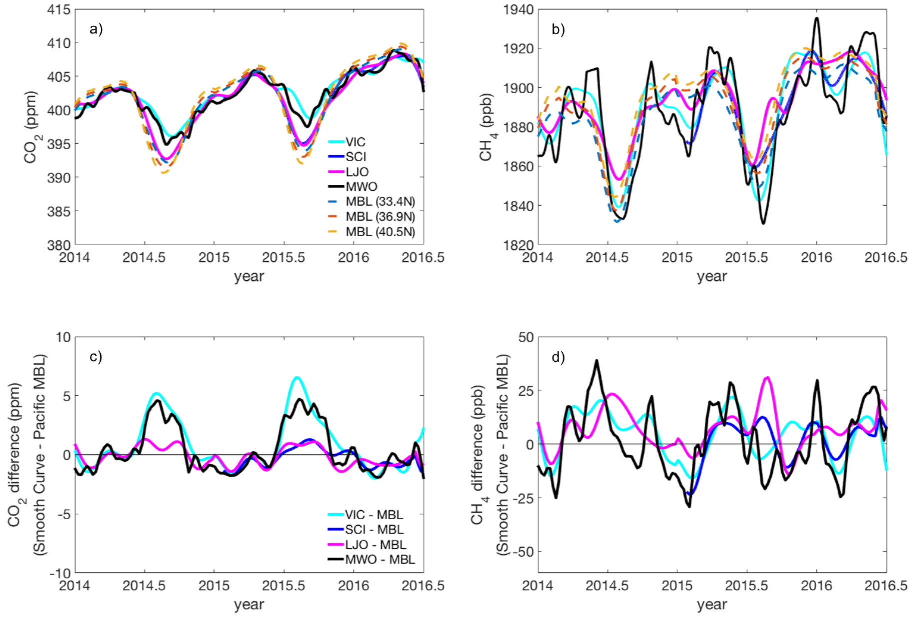

Figure 4. Comparison of background estimates for Los Angeles for CO$_2$ (panels *a and c*) and CH$_4$ (panels *b and d*) at various sites from January 2014 to June 2016. *Panels a-b:* Smooth curve results for Victorville (VIC, cyan); San Clemente Island (SCI, blue); La Jolla (LJO, magenta); Mt Wilson (MWO, black); and a 2-D Pacific marine boundary layer curtain estimate (Pac. MBL, light blue, red, and yellow dashed lines show results for at 33.4°, 36.9°, and 40.5° N, respectively). The SCI, VIC, and LJO curves were generated using data selected based on stability criteria. The MWO curve was generated using night-time flask data collected every 3-4 days. *Panels c-d:* Background estimates from each site plotted as a difference from the MBL curtain at 33.4° N.

Formatted: Font:9 pt, Bold, Complex Script Font: 9 pt

Deleted: left

Deleted: right

Deleted: during 2014 to 2015

Deleted: *Upper p*

Deleted: yellow, red, and

Deleted: n

Deleted: *Lower p*

Deleted: 40

Deleted: .5

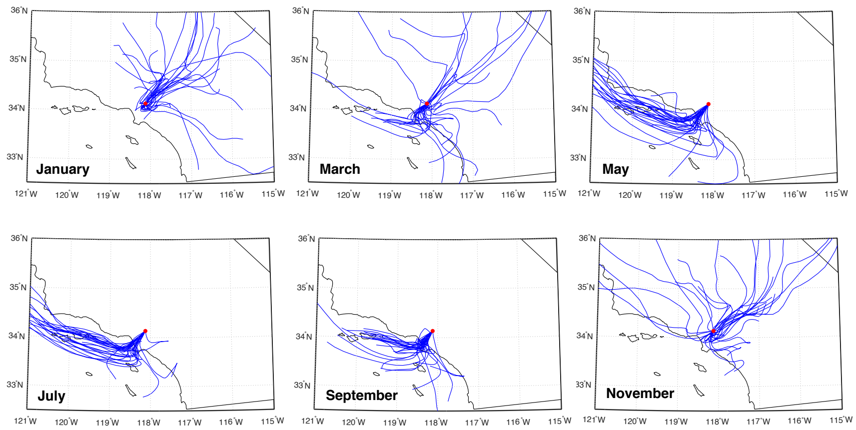

Figure 5. HYSPLIT back trajectories estimated for the previous 24-hours, ending in Pasadena, CA (red circle, at the CIT measurement site) at 14:00 LST. Results are shown for January, March, May, July, September, and November 2015 (from top left to bottom right) using NAM12 hourly winds.

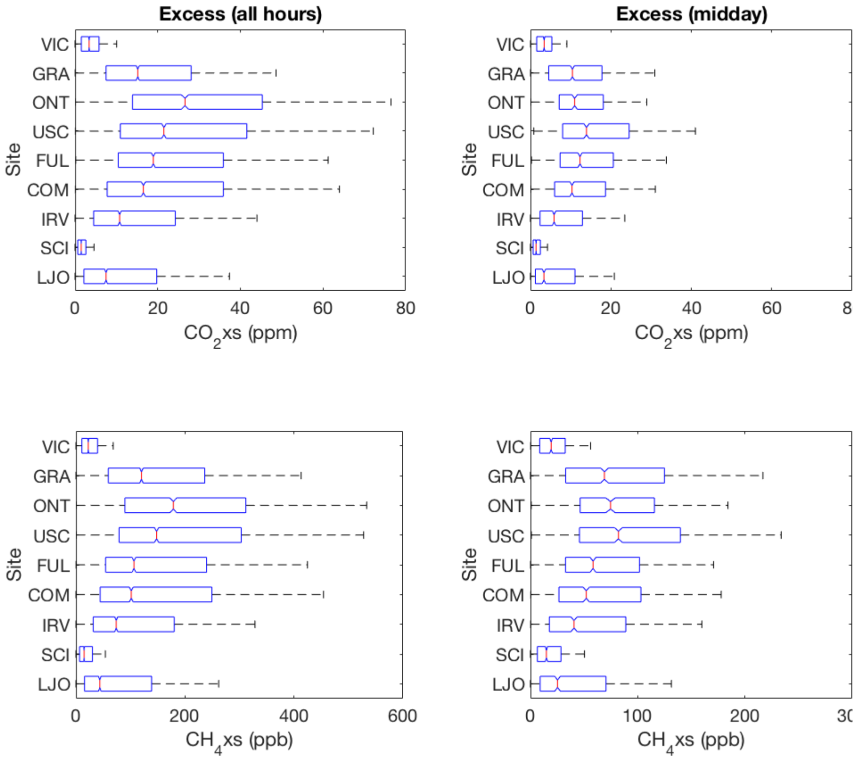

Figure 6. Boxplot of enhancements (CO_2xs and CH_4xs) in the LA megacity observed during 2015 relative to the San Clemente Island background estimate. Results are shown for CO_2xs (upper panels) and CH_4xs (lower panels) and for all hours (left panels) and mid-afternoon hours (12-16:00 LT, right panels). The sites are arranged by latitude from north to south (top to bottom): Victorville (VIC), Granada Hills (GRA), Ontario (ONT), Downtown LA (USC), California State University Fullerton (FUL), Compton (COM), University of California, Irvine (IRV), San Clemente Island (SCI) and La Jolla (LJO). Boxes outline the 25th and 75th percentiles of the sample data, respectively and red horizontal lines show the median values at each site. Values outside the 25th and 75th percentiles are not shown here, but are plotted in Figure S11. (Note: Only positive enhancements are shown. Results for the ONT site are for September to December 2015, while all other results are annual averages. Results from the USC site are shown for the G2401 analyzer only).

Formatted: Font:Bold

Deleted: Δ

Deleted: Δ

Deleted: Δ

Deleted: midday

Deleted: in order

Deleted: going

Deleted: plotted

Deleted: Note: Outliers are included in the statistics, but are not shown here. Figure S6 shows the same results, with outliers plotted. Observations

Deleted: began in

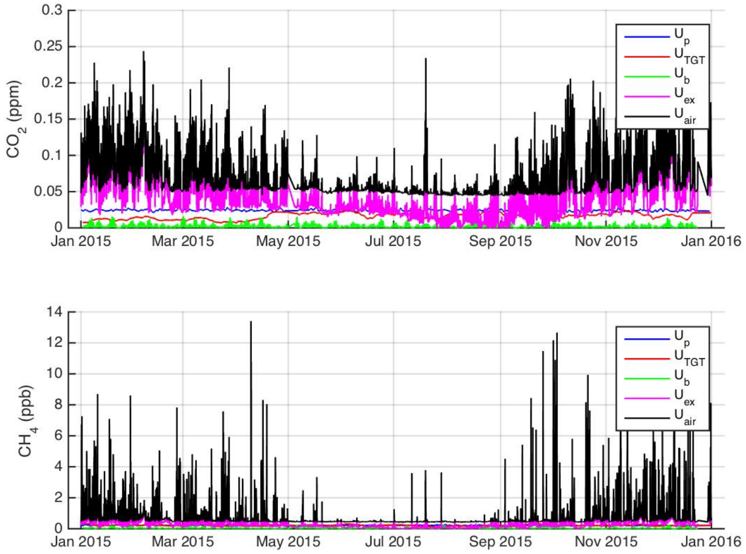

Figure 7. Time series of uncertainties in the La Jolla (LJO) air observations. U_p is the analyzer precision, U_{TGT} is the uncertainty derived from the target tank measurements, U_b is the calibration baseline uncertainty, and U_{extrap} (abbreviated U_{ex} in this figure) is the extrapolation uncertainty, or the uncertainty due to the single-point calibration strategy. U_{extrap} was estimated using a mean ε for 9 analyzers see text and Supplemental materials). The total analytical uncertainty in the air measurements (U_{air}) is calculated as described by Eqs. 5-7.

Deleted: u_p

Deleted: u_{TGT}

Deleted: u_b

Deleted: u_{extrap}

Deleted: u_{extrap}

Deleted: U_{air}

Table 1. Site information for the Los Angeles Megacity Carbon Project surface network. Continuous measurements from the CIT, CNP, MWO, SBC, and PVP sites are not included as part of this study.

Code	Full Site Name	Elev. (m agl)	Elev. (m asl)	Lat (◦N)	Long (◦W)	Analyzer
VIC	Victorville[1]	100/100/50	1370	34.61	117.29	Picarro G2301
GRA	Granada Hills[1]	51/51/31	391	34.28	118.47	Picarro G2401
USC-1	University of Southern California/Downtown LA[2,3]	50	55	34.02	118.29	Picarro G2301
USC-2	University of Southern California/Downtown LA[2,3]	50	55	34.02	118.29	Picarro G2401
COM	Compton[1]	45/45/25	9	33.87	118.28	Picarro G2401
FUL	Fullerton (CSU Fullerton)[2]	50	75	33.88	117.88	Picarro G2401
IRV	Irvine (UC Irvine)[2]	20	10	33.64	117.84	Picarro G2301
SCI	San Clemente Island[1]	27	489	32.92	118.49	Picarro G2401
ONT	Ontario[1]	41/41/25	260	34.06	117.58	Picarro G2301
CNP	Canoga Park[*]	15	245	34.19	118.6	Picarro G2301
LJO	La Jolla (Scripps Pier)[2]	13	0	32.87	117.25	Picarro G2301
CIT-1	Pasadena (Caltech, Arms Laboratory)[2,4,*]	10	230	34.14	118.13	
CIT-2	Pasadena (Caltech, Millikan Library)[4,*]	48	230			Picarro G2401
MWO	Mt Wilson[2,5,*]	3	1670	34.22	118.06	
PVP	Palos Verdes Peninsula[2,*]	3	320	33.74	118.35	
SBC	San Bernardino[1,2,*]	27/58	300	34.09	117.31	Picarro G2301

(1) Tower sites include VIC, GRA, COM, SCI, ONT, and SBC. All other sites have rooftop configurations (USC, FUL, IRV, CIT, and CNP), with air inlets plumbed to the four corners of the building, sampling each corner every 15 minutes (similar to McKain *et al.,* 2015). For rooftop configurations, "upwind" hourly averages are computed using data from the upwind corner of the building determined based on the corner with the highest wind speed measurement. Rooftop inlet height indicates the total height above the surface (building + mast).

(2) Indicates flask collection site for ^{14}C observations (during current or past studies). CO_2 flask observations began near the LJO site in 1979, but are not included as part of this study. The Earth Networks configuration at LJO was implemented in January 2012 with an inlet is located near Scripps pier.

(3) USC: At the time of this study, the USC site had two Picarro analyzers installed (model G2301 and G2401), referred to here and in the text as USC-1 and USC-2, respectively.

(4) CIT: Flask observations at Caltech Arms Laboratory site (CIT-1) began in 1998. The Arms site also has a Picarro G1101-i (isotopic CO_2 analyzer) with continuous measurements of $^{12}CO_2$, $^{13}CO_2$ since described previously (Newman et al., 2008; 2013; 2016) roughly 2001 and LGR N_2O/CO-EP analyzer measuring N_2O and CO. The Caltech Millikan Library site (CIT-2) was installed nearby in December 2015 and includes a Picarro G2401 analyzer. The Millikan site has a 4-corner rooftop sampling strategy identical to other rooftop sites, while the Caltech Arms Laboratory site is a building site with a different configuration. Results are not included as part of this study.

(5) MWO: Flask data have been collected by NOAA/ESRL since 2010 and are included as part of the background analysis in this study. At the time of this study, there were three continuous analyzers installed at the CLARS facility near MWO, which are managed by the Air Resources Board: Picarro G2201-i analyzer measuring CH_4/$^{13}CH_4$/CO_2, Picarro G5310 measuring N_2O/CO/CO_2, and LGR Model 913-0015 measuring N_2O/CO.

(*) Continuous measurements from the CIT, CNP, MWO, SBC, and PVP sites are not included as part of this study. Some data from the CIT-1, PVP, MWO, and SBC sites have been described previously (e.g., Hsu et al., 2010; Jeong et al., 2013; Newman et al., 2013). At the time of this study, the PVP site also had a continuous CO_2 analyzer installed (PP-Systems CIRAS-SC) and the SBC site also had an LGR N_2O/CO-EP.

Table 2. Statistics for CO$_2$ observations from the nine sites shown in Figure 2. Annual average, SD, 16th, 50th (median) and 84th percentiles, minimum and maximum, and RMS values were computed based on the hourly average observations collected during calendar year 2015, with results shown for observations collected during "All hours" and during "Mid-afternoon hours" only (12-16:00 LT).

CO$_2$ (ppm)		**VIC**	**GRA**	**ONT***	**USC**	**FUL**	**COM**	**IRV**	**SCI**	**LJO**
All hours	**mean**	404.7	421.4	434.0	434.8	429.0	430.5	419.4	402.4	412.9
	1σ S.D.	3.7	17.0	25.2	31.2	23.3	30.3	19.3	4.3	14.9
	min	393.5	399.0	400.0	397.5	398.1	395.9	392.6	390.7	388.8
	16th	401.3	407.5	410.9	410.0	409.4	407.4	403.9	397.9	400.4
	median	404.4	416.3	428.1	424.4	421.3	419.5	413.0	403.1	407.3
	84th	407.8	435.8	457.1	460.7	451.2	457.4	436.9	406.1	428.8
	max	442.6	532.6	561.1	621.8	572.9	625.8	531.9	427.7	498.2
	RMS	0.8	3.9	3.4	7.0	5.1	6.9	4.2	1.0	3.4
Mid-afternoon	**mean**	404.4	414.6	415.4	421.6	418.6	418.0	412.0	402.4	407.9
	1σ S.D.	3.6	12.8	11.8	17.5	14.9	16.9	13.5	4.4	10.6
	Min	395.9	399.2	400.0	397.5	398.7	396.9	392.6	391.2	392.5
	16th	401.2	404.9	406.2	408.2	407.2	406.0	401.4	397.9	398.5
	median	404.0	411.2	412.3	416.5	414.4	412.9	408.2	403.1	405.1
	84th	407.3	423.5	423.3	435.0	430.0	429.3	422.7	406.1	417.9
	max	442.6	521.6	487.8	530.0	498.8	558.1	494.9	425.2	468.1
	RMS	0.8	2.9	1.6	3.9	3.3	3.9	2.9	1.0	2.4

*Statistics for the ONT site are based on measurements from Sept-Dec 2015 only.

Deleted: on the hourly average

Deleted: for

Deleted: values

Deleted: . Results are shown for all hours

Deleted: midday

Deleted: roughly

Deleted: **Midday**

Table 3. Statistics for CH_4 observations from the nine sites shown in Figure 2. Mean, SD, 16th, 50th (median) and 84th percentiles, minimum and maximum, and RMS values were computed based on the hourly average observations collected during calendar year 2015, with results shown for observations collected during "All hours" and during "Mid-afternoon hours" only (12-16:00 LT).

CH_4 (ppb)		**VIC**	**GRA**	**ONT***	**USC**	**FUL**	**COM**	**IRV**	**SCI**	**LJO**
All hours	**mean**	1901.7	2103.9	2126.1	2126.5	2079.3	2090.7	2045.7	1901.4	2009.5
	1σ S.D.	34.2	331.3	231.5	227.9	218.0	240.8	246.7	39.9	247.0
	min	1824.9	1828.8	1860.3	1864.9	1849.9	1848.6	1845.6	1823.3	1838.2
	16th	1869.4	1927.3	1956.6	1946.2	1923.7	1914.9	1902.5	1866.4	1883.7
	median	1898.5	2003.6	2073.6	2047.2	1998.1	1998.4	1966.7	1897.6	1925.2
	84th	1933.4	2228.1	2287.1	2321.3	2245.8	2296.3	2183.5	1928.9	2108.6
	max	2383.1	6946.1	8675.7	4511.1	4474.8	3788.6	8432.4	2348.3	5439.1
	RMS	7.2	76.0	31.4	51.1	47.5	55.1	53.5	8.9	55.7
Mid-afternoon	**mean**	1898.6	1985.6	1990.7	2009.9	1978.2	1977.2	1962.6	1900.9	1935.3
	1σ S.D.	32.9	130.5	93.3	116.4	100.2	109.8	101.5	37.9	77.5
	min	1832.7	1828.8	1862.5	1864.9	1849.7	1848.9	1845.6	1824.7	1838.3
	16th	1866.5	1902.9	1924.7	1923.6	1907.5	1901.6	1889.7	1866.4	1877.3
	median	1896.7	1949.8	1969.3	1973.0	1947.6	1943.7	1929.2	1897.3	1911.3
	84th	1928.6	2056.3	2042.2	2095.7	2041.2	2050.3	2036.4	1927.9	1997.6
	max	2105.3	3567.8	2634.0	2677.9	2710.1	3109.6	2960.0	2231.4	2758.3
	RMS	7.0	29.9	12.7	26.2	22.0	25.2	22.1	8.4	17.5

*Statistics for the ONT site are based on measurements from Sept-Dec 2015 only.

Deleted: on the hourly average

Deleted: for

Deleted: Annual average

Deleted: values

Deleted: . R

Deleted: are

Deleted: a

Deleted: midday

Deleted: roughly

Deleted: **Midday**

Table 4. Statistics for the CO_2xs observations from eight of the sites shown in Figure 2. Mean, SD, 16th, 50th (median) and 84th percentiles, minimum and maximum, and RMS values were computed based on the hourly average enhancements calculated during calendar year 2015. Results are shown for observations collected during "All hours" and "Mid-afternoon hours" only (12-16:00 LT). For USC, results are shown for the G2401 analyzer only. ONT results are not shown because measurements were only available from Sept-Dec 2015.

CO_2xs		**VIC**	**GRA**	**USC**	**FUL**	**COM**	**IRV**	**SCI**	**LJO**
All hours	**mean**	4.2	19.9	30.8	26.3	26.7	17.1	2.0	12.7
	1σ S.D.	3.5	16.8	28.6	22.0	27.5	17.5	2.2	13.5
	min	0	0	0.1	0.1	0.1	0	0	0
	16th	1.0	5.1	8.1	7.9	5.8	2.9	0.4	1.3
	median	3.4	15.2	21.5	18.9	16.5	10.8	1.5	7.5
	84th	7.3	35.1	53.8	46.9	49.9	32.5	3.3	26.4
	max	41.0	126.5	222.6	171.2	203.4	126.8	23.0	93.0
	RMS	1.0	5.4	9.0	6.8	8.8	5.3	0.6	3.9
Mid-afternoon	**mean**	3.9	12.8	18.8	16.4	15.2	10.1	1.9	7.6
	1σ S.D.	3.2	11.1	15.9	13.8	15.2	11.8	2.0	9.5
	min	0	0	0.8	0.3	0.1	0	0	0
	16th	1.0	2.8	6.1	5.7	4.9	1.5	0.5	0.7
	median	3.4	10.4	13.9	12.3	10.3	5.9	1.4	3.4
	84th	6.6	22.3	31.3	25.9	24.1	18.9	3.1	16.6
	Max	41.0	99.1	124.8	94.4	152.9	93.2	21.3	66.4
	RMS	0.9	3.5	5.0	4.3	4.9	3.5	0.5	2.7

Deleted: on

Deleted: annual average Δ

Deleted: for

Deleted: Annual average

Deleted: all

Deleted: midday

Deleted: **Midday**

Table 5. Statistics for the CH$_4$xs observations from eight of the sites shown in Figure 2. Mean, SD, 16th, 50th (median) and 84th percentiles, minimum and maximum, and RMS values were computed based on hourly average enhancements calculated during calendar year 2015. Results are shown for enhancements estimated during "All hours" and "Mid-afternoon hours" only (12-16:00 LT). For USC, results are shown for the G2401 analyzer only. ONT results are not shown because measurements were only available from Sept-Dec 2015.

CH$_4$xs		**VIC**	**GRA**	**USC**	**FUL**	**COM**	**IRV**	**SCI**	**LJO**
All hours	**mean**	29.8	217.0	224.0	183.5	188.9	144.0	25.3	129.9
	1σ S.D.	26.0	335.1	212.8	209.2	219.9	195.9	32.1	250.5
	min	0	0	0.8	0.1	0	0.1	0	0
	16th	6.6	39.8	59.6	40.6	30.3	21.4	4.3	9.1
	median	22.5	120.1	147.9	106.4	101.4	73.9	14.9	43.7
	84th	50.3	328.3	403.8	331.8	372.4	268.5	43.6	216.8
	max	484.9	5085.0	2615.0	2611.4	1614.0	2821.3	453.3	3520.4
	RMS	6.8	63.5	61.4	48.6	52.9	38.6	6.0	34.3
Mid-afternoon	**mean**	24.6	99.2	113.8	85.6	84.4	72.2	23.6	53.6
	1σ S.D.	23.2	119.4	105.8	88.9	98.0	92.2	29.2	68.4
	min	0.2	0	0.8	0.1	0.3	0.2	0	0
	16th	5.2	20.3	35.1	24.4	18.3	11.0	3.7	6.1
	median	19.3	69.0	82.0	58.3	52.0	40.6	14.9	25.3
	84th	43.0	162.3	187.7	139.0	140.3	125.9	40.5	114.1
	max	187.2	1666.3	785.9	813.3	857.5	1063.8	313.7	508.7
	RMS	5.4	37.1	33.4	27.2	31.0	27.4	7.6	19.7

Deleted: on

Deleted: annual average Δ

Deleted: for

Deleted: Annual average

Deleted: values

Deleted: a

Deleted: midday

Deleted: roughly

Deleted: Results from

Deleted: **Δ**

Deleted: **Midday**

Table 6. Summary of the average uncertainty estimates for the LJO analyzer during 2015. Each component of the total measurement uncertainty, where: $\overline{U}_{air}$ is the total mean annual uncertainty in the air measurements collected during 2015 and calculated as described by Eqs. 5-7, $\overline{U}_{excess}$ is the average annual uncertainty in the enhancement, U_{h2o} is the uncertainty due to the treatment of water vapor, $\overline{U}_{TGT}$ is the mean uncertainty derived from the target tank measurements, $\overline{U}_{p}$ is the mean analyzer precision, $\overline{U}_{b}$ is the mean calibration baseline uncertainty, and $\overline{U}_{extrap}$ is the extrapolation uncertainty, or the uncertainty due to the single-point calibration strategy, which was estimated using a mean ε for 9 analyzers (see text and Supplemental materials).

Uncertainty Estimates	**CO_2 (ppm)**	**CH_4 (ppb)**
U_{h2o}	0.0233	0.221
U_{scale}	0.03	0.31
$\overline{U}_{TGT}$	0.0166	0.2126
$\overline{U}_{p}$	0.0242	0.2205
$\overline{U}_{b}$	0.0028	0.0444
$\overline{U}_{extrap}$	0.0477	0.4618
$\overline{U}_{air}$	0.0699	0.7224
$\overline{U}_{excess}$	1.36	11.89

Supplemental Materials

for

Carbon Dioxide and Methane Measurements from the Los Angeles Megacity Carbon Project: 1. Calibration, Urban Enhancements, and Uncertainty Estimates

In this document, we describe: (1) Data acquisition and QA/QC protocols; (2) the "Alternate Calibration Method," which is a correction applied to the air data from La Jolla and Victorville using a 2-point calibration method; (3) Data selection criteria and curve fitting parameters for the CCGCRV software used to estimate background; (4) Estimates of epsilon (the slope component of the extrapolation uncertainty) for CO_2 and CH_4 based on laboratory measurements using CRDS analyzer units similar to those deployed in the field; (5) Uncertainty due to permeability of the Nafion drier determined from laboratory experiments; (6) Results from an Allan deviation analysis conducted using daily calibration runs from the La Jolla analyzer during January 2016; (7) Example plots showing the CO_2 and CH_4 calibration baseline uncertainty using three possible time series of Picarro sensitivity for the standard tank measurements from the La Jolla site during January 2016; (8) Results for the uncertainty associated with background (U_{BG}) for the San Clemente Island, Victorville, and La Jolla estimates.

Deleted: (1) Estimates of epsilon (the slope component of the extrapolation uncertainty) for CO_2 and CH_4 based on laboratory measurements using CRDS analyzer units similar to those deployed in the field; (2) Uncertainty due to permeability of the Nafion drier determined from laboratory experiments;

Deleted: 3

Deleted: 4

Deleted: (5) Plot of the uncertainty associated with background (U_{BG}) based on the San Clemente Island smooth curve result.

1) Data Acquisition and Quality Control

Deleted: Appendix A ... [1]

Deleted: A/QC

1.1) Data acquisition

The LA in situ network includes sites deployed by Earth Networks, Inc. (http://www.earthnetworks.com/OurNetworks/GreenhouseGasNetwork.aspx). The GCWerks software manages the data flow. This software was originally developed for use in the Advanced Global Atmospheric Gases Experiment (AGAGE) network to provide a secure point of access to acquire data from remote instruments and has since been adapted for data management of CRDS analyzers using a Linux-based system (http://www.gcwerks.com). GCWerks also assists in the operation of the LA Megacity sites by reporting instrument diagnostics, sending user defined email alarms, applying pre-defined automated filter and flagging criteria to remove data impacted by instrument errors, and allowing graphical display of results. Several instrument diagnostics and quality control parameters including pressures, flow rates, cycle time, cavity pressure and cavity temperature are monitored in GCWerks to track the instrument status and measurement quality. The calibration correction (using the default, single-point calibration method) is also applied by GCWerks based on daily runs of the calibration standard tank (see Section 2 of the manuscript).

A master copy of GCWerks stored on the EN server ingests and merges the high-frequency CRDS greenhouse gas mole fractions and meteorological data, as well as the calibration information, port assignments,

Formatted: After: 0.25"

tank assignments, etc., on an hourly basis. The imported data are stored as binary strip-chart files, which are over 30 times smaller than the hourly Picarro files for fast data processing and copying. Metadata associated with the LA measurement sites is also stored and maintained on the EN server, including the most current versions of the ports.log and standards files. The standards file contains all the information about the assigned calibration tank values. The ports.log indicates the assignments for each of the air inlets and calibration standards, as well as the time period to reject before calculating averaged values from the native resolution Picarro data. Daily Picarro results are exported into yearly .csv files, which are checked offline against the standards files for additional updates (e.g., calibration tank assignments and data that requires manual flagging). Remote copies of GCWerks are also run by site operators for data exploration via VNC connection.

1.2) Data quality control and automated filters

Deleted: A

Deleted: QA/QC

GCWerks applies some basic automated quality control flags, which filter and/or reject some of the Level 0 data points. We apply automated filters to the high-frequency data in GCWerks before subsequent processing. Filtered data are displayed in GCWerks and are configured in the gcwerks.conf file. The filter criteria are listed in Table S1 and apply to individual high-resolution data points (letter codes: P, S, W, C, T).

Deleted: A

Some data are also rejected to account for the stabilization period after the inlet is switched. The first 10 minutes of data are excluded from further analysis after switching from a calibration tank to an air inlet and the first minute is excluded when switching between air inlets. This allows for flushing time for the tank regulator and plumbing and stabilization of the measurement after valve switching. Data that is automatically or manually flagged or rejected data are also displayed in GCWerks with letter codes (F= flagged data and x = rejected data).

Manual data flagging is occasionally needed to ensure good quality control of the greenhouse gas data (e.g., to ensure the flags were applied correctly in the previous step, or to address technical issues or instrument errors that are outside the scope of the automated filters, such as when a field technician visits the site and impacts the regular sampling protocol). After automated filters are applied, the data are screened manually using a parameter called N filtered in GCWerks to identify instances where automated filters have been applied. Manual data flags are applied by Earth Networks based on recommendations from the LA Megacity Data Working Group, a team of scientists from NASA's Jet Propulsion Laboratory, Scripps Institution of Oceanography, the National Institute of Standards and Technology, and Earth Networks. Manual flags are applied on a case-by-case basis. The decision to flag the data is usually based on information or observations that suggest instrument issues. Many of these cases include technician site visits that require modifications to the plumbing on the instrument of calbox. For example, when a calibration standard is replaced or if an analyzer is removed and/or replaced during repair, room air may enter the instrument, which is not of scientific interest. In some instances, we identify problematic by first looking for large deviations in the cavity pressure, sample pressure, inlet pressure, and/or in the measured mole fraction data and then comparing the data alongside notes from technician logs. The numerous parameters monitored by GCWerks help narrow down the cause of anomalous observations. The N filtered parameter is also monitored and cases where a large number of data have been filtered are analyzed in more detail to determine if additional manual flags are

Deleted: D

Formatted: After: 0.25"

required. The manual flags are applied on the EN server to indicate those data that are not recommended for further scientific evaluation or interpretation within the scope of the project.

The corrected data is generated by GCWerks at 1-minute average intervals and generated as a .csv file for export and further analysis outside of the GCWerks framework. These .csv report files are uploaded to a primary Earth Networks/GCWerks server and are synced nightly and later used to compute the hourly average (Level 3) product.

We primarily discuss the 1-hour average CO_2 and CH_4 air observations in Sections 3 and 4, which are from individual inlet heights (for tower sites), and from a combination of the 4 corner inlets (for rooftop sites). These hourly average data are a Level 3 product, which is averaged from the uncorrected (2-5 s) Picarro data. For rooftops, we used a method similar to McKain et al. (2015) to calculate the 1-hour average air observations using only "upwind" observations (determined from the 1-minute average data). Additionally, we used wind speed and direction observations to verify the "upwind" side of the building. We constructed an "upwind" index for each 1-minute CO_2 or CH_4 observation. The measurement was determined to be "upwind" if the building corner had the highest wind speed and the wind direction also corresponded to the same side of the building.

Deleted: The measurements discussed in Sections 3 and 4 are mainly the

Deleted: each

Deleted: , which we term

2) Alternate calibration method

Deleted: A

An "Alternate Calibration Method" was explored using a linear fit between two tanks (one "near-ambient" tank and one ''high concentration" standard tank) where data was available. Each calibration run is used to derive a slope and intercept, which are then interpolated in time:

$$Xcorr\ alternate = m * X'_{air} + b \qquad \text{(Eq. S1)}$$

Deleted: A

where the slope m and intercept b. The Alternate Calibration Method uses the high concentration standard to determine the slope, m, and intercept, b, while the default (single-point calibration) method assumes a zero reading at zero measurement. Therefore, the Alternate Method becomes equivalent to the default calibration method if b = 0 and the slope m does not vary with mole fraction, so that m = 1/S for all points. Both methods of calibration assume linearity, in that the slope m (or 1/S), is a constant over all mole fractions.

Deleted: cal

Air data from the LJO and VIC sites were corrected using the two methods to quantify the effect of different calibration methods on the final air mole fraction data. Both of these sites had limited measurements of a high mole fraction (span) tank available at the time of this study. Figures S2 and S3 show the difference in air data from the LJO analyzer corrected with the 2-point calibration method and the single-point calibration method for CO_2 (upper panels) and CH_4 (lower panels). Figure S3 shows similar results for air data collected from the VIC analyzer. Overall, the single-point calibration method underestimates the CO_2 levels by about 0.2 ppm out of 100 ppm and underestimates the CH_4 levels by about 6 ppb out of 6000 ppb, or about 1 part in 1000 for the LJO site (Figure S2). The results were similar when the same analysis was performed using air data from the VIC analyzer (Figure S3).

Deleted: A

Deleted: A

Deleted: A3

Deleted: A2

Deleted: A3

Formatted: After: 0.25"

3) Background selection criteria and curve fitting parameters for CCGCRV

Our data selection criteria for CO_2 loosely follow the discussion in Thoning *et al.* (1989), but differ slightly for the LA sites. As described in the text, our data selection approach relies on several criteria: (1) a small degree of variability within a one hour period, and 2) small hour-to-hour variability, and (3) persistence of the first two conditions for several hours. Based on these criteria, we exclude observations that are impacted by local emissions or recirculation effects. The selection criteria for SCI were as follows: (1) First, check for stability of the CO_2 and CH_4 observations within 1-hour and retain measurements if the 1-hour SD is <0.3 ppm CO_2 and <3 ppb CH_4; (2) Next, find small hour-to-hour changes in CO_2 concentration and retain measurements if the hour-to-hour difference is less than 0.25 ppm CO_2. No hour-to-hour criteria were used for CH_4; (3) Finally, retain only those observations with several (6 or more) consecutive hours that meet criteria 1 and 2.

To determine the filter criteria, we first evaluated the standard deviation of the one hour average observations (Figure S4). During 2015, 70%, 42%, and 30% of the data had a one hour S.D. <0.3 ppm CO_2, 67%, 57%, and 42% of the data had a one hour S.D <3 ppb CH_4 filter criteria, and 60%, 35%, and 29% of the data met both criteria for the SCI, VIC, and LJO sites, respectively. We began by applying these criteria to all 3 sites since a significant fraction of the data were within these limits. Next, we chose the hour-to-hour stability cutoff (0.25 ppm CO_2) based on Thoning *et al.* (1989). For the final criteria, we performed several tests by setting the number of consecutive hours between 3 and 6 hours and analyzing the remaining observations.

We found that the LJO and VIC observations were most sensitive to the filter parameters, especially the hour-to-hour stability and number of consecutive hours (criteria 2 and 3). For VIC, we found that requiring 6 or more consecutive hours of stable conditions resulted in large data gaps over the entire season during summer months, making the background estimate highly uncertain during this period. After several adjustments to the filter criteria, we were able to reduce the gaps in the VIC background observations to <1 month by applying the following changes: 1) increasing the hour-to-hour stability from 0.3 ppm CO_2 to 0.5 ppm CO_2 and 2) decreasing the number of consecutive hours with stable conditions from six hours to four hours. For LJO, the original filter criteria did not produce large gaps (>1 month). Furthermore, increasing the allowable hour-to-hour stability or decreasing the number of consecutive hours resulted in a few anomalously high CO_2 and/or CH_4 observations being included in the result, which is unfavorable (and likely due to a persistent polluted air mass passing over the site rather than clean background air). For these reasons, we applied the same criteria at LJO and SCI.

We have considered possible impacts of PBL growth on the background analysis. As described in the main text, we use only nighttime flask samples for the MWO background estimate because this site is more sensitive to the LA Basin during daylight hours due to growth of the PBL and upslope winds. However, our filtering criteria for SCI, LJO, and VIC do not account for diurnal variations, e.g., due to variations in the planetary boundary layer height or due to potential daytime drawdown of CO_2 due to photosynthetic uptake. Initially, we made plots of the monthly average diurnal variability for the SCI, LJO, and VIC sites. However, it was not apparent how the diurnal cycle would aid in the interpretation of background because most of the time the diurnal changes at these sites are dominated by impacts from local emissions (especially at LJO and to a lesser extent at the other two background

Formatted: After: 0.25"

sites due to outflow). At the marine background sites (LJO and SCI), it is the growth the marine boundary layer (MBL) rather than the PBL over the land, that is relevant to the interpretation of background. However, the MBL growth effect is most relevant when a site located very far off-shore, such that nighttime continental outflow is not present. Under these conditions, changes in the MBL with time of day are likely to be very small. The LJO is near sea level and is within the MBL, but is frequently impacted by local sources. The SCI site can be either within or above the MBL due to its elevation (~489 m asl), but is still occasionally impacted by continental outflow. For these reasons, we do not limit the background consideration to certain times of day. The agreement between the SCI and LJO marine background estimates (within ~±1 ppm CO_2 and ~±10 ppb CH_4) suggests that there is not a large gradient between the CO_2 and CH_4 levels in the surface MBL and above the MBL. In summary, for the SCI, LJO, and VIC background sites, our underlying assumption is that if the PBL (or MBL) grows, it will not further dilute the CO_2 or CH_4 levels or cause additional large variations if the site is truly sampling background conditions.

After applying the selection criteria respective to each site, the CCGCRV curve fitting software was used to estimate a "smooth curve" fit to the remaining observations (Thoning et al., 1989; http://www.esrl.noaa.gov/gmd/ccgg/mbl/crvfit/crvfit.html). The following fit parameters were used in CCGCRV: short-term cutoff filter=80 days, long-term cutoff filter=667 days, npoly=3, nharm=4. Data were fit iteratively, continually excluding outliers greater than ±2σ from the smooth curve fit until no more outliers could be removed. A multi-species filter was also applied, so that if either CO_2 or CH_4 were outliers from the smooth curve, then both observations were omitted. The MWO flask data were fit using a similar approach (but only using nighttime flask data to prevent potential contamination due to upslope winds). For MWO, the following fit parameters were used in CCGCRV: short-term cutoff filter=30 days, long-term cutoff filter=667 days, npoly=3, nharm=4, and the data were fit iteratively excluding outliers as described above. The full datasets, selected data and "smooth curve" results are shown in Figure 3 in the main text and a comparison of the final smooth curve results for each site is shown in Figure 4 (top panels). Figure S10 shows the same results with uncertainty estimates calculated as described in Section 6.2 of the main text. Overall, we have achieved a reasonable level of convergence between the background estimates for three sites with very different variability in CO_2 and CH_4 mole fractions. A metric of success exhibited by our results is that the background reference curve estimates agree within ~±1 ppm CO_2 and ~±10 ppb CH_4 for the marine sites (LJO and SCI) and continental sites (MWO and VIC, see Figures 4 and S10).

4) Uncertainty due to Nafion drier permeability

Deleted: A3

Deleted: ... [2]

The laboratory experiments described here were performed at the Scripps Institution of Oceanography to estimate the uncertainty in the water vapor correction due to bias caused by the permeation of CO_2 and CH_4 across the membrane of the Nafion drier. We measured two dry standard tanks for 1200 seconds each, alternating one directly after the other. The measurement system setup was identical to those used at our field sites, with a Nafion dryer located upstream of the instrument. The water vapor concentrations at the start of the measurements were 0.095%, reflective of the Nafion dryer conditions during the ambient air measurements just prior to this experiment. As the measurements continued, the Nafion dryer gradually dried out, which reduced the permeation of CO_2 and CH_4 across the membrane. This effect leads to a small increase in the CO_2 and CH_4 levels measured on the Picarro

Formatted: After: 0.25"

analyzer (Figure S6). In this experiment, we assume that other factors such as instrument drift are negligible over the duration of this experiment (approximately 16 hours).

The uncertainty due to the Nafion permeation effect is derived from the slope of measured CO_2, CH_4 concentrations against water vapor concentrations during our experiment, as shown in Figure S6. CO_2 concentrations are found to decrease at a ratio of -1.15 ppm per 1% change in water vapor concentration in the range of 0 to roughly 0.095%, while CH_4 concentrations are found to be small at a ratio of 0.029 ppb per 1% water vapor concentration change within a range of 0.03 to roughly 0.095%. As the water vapor concentrations in our field measurements lie within a range of 0.01±0.001%, we estimate the potential bias introduced by the 0.001% range in water vapor concentrations to be -0.0115 ppm for CO_2 and 0.000029 ppb for CH_4.

Note that while the permeability of CH_4 through the Nafion membrane is shown to change dramatically in water vapor concentrations lower than 0.03%, this effect can be effectively ignored for our purposes considering the range of water vapor concentrations measured at our sites.

Also, since the relationship between permeation through the Nafion membrane and water vapor concentration has been established, it is also possible to correct for this bias and report an uncertainty on the confidence of our understanding of this relationship. This correction may potentially be added in the future, which would further reduce the uncertainties due to this effect.

Deleted: 3

Deleted: 3

Formatted: After: 0.25"

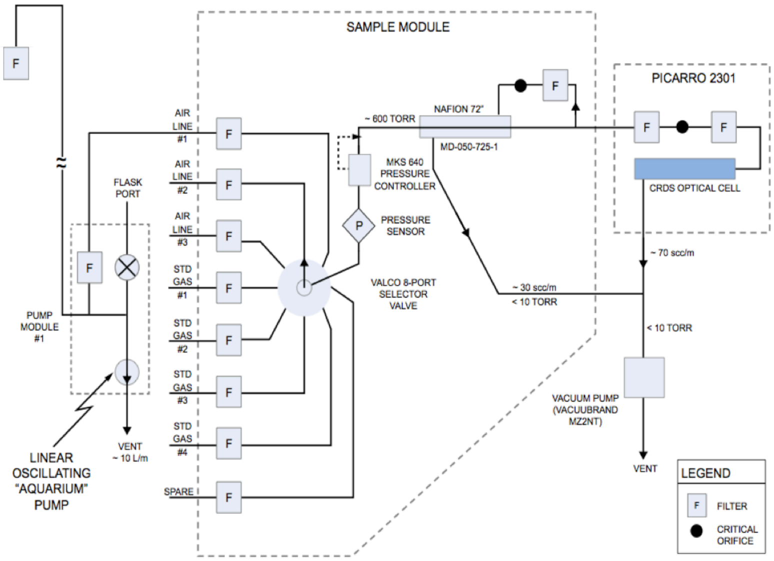

Figure S1. Diagram showing the standard gas-handling configuration for an Earth Networks greenhouse gas monitoring tower sampling from a single air inlet (see text). Figure and caption adapted from Welp et al. (2013).

Deleted: **A**

Formatted: After: 0.25"

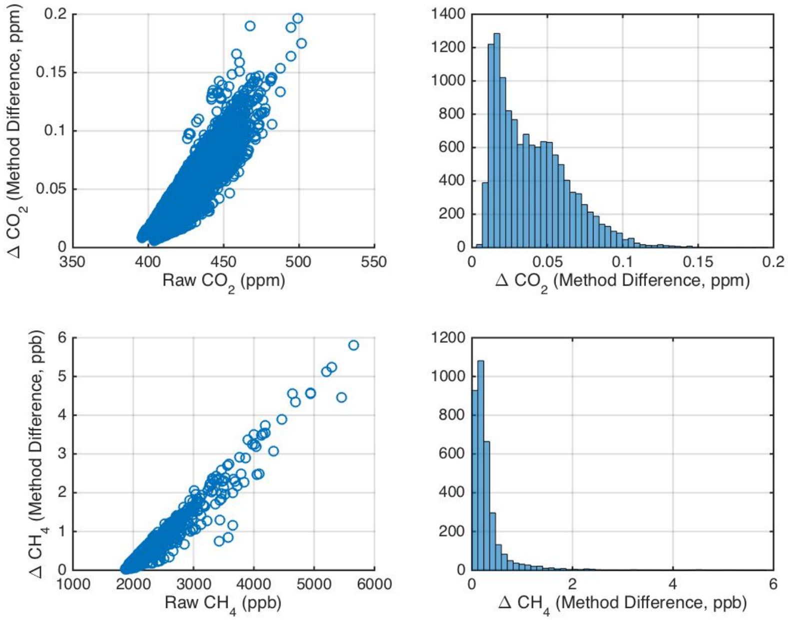

Figure S2. "Alternate Calibration Method" plotted versus uncorrected CO_2 and CH_4 air sample measurements for the LJO site. A limited number of measurements of a high mole fraction CO_2 and CH_4 standard were available at the LJO field site between October 2015 and March 2016. "Method Difference" indicates the difference in the correction of the air data using a single-point relative to a 2-point calibration. Histograms show that the uncertainty associated with using a single-point calibration is <0.2 ppm CO_2 and <4 ppb CH_4 for air measurements collected during this period.

Deleted: **A**

Deleted: raw

Formatted: After: 0.25"

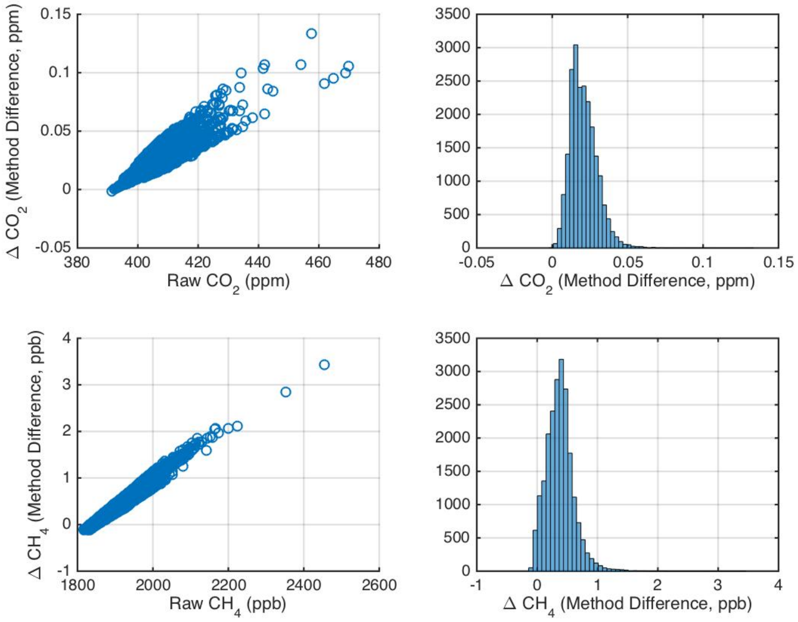

Figure S3. Same as Figure S2, except for the VIC site, which also had limited measurements of a high mole fraction CO_2 and CH_4 standard available at the time of this study. Histograms show that the uncertainty associated with using a single-point calibration is <0.15 ppm CO_2 and <4 ppb CH_4 for the majority of the air measurements collected during this period. Overall, the corrections are slightly smaller because the CO_2 and CH_4 enhancements at VIC are smaller relative to LJO.

Deleted: A

Deleted: A2

Formatted: After: 0.25"

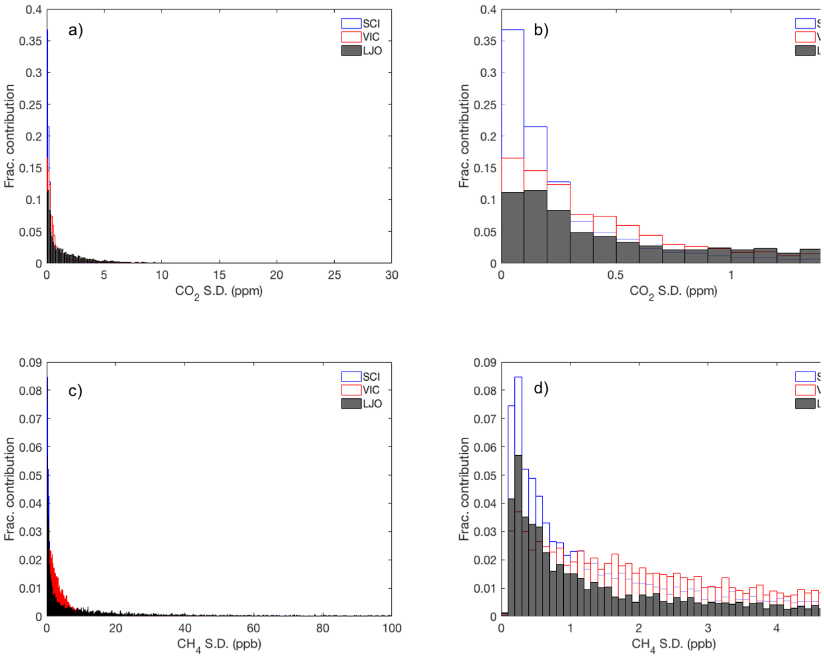

Figure S4: Histograms of the standard deviation of hourly CO_2 (panels *a and b*) and CH_4 (panels *c and d*) observations from the SCI (blue), VIC (red), and LJO (grey) sites. Left panels show histograms for all data. Right panels show the same data with the x-axis truncated for values >1.5 ppm CO_2 and >5 ppb CH_4.

Formatted: Font:(Default) +Theme Headings CS (Times New Roman), 10 pt, Font color: Text 1, Complex Script Font: +Theme Headings CS (Times New Roman), 10 pt

Formatted: After: 0.25"

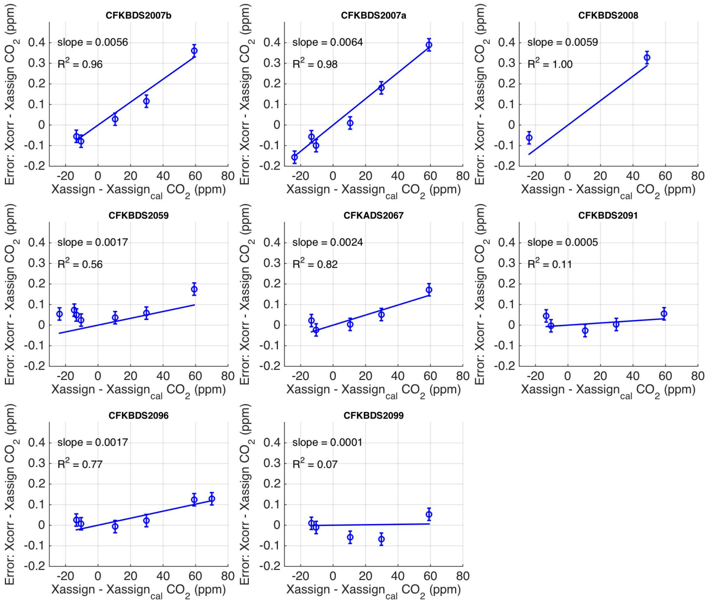

Figure S5. Estimates for epsilon (ε), the slope component of the extrapolation uncertainty (U_{extrap}) for CO_2 based on measurements from seven Picarro CRDS analyzer units. All calibrations were performed on the same suite of tanks at the NOAA/ESRL calibration laboratory. $Xassign_{cal}$ is the assigned value of the calibration standard on the WMO scales (in this case the tank with CO_2 value closest to 400 ppm). The calibration standard was used to correct the uncorrected measurements of other standard gases using Eq. 2 in the main text. *Xassign* is the assigned value of the other standard tanks on the WMO scale (i.e., the span tanks with varying concentrations), and *Xcorr* is the calibrated data. The slope of the residual (*Xcorr* – *Xassign*) is plotted as a function of the concentration difference between each of the standard tanks and the assigned calibration tank ($Xassign_{span}$ – $Xassign_{cal}$), and is a measure of ε. All tanks were calibrated on the WMO/NOAA scales at the NOAA/ESRL laboratory. All Picarro analyzers shown here are similar models to those deployed in the LA network. The same suite of standard tanks was run on each analyzer prior to deployment for various field campaigns (with the exception of CFKBDS2008). CFKBDS2007a and CFKBDS2007b indicate two different calibrations of the same analyzer. All regressions are forced through zero. Error bars show the scale reproducibility (1σ) for the tank values reported by NOAA/ESRL (0.03 ppm CO_2; *Andrews et al.*, 2014 and *B. Hall*, personal communication).

Deleted: S1

Deleted: u_{ex}

Deleted: ,

Deleted: is tank

Deleted: raw

Deleted: –

Deleted: -

Deleted: The same suite of standard tanks was also run on each analyzer prior to deployment for various field campaigns (with the exception of CFKBDS2008).

Deleted: Figures for CFKBDS2007a and CFKBDS2007b indicate two different calibrations of the same analyzer.

Formatted: After: 0.25"

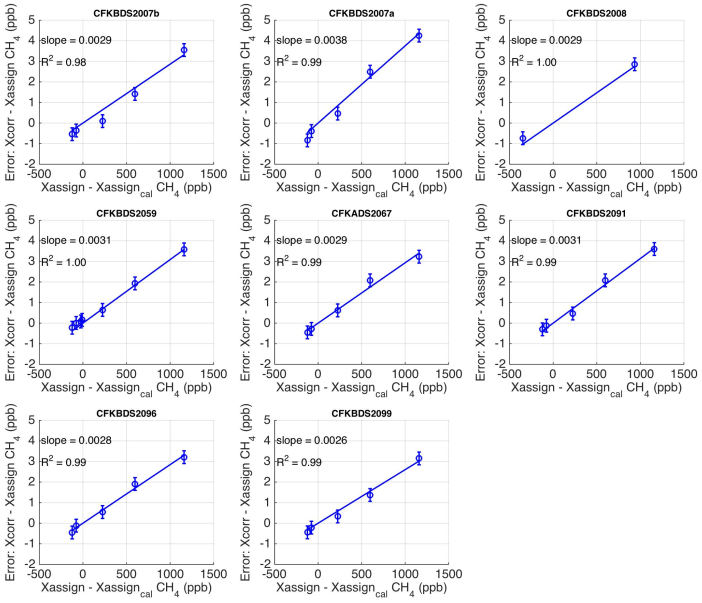

Figure S6. Estimates of epsilon (ε), the slope component of the extrapolation uncertainty (U_{extrap}) for CH_4 using the same suite of tanks as in Figure S4. All regressions are forced through zero. Error bars show the scale reproducibility (1σ) for tank values reported by NOAA/ESRL (0.31 ppb; CH_4 Andrews et al., 2014).

Deleted: S2

Deleted: u_{ex}

Deleted: 2

Formatted: After: 0.25"

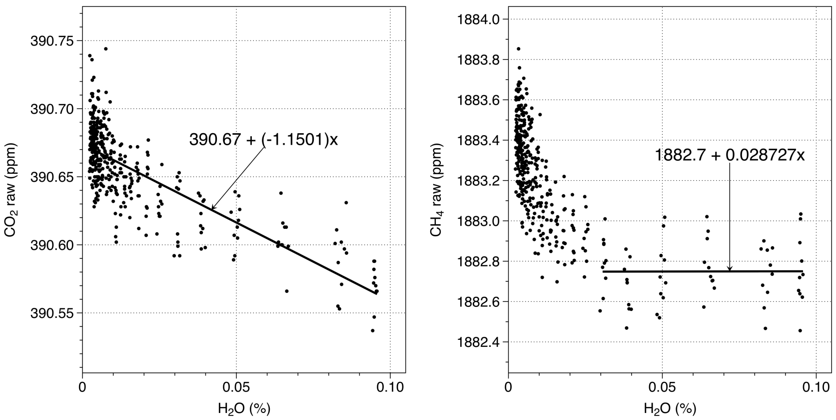

Figure S7. Results of Nafion permeation experiment. A slight increase in the measured CO_2 and CH_4 levels (shown here as uncalibrated CRDS readings) was found as the Nafion membrane dried out, leading to less permeation across the membrane throughout the experiment. We assume that these changes in the measured concentrations are not due to any other factors such as instrument drift. For simplification, only one of the two tanks measured during the experiment is shown. For CO_2, the relationship between measured concentrations and water vapor concentration is derived for the complete water vapor concentration range. For CH_4 we only consider the range of 0.03 to 0.095% H_2O since the permeation effect is different at lower water vapor concentrations, and the water vapor concentration for the field measurements in our network are within the 0.01±0.001% range.

Deleted: S3

Formatted: After: 0.25"

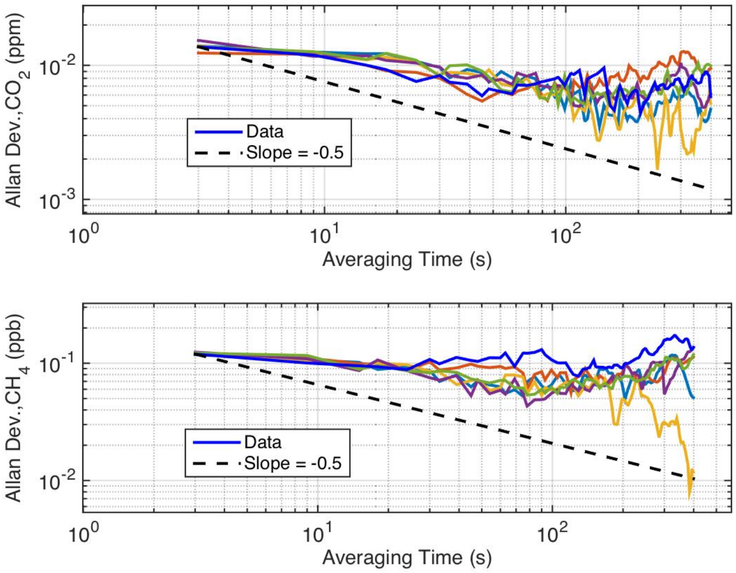

Figure S8. Allan deviation analysis from a subset of the daily calibration runs collected on the LJO analyzer during January 2016 (every 5th run is plotted for clarity). The results show that the characteristics of the noise in the analyzer vary with time. In general, the results for the calibrations are not all the same and do not fit a white-noise profile (indicated by the dashed line with slope of -1/2), indicating correlation in the noise at various longer time scales.

Deleted: S4

Formatted: After: 0.25"

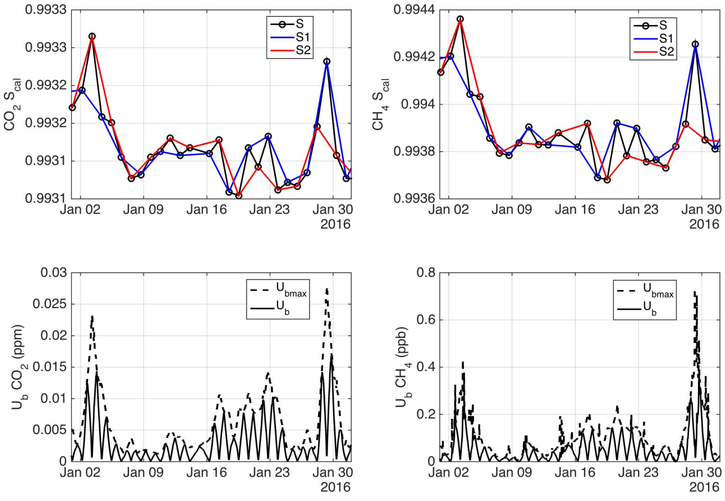

Figure S9. Example showing three possible time series of Picarro sensitivity for the standard tank measurement (upper panels) and the impact on estimates of calibration baseline uncertainty (lower panels). Results are shown for LJO data collected during January 2016. Upper panels: S is the sensitivity of the standard at the times when the reference tank was sampled (black points), which is calculated as the ratio of the measured analyzer mole fraction for the reference gas and the tank’s assigned value (see text). The sensitivity of the standard is linearly interpolated in time, as shown by the black lines for CO_2 (left) and CH_4 (right). The traces, labelled S1 (blue lines) and S2 (red lines), show two alternate realizations of the analyzer sensitivity based on different interpolation methods (e.g. interpolating at points halfway between the sequential standard tank measurements, leaving out every other point). Lower panels: Calibration baseline uncertainty (U_b and U_{bmax}) calculated for CO_2 (left) and CH_4 (right). U_b reduces to zero at the times when the calibration gas was run because the tank value is measured at that time.

Deleted: S5

Deleted: are

Deleted: u_b

Deleted: u_{bmax}

Deleted: u_b

Formatted: After: 0.25"

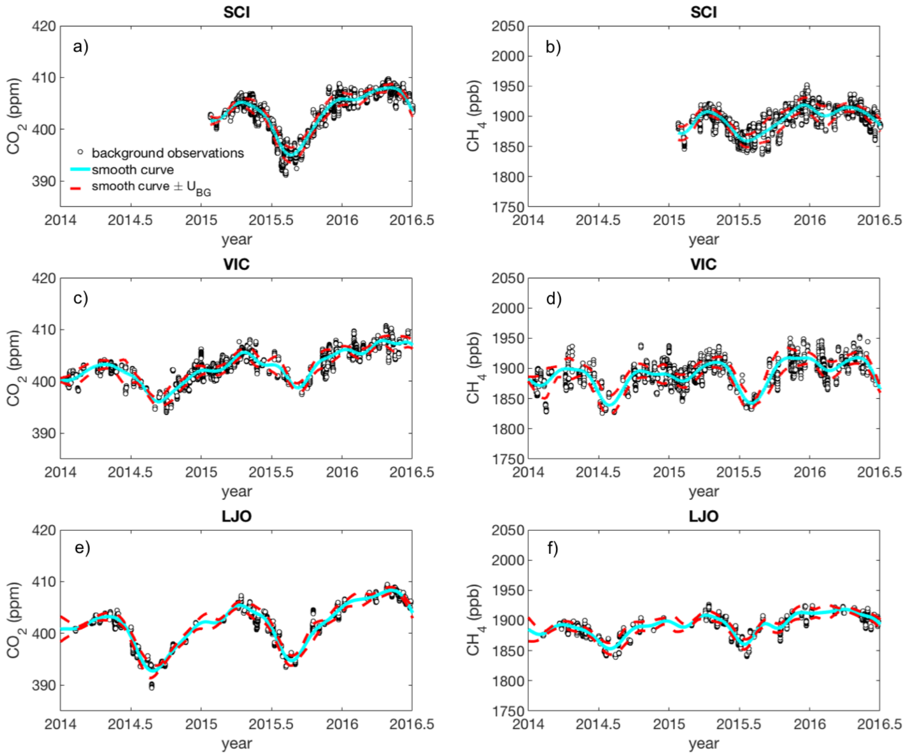

Figure S10. Background observations (black circles), smooth curve estimates (cyan lines) and uncertainty estimates (red dashed lines) for San Clemente Island (panels *a*-*b*), La Jolla (panels *c*-*d*), and Victorville (panels *e*-*f*) for CO_2 and CH_4. During 2015, the annual average uncertainty in the SCI smooth curve estimate is 1.4 ppm CO_2 and 11.9 ppb CH_4.

Formatted: Font:(Default) +Theme Headings CS (Times New Roman), 10 pt, Bold, Complex Script Font: +Theme Headings CS (Times New Roman), 10 pt

Formatted: After: 0.25"

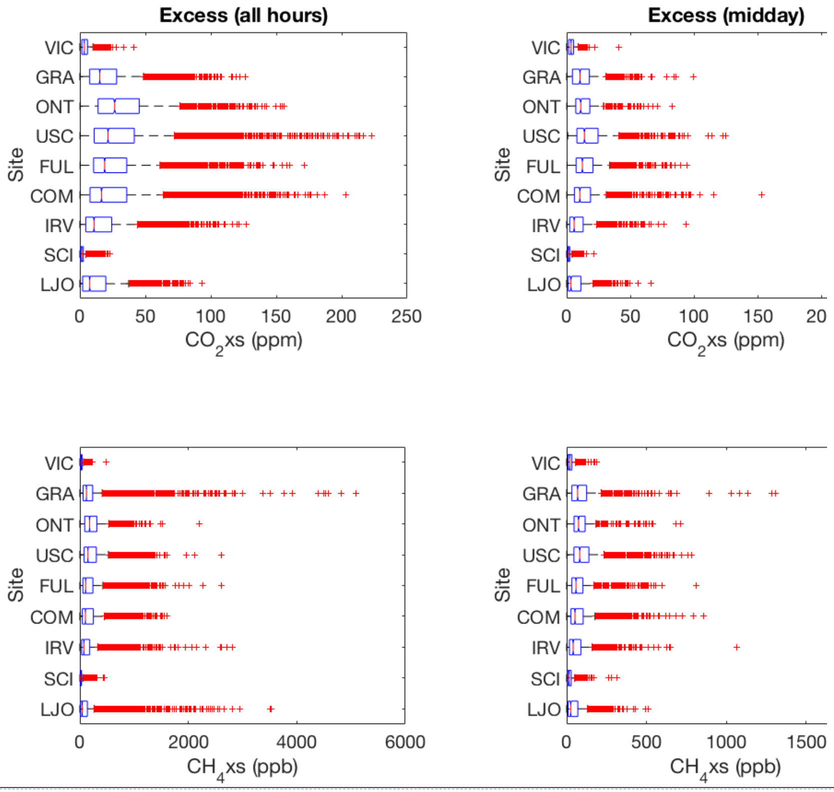

Figure S11: Boxplot of enhancements (CO$_2$xs and CH$_4$xs) in the LA megacity during 2015. Results for CO$_2$xs (upper panels) and CH$_4$xs (lower panels) are shown for all hours (left panels) and mid-afternoon hours (12-16:00 LT, right panels). The sites are arranged by latitude from north to south (top to bottom): Victorville (VIC), Granada Hills (GRA), Ontario (ONT), University of Southern California (USC), Fullerton (FUL), Compton (COM), Irvine (IRV), San Clemente Island (SCI) and La Jolla (LJO). Boxes outline the 25th and 75th percentiles of the sample data, respectively and red vertical lines show the median value at each site. The maximum whisker length is specified as 1.0 times the interquartile range (i.e. [$q_3 + w^*(q_3 - q_1)$] and [$q_1 - w^*(q_3 - q_1)$], where q_1 and q_3 are the 25th and 75th percentiles and w=1.0). Red pluses (+) indicate enhancements greater (or less than) the maximum whisker length to show the full range of variability. (Note: Results for the ONT site include observations for September –December 2015 only, while all other results are annual averages. Results from the USC site are shown for the G2401 analyzer only).

Formatted: Font:(Default) +Theme Headings CS (Times New Roman), 10 pt, Complex Script Font: +Theme Headings CS (Times New Roman), 10 pt

Formatted: After: 0.25"

Table S1. Automated flagging and filtering criteria applied to the CRDS measurements using the GCWerks software. Data meeting the filter criteria are flagged to identify periods when the CRDS analyzer may be subject to large errors and greenhouse gas observations collected during such periods were excluded from further analysis. Flags and filters are applied to high-resolution (roughly 2.5 second) CRDS readings.

Deleted: A

Symbol	Filter name	Frequency	Criteria
P	Cavity pressure[1]	3-5 sec	Cavity pressure out of range (139.9-140.1 Torr)
T	Cavity temperature	3-5 sec	Cavity temperature out of range 44.98-45.02 °C
W	High water	3-5 sec	Water value too high (>10%)
C	Cycle time[1,2]	3-5 sec	Cycle time too high (>8 seconds/cycle)
S	Standard deviation[3]	Varies	For measured compound or water only Calibration standards only: applies to 20-min window, filters values >3σ Air data only: applies narrow 2-minute moving window, filters values >10σ

Formatted: Superscript

(1) Indicates the filter contains a user defined or specified value within GCWerks.

(2) Cycle time is defined as the time between subsequent trace gas measurements. Note: For periods in which a data point is separated from adjacent points by more than the specified maximum cycle time, all 3 points will be filtered. For Los Angeles, the default maximum for cycle time filter is 8 seconds. Representatives from Picarro Inc. recommend the cycle time value should not normally exceed 5 seconds (C. Rella, *personal communication*).

(3) For each measured compound (and water) any data points outside of the user-defined number of standard deviations are automatically filtered. The filter is applied recursively until no more points are filtered in each mean. For calibration tank measurements, the remaining 10-minute period (after the initial 10 minute rejection period) is filtered at once (i.e., no moving window) using a 3σ SD filter. For air data, a narrow 2-minute moving window is used to only filter extreme outliers (>10σ SD, default) that may result from instrument errors. The moving windows overlap 1-minute, and the center 1-minute is filtered, while ends (first and last 30 seconds of each air measurement) are not filtered.

Formatted: After: 0.25"

Table S2. Estimates of ε, the slope component of U_{extrap}, the uncertainty due to the single-point calibration strategy, based on laboratory experiments and field data. Two values are from analyzers deployed at the LJO and VIC sites using limited measurements of a high mole fraction tank deployed in the field. Additional estimates of ε were collected from laboratory calibrations at NOAA/ESRL using CRDS analyzers with similar model numbers (see Figures S4 and S5). Two different sets of calibration results are available for one of the analyzers (CFKBDS-2007a and -2007b).

no.	Analyzer model	CO_2 slope (ε) (ppm/ppm)	R^2	CH_4 slope (ε) (ppb/ppb)	R^2
1a	CFKBDS-2007a	0.0064	0.98	0.0038	0.99
1b	CFKBDS-2007b	0.0056	0.96	0.0029	0.98
2	CFKBDS-2008	0.0059	n/a	0.0029	n/a
3	CFKBDS-2059	0.0017	0.56	0.0031	1.0
4	CFKADS-2067	0.0024	0.82	0.0029	0.99
5	CFKBDS-2091	0.0005	0.11	0.0031	0.99
6	CFKBDS-2096	0.0017	0.77	0.0028	0.99
7	CFKBDS-2099	0.0001	0.07	0.0026	0.99
8	LJO	0.0027	n/a	0.0012	n/a
9	VIC	0.0018	n/a	0.0060	n/a

Formatted: After: 0.25"

Table S3. Estimates of the uncertainty in the single-point calibration method based on laboratory experiments and limited measurements of high concentration standards deployed in the field. Corrections to the air data estimated assuming a 100 ppm CO_2 and 4 ppm CH_4 enhancement above the "near ambient" calibration standard and various estimates for ε.

	CO_2 slope (ε) (ppm/ppm)	**CH_4 slope (ε) (ppb/ppb)**	**CO_2 correction given a 100 ppm enhancement (units: ppm)**	**CH_4 correction given a 4 ppm enhancement (units: ppb)**
Analyzer 1 (a and b)	0.0060±0.0005	0.0033±0.0006	0.60±0.05	13.2±2.4
Analyzers 1-7*	0.0026±0.0024	0.0030±0.0002	0.26±0.24	12.0±0.8
Analyzers 1-9*	0.0025±0.0021	0.0031±0.0012	0.25±0.21	12.4±4.8
LJO analyzer	0.0027	0.0012	0.27	4.8
"Alternate calibration method"**	n/a	n/a	0.2	<6

*Two different calibrations available for analyzer 1 (a and b) were averaged together first, to get a single value for analyzer CFKBDS-2007, before averaging with the other analyzers. See Table S2.

** See Figures S2 and S3.

Formatted: After: 0.25"

References

Andrews, A. E., Kofler, J. D., Trudeau, M. E., Williams, J. C., Neff, D. H., Masarie, K. A., Chao, D. Y., Kitzis, D. R., Novelli, P. C., Zhao, C. L., Dlugokencky, E. J., Lang, P. M., Crotwell, M. J., Fischer, M. L., Parker, M. J., Lee, J. T., Baumann, D. D., Desai, A. R., Stanier, C. O., De Wekker, S. F. J., Wolfe, D. E., Munger, J. W. and Tans, P. P.: CO_2, CO, and CH_4 measurements from tall towers in the NOAA Earth System Research Laboratory's Global Greenhouse Gas Reference Network: instrumentation, uncertainty analysis, and recommendations for future high-accuracy greenhouse gas monitoring efforts, Atmos. Meas. Tech., 7(2), 647–687, doi:10.5194/amt-7-647-2014, 2014.

Welp, L. R., Keeling, R. F., Weiss, R. F., Paplawsky, W. and Heckman, S.: Design and performance of a Nafion dryer for continuous operation at CO_2 and CH_4 air monitoring sites, Atmos. Meas. Tech., 6(5), 1217–1226, doi:10.5194/amt-6-1217-2013, 2013.

Formatted: After: 0.25"